Appendix III

Volunteer-Plant Containment Pool Computational Fluid Dynamics Analysis

III.1 Introduction

A three-dimensional computational fluid dynamics (CFD) model was developed to analyze the flow patterns developed in the U.S. Nuclear Regulatory Commission (NRC) volunteer-plant reactor containment during loss-of-coolant accidents (LOCAs). The CFD modeling assessed the water velocities and flow patterns developed during sump pump operation to support estimates of subsequent LOCA-generated sump pool debris transport. Water sources to the sump pool included effluents from the LOCA break and containment spray drainage. The locations and flow rates of each of these water sources and the recirculation pumping rates determined the characteristics of the sump pool that subsequently determined whether, and what fraction of, the debris deposited into the pool could transport to the recirculation sump screens. Experiments conducted at the University of New Mexico determined threshold transport velocities for debris from pressurized-water reactor (PWR) insulating materials (NUREG/CR-6772, 2001). These threshold velocities were used to set the velocity contours of the CFD flow diagrams to facilitate the determination of whether debris would likely transport. Section III.2 discusses the CFD simulations.

A logic chart debris-transport model was developed to supplement the CFD analyses so that information from the CFD simulations can be used with the blowdown/washdown transport analyses documented in Appendix VI to determine estimates of debris transport to the recirculation sump screens. The pool velocity and turbulence characteristics determine areas of the pool where debris entrapment may occur. The flow streamlines can be used to determine whether debris entering the pool at a discrete location would likely pass through one of the potential entrapment locations. The debris transport process was decomposed using a logic chart approach to facilitate the individual transport steps—steps that could be determined analytically or experimentally, or simply judged. The subsequent quantification of the chart then provided an estimate of the overall sump pool debris transport. Section III.3 discusses the debris transport estimates.

III.2 Analysis of the CFD Simulation

III.2.1 Modeling Methodology, Assumptions, and Conditions Simulated

The commercial CFD program Fluent™ was used to compute the volunteer-plant containment pool flows for large and small LOCA breaks. The containment geometry was available in Autocad™ format and was imported into the Fluent™ preprocessor and grid generator. As shown in Figure III-1, the model geometry included all of the structures, stairwells, and sumps, but the containment pool was modeled only to a depth of 6 ft. This is the maximum anticipated depth of water during steady-state operation of the spray system and sump pump operating in the recirculation mode.

Figure III-2 shows the splash locations, which can be seen as the extruded volumes above the containment pool in Figure III-1. Appendix VI explains in detail the splash locations and flow rates shown in Figure III-2. The CFD model included the following modifications to the splash locations and flow rates:

- One of the four "yellow" floor drains from Level 832, with a total flow rate of 397 gpm in Figure III-2, is located on top of a wall. Thus, the adjacent yellow splash located in the corridor had double the individual flow rate. (For all the Level 832 floor drains, the total mass flow was evenly distributed to all locations, with the exceptions noted here.)
- The liner film flow of 700 gpm was uniformly distributed.
- The Level 808 sprays of 1080 gpm were neglected entirely.

Thirteen LOCA break conditions were simulated. These included eight large LOCA conditions (four break locations, each considered with and without the spray flows) and five small LOCA conditions (four break locations without spray flows and one location with spray flows). The analysis considered both large and small LOCA breaks because each can cause the sump screens to become clogged in a different way. The large LOCA break and spray flows will result in a large pool depth and the wetting of all of the screen surface area. The large LOCA break will likely generate more debris that can migrate to the sump screens, causing an unacceptable head loss because of the amount of debris collected. The small LOCA break may not cause the spray systems to activate and could result in a water depth that wets only the lower portion of the sump screens. This has the potential of forming a thin bed debris mat over a small portion of the screen area resulting in an unacceptable head loss. If the spray flow systems do not activate, depending on break location, a larger portion of the pool flows do not have velocities in excess of the debris threshold velocities and do not participate in the recirculation flow. Therefore, the debris generated in those regions does not migrate to the sump screens.

The four break locations considered correspond to a break occurring in one of the four quadrants (steam generator (SG) compartments) in Figure III-2. The total break flow was assumed to be 7400 and 1611 gpm for the large and small LOCA break flows, respectively. It was assumed that the upper two SG compartments were physically separate from the lower two compartments. Thus, if the break were postulated to occur in the upper left quadrant, 75 percent of the break flow would be partitioned to the upper left and 25 percent to the upper right quadrants; none of the break flow would be in the lower two quadrants. The 75/25-percent partitioning was determined arbitrarily, but it seemed to be a realistic assumption. Additionally, a transient pool fillup simulation was initiated for a large LOCA break in the upper-left quadrant. Only the break flows were simulated in the upper half of the SG compartments with the break flow partitioned as described above. The above apportionment of the flow represents an estimate of the volunteer-plant break resulting from the SG compartment configuration. The SGs are raised above the pool floor level and do not participate in the recirculation flow. Thus, the break flow enters the pool by flowing down the SG stairwells, and the water sheets across the SG compartment and does not pool to any significant depth. Although the 75/25-percent apportionment was assumed, a thorough analysis of how the break flow would enter the pool is needed. Each plant would require such an analysis, which would benefit from the plant personnel's expert knowledge of the containment configuration. The above apportionment merely illustrates the types of flows that would enter the pool.

The simulation used three boundary condition types. All hard surfaces (walls, floors, etc.) were specified to be a no-slip wall condition. The spray system splash and LOCA break flows were specified as a mass flow inlet condition, and the sumps were set to a pressure outflow boundary condition. Because the break flow sheeting described previously was not included, the break and spray flows present in the SG compartment were applied as a mass inflow boundary on a vertical surface at the exit of the SG entrance steps of each quadrant (i.e., a mass flow boundary condition located at the "door" of the SG entrance steps, for instance). The spray/splash mass flow boundary conditions were placed on the "top" of each extruded spray location, as shown in Figure III-1. This extruded volume was found to be easier to handle in Fluent™ rather than trying to set the boundary condition on the "top" of the pool surface.

The combination of mass inflow and pressure outflow satisfies the mass continuity condition without unnecessary complications from numeric and other boundary condition errors. In theory, a mass outflow condition at the bottom of the sump could be specified, but that condition results in numerical instabilities when prescribed. By using a pressure outflow condition at the sumps, the pressure is allowed to "float" to satisfy the incompressible continuity equation. In other words, the code adjusts the pressure at the bottom of the sump to balance the mass flow entering and exiting the pool. This method avoids the introduction of artificial pressure waves in the solution which can be created by specifying mass inflow and outflow conditions.

A second-order-accurate numerical method was used to solve the incompressible Navier-Stokes equations, in conjunction with a renormalized group-theory turbulent-kinetic-energy (TKE) and dissipation turbulence closure (RNG κ-ε). This closure was chosen because of its ability to treat swirling flows, but in practice, little difference was found between the RNG κ-ε and the more traditional κ-ε closure for these simulations. The pressure equation was solved using a pressure-implicit split-operator (PISO) numerical method, as described in the Fluent™ documentation. For the steady-state pool flow analyses, the pool volume was assumed to be completely full of liquid water and initialized to zero velocity. The inflow boundary conditions were flowing from the start, and the solution was allowed to proceed until a steady-state condition was achieved. The normalized residuals of the continuity, momentum, and κ and ε equations were monitored until convergence was achieved, typically after about 400 iterations. For the steady-state pool flow analysis, an additional convergence criterion was to integrate the mass flow rate at the two sump pressure outflow boundaries and compare it with the mass inflow. Achievement of a mass balance, in addition to a drop in the normalized residuals, was necessary for the simulation to be deemed converged.

III.2.2 Results and Discussion

This section contains the results of the CFD simulations. These simulations illustrate what can be achieved with a CFD analysis of the containment pool flows. Application to a particular plant containment would require a more rigorous set of simulations to be performed, including grid convergence tests (e.g., does doubling the number of grid points change the results significantly).

One figure of merit was to determine the fraction of the pool flow volume that produced velocities in excess of the debris migration threshold velocities. Based on the experimental measurements reported in NUREG/CR-6772, the reflective metal

insulation (RMI) and fiber flock transport threshold velocities were determined to be 0.085 and 0.037 m/s, respectively. The following analyses use only one debris transport threshold velocity for fiber and one for small RMI.

III.2.2.1 Transient Containment Pool Fillup

This simulation used a volume-of-fluid (VOF) method. The containment pool was initially filled with air, and water was allowed to enter the pool from the SG entrance stairs. The simulation included only the break flows for a large LOCA break, located in the upper-left quadrant. As noted in Section III.2.1, the break flow is partitioned such that 75 percent of the water leaves the upper-left SG compartment stairwell and 25 percent leaves the upper-right SG compartment stairwell. This condition corresponds to the time immediately after a break occurs and before the spray system is activated. All walls were treated as no-slip surfaces, and because the fillup phase was simulated, the sumps were also treated with no-slip surfaces instead of pressure outflow boundary conditions. The top boundary of the simulated pool was prescribed as a pressure outflow boundary condition instead of as a no-slip wall. This treatment allows the air to leave the domain as the water displaces it. The containment pressurization that occurs during a LOCA was not modeled because it has minimal effect on pool transport.

Figure III-4 through Figure III-12 show the volume fraction of water, at a height of 0.01 m above the containment floor, as the containment pool fills at 0.34, 0.94, 11.4, 21.4, 31.4, 41.4, 51.4, 71.4, and 111.4 seconds after the water leaves the SG compartment stairwells. The color scheme shown corresponds to a red color for 100-percent water in the computational cell and blue for 100-percent air in the cell. Other colors indicate that the computational cell has both air and water partially filling the cell. Figure III-4 through Figure III-12 show the areas that are first swept by the water, as well as how the containment pool fills. This simulation shows the areas that fill first and thus provides information needed to design systems to divert debris to areas of the pool that do not participate in recirculation flow. In general, the water leaves the SG compartment, flows out the doorway, and hits the circular outer wall. Then, the water flows circumferentially around the containment until the two water streams meet near the sumps. The water then starts to enter the areas between the upper and lower SG compartments. For this plant configuration, these two areas between the upper and lower SG compartments are the only “quiet” zones (i.e., they have flow velocities much lower than the debris threshold) in the pool when all break locations are considered in the subsequent steady-state pool flow analysis.

Figure III-13 through Figure III-21 show the fluid velocity during the fillup at the same set of time increments previously discussed for volume fractions. Note that when the water volume fraction and fluid velocity plots are compared, there is motion ahead of the water. This motion is the air moving in response to the approaching front of water. During fillup, the water velocity near the front is in the range of 2–3 m/s, well in excess of the debris transport threshold velocities of 0.037 and 0.085 m/s for fiber and RMI, respectively.

III.2.2.2 Steady-State-Flow Analysis

To study the containment pool’s steady-state-flow dynamics, the simulated volume was considered to be completely full of water. In the case of a small LOCA break, the simulations did not include the spray flows; however, for the large LOCA break, they did include spray flows. With the simulated pool full of water, the break and spray flows

were introduced as mass inflow boundary conditions, and the sumps were set to a pressure outflow boundary condition. These simulations produced a stimulated steady-state-flow condition for further debris transport analysis, discussed in Section III.3.

Figure III-22 through Figure III-29 show the steady-state-flow pattern developed for a small LOCA break condition, without spray flows, and Figure III-30 to Figure III-37 show large LOCA break conditions, including spray flows. These figures show contours of water velocity at a height of 0.01 m above the containment floor and show a velocity range from 0 m/s up to the threshold velocity for fiber or RMI, 0.037 and 0.085 m/s, respectively. From these plots, the area enclosed by the threshold velocity contour can be computed, and by dividing by the entire available flow area in the containment, a percentage of area in excess of the threshold velocity may be calculated. Table III-1 summarizes these percentages, or fractional areas in excess of the threshold velocity, for both large and small LOCA break conditions.

Figure III-38 through Figure III-47 show streamlines for origins near the splash locations for a large LOCA break at two different locations, an upper-left break and a lower-right break. A rake of particles was released from ($-15 < X < -5$, $Y=10$) and also from ($0 < X < 5$, $Y=15$) and allowed to follow the flow. From these streamlines, debris trajectories can be determined and their fate postulated. Figure III-38 and Figure III-39 show the streamlines superimposed on the background velocity map that were color coded using the fiber (0.037 m/s) and RMI (0.085 m/s) threshold velocity, respectively. Figure III-41 and Figure III-42, color coded according to the flow speed, using the fiber and RMI threshold velocity, respectively, show an oblique view of the three-dimensionality of the streamlines. Thus, it can be deduced that if the velocity (speed) along a particular streamline became smaller than the debris type threshold velocity, the debris would not be so likely to migrate to the sump screen. By using rakes and streamline analysis at potential debris entry locations, a method for determining whether the debris will transport to the sump screens could be developed.

Figure III-42 through Figure III-45 show a similar set of plots for the large LOCA break located in the lower-right quadrant. The streamline patterns are quite different for the lower-right break location when compared to the upper-left break location.

Figure III-46 shows a vortex induced by the splash located in the upper-right quadrant in Figure III-42. Here the streamlines are color coded by velocity using the fiber velocity threshold. Because the water enters the pool from above and penetrates to the containment floor, a vortex with significant vertical motion is created. Figure III-47 shows the streamlines color coded by TKE. This type of information would be useful in determining debris degradation mechanisms, particularly for fibrous debris. In Figure III-46 to Figure III-47, the streamlines show the type of rotation that debris can encounter near the entry of a splash into the pool. The water flow produces vortices around the splash entry and could potentially shred debris into finer particles and pieces than those generated by the break itself.

Table III-1. Percentage of Containment Pool Flow Area in Excess of the Debris Transport Threshold Velocity (Total Pool Area = 767.7 m^2)

Break Location	Break Size	RMI (%)	Fiber Flocks (%)
Upper Right	Large	35	60

Break Location	Break Size	RMI (%)	Fiber Flocks (%)
Upper Left	Large	30	54
Lower Left	Large	22	43
Lower Right	Large	22	41
Upper Right	Small	5	31
Upper Left	Small	2	25
Lower Left	Small	5	14
Lower Right	Small	5	19

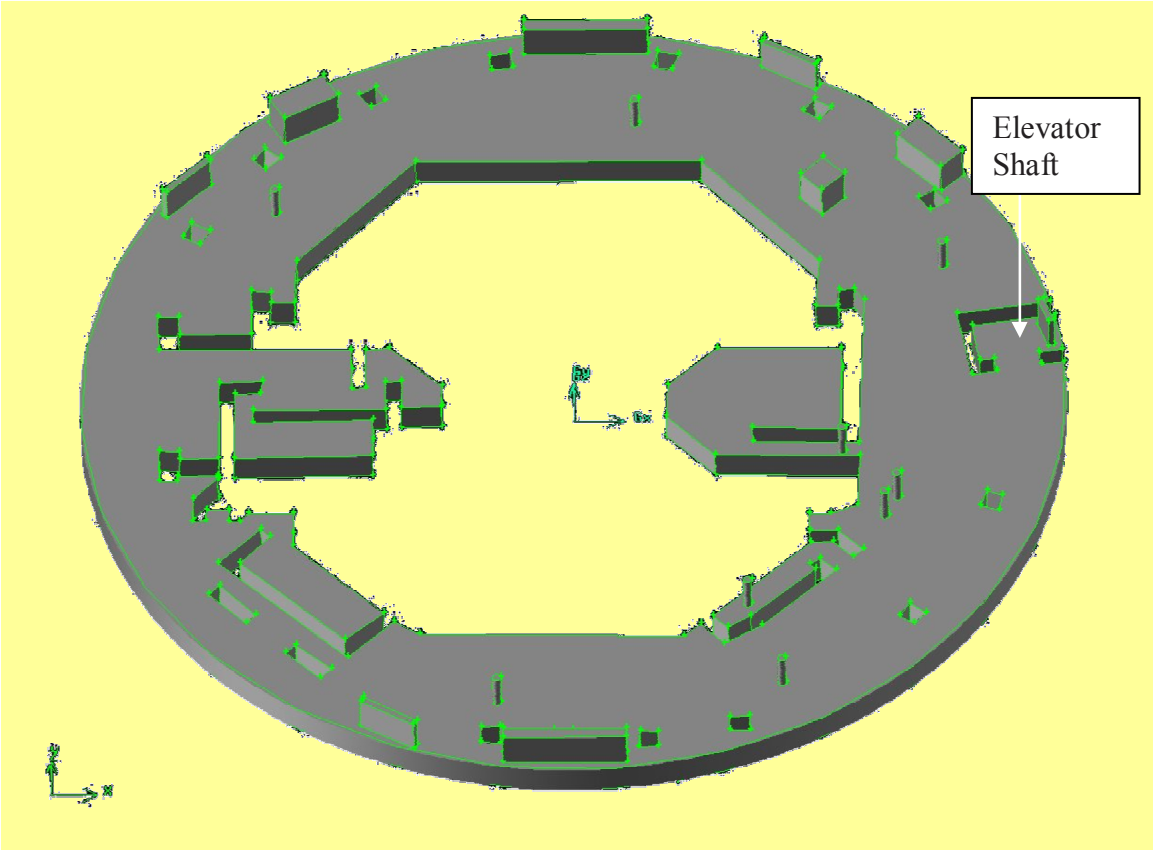

Figure III-1. Volunteer-Plant Geometry and Flow Region Modeled
(Note: Splash Locations Are Shown Extruded above the Nominal Pool Depth)

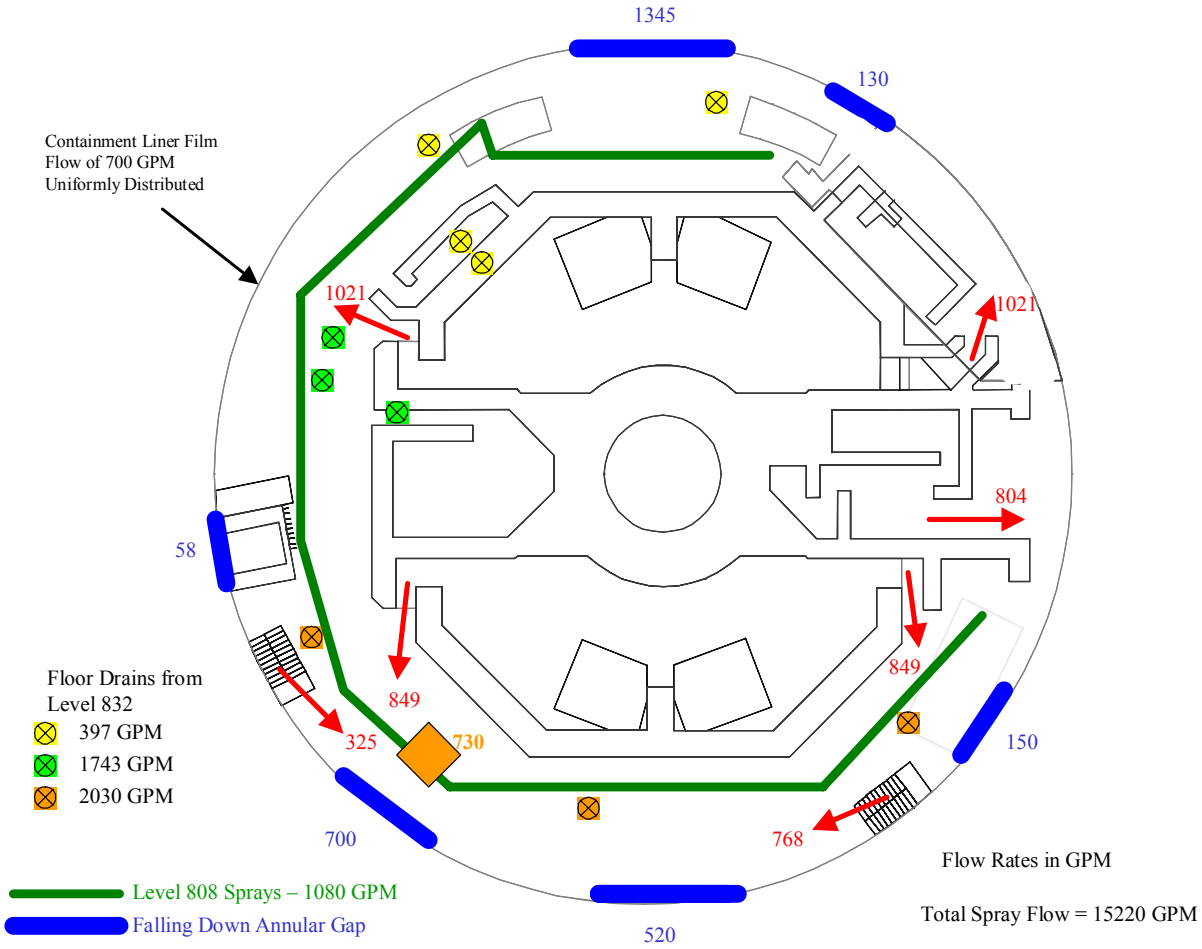

Figure III-2. Spray Flow Rates (gpm) and Locations for the Volunteer-Plant Pool Flow Calculations

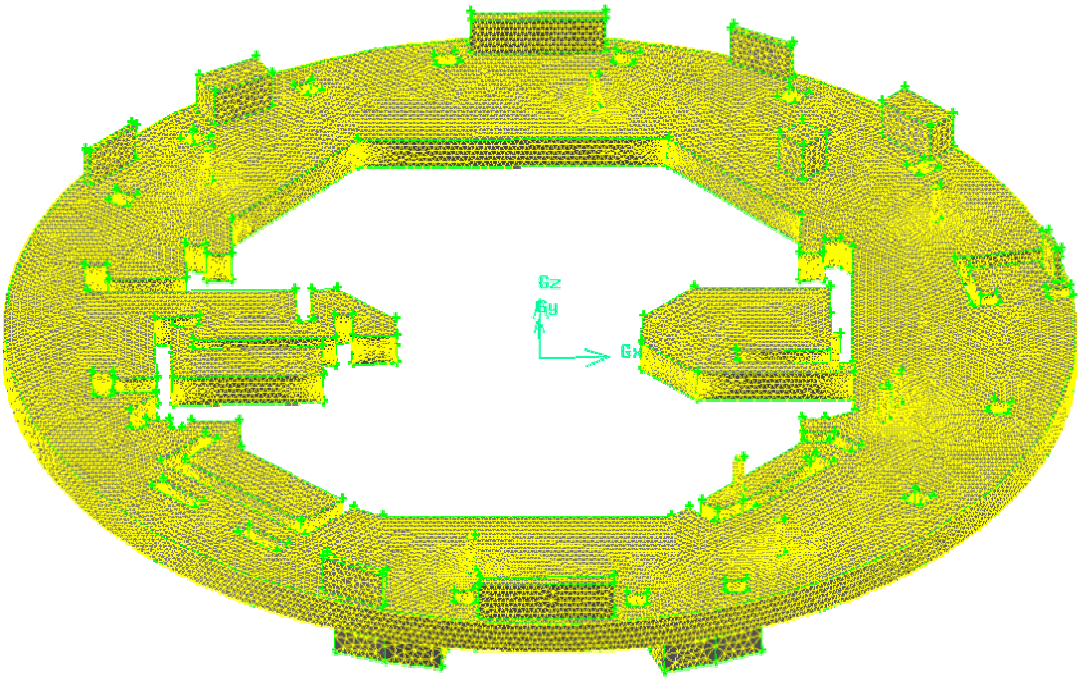

Figure III-3. Unstructured Mesh Created for Containment Pool Flow Calculations

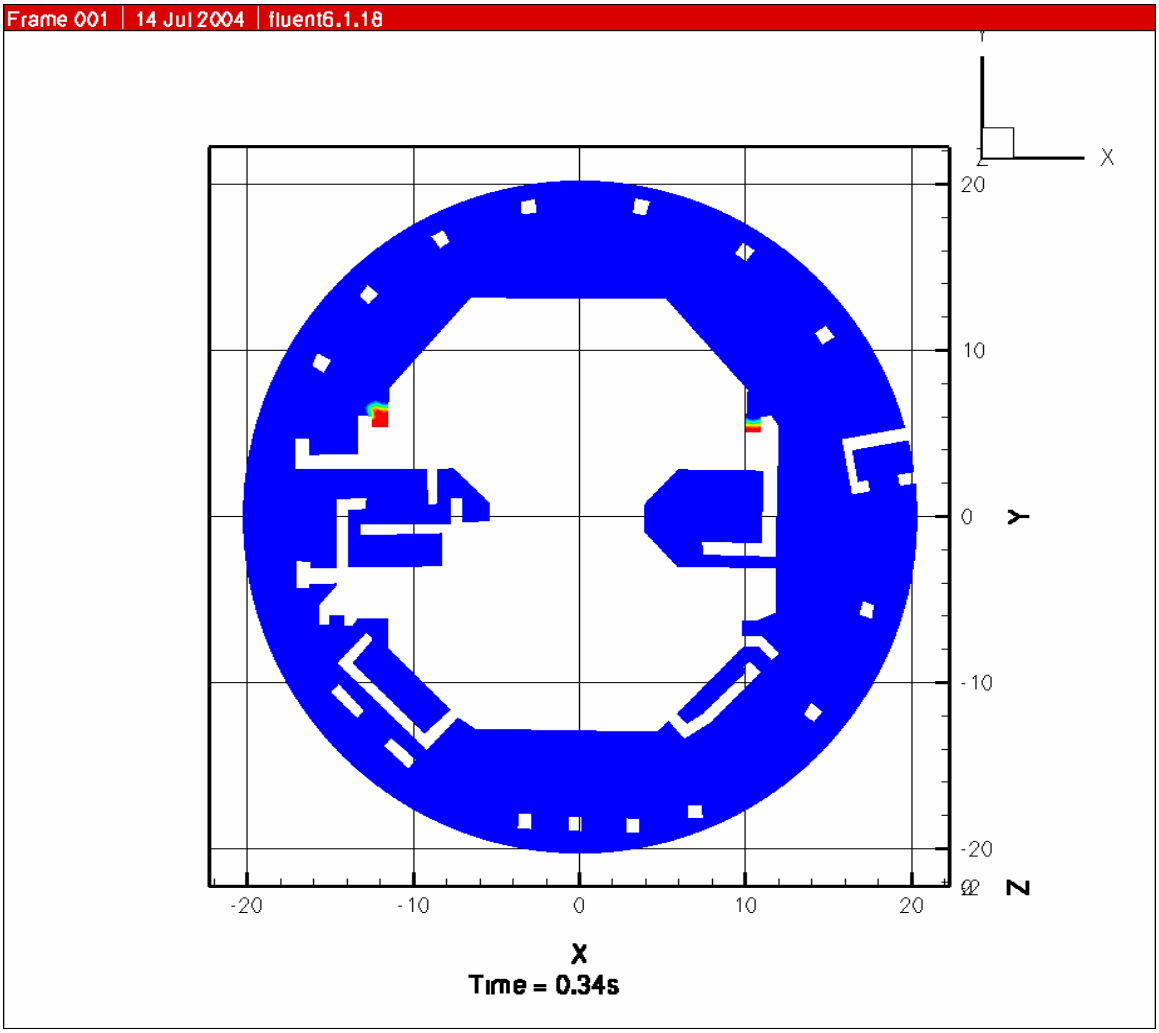

Figure III-4. Transient Volume of Fluid during the Simulation of Containment Pool Fillup

Figure III-4 shows the computational cell volume fraction of Water at a height of 0.01 m above the containment floor. The red color represents 100-percent water (0-percent air), while blue represents 0-percent water (100-percent air). The bottom of the figure shows the time of the snapshot in seconds after the breakflow is initiated.

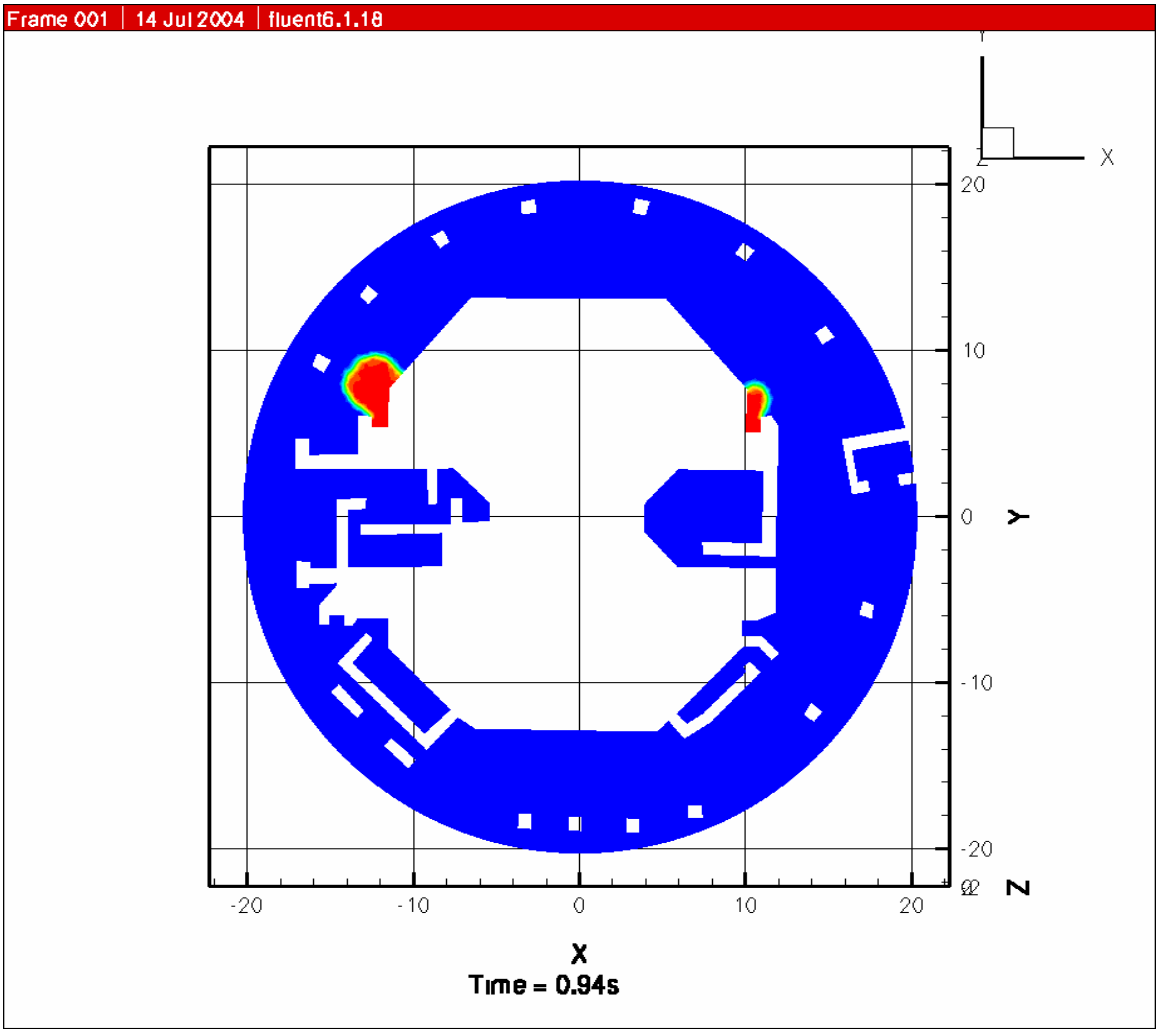

Figure III-5. Same as Figure III-4 for t = 0.94 Seconds

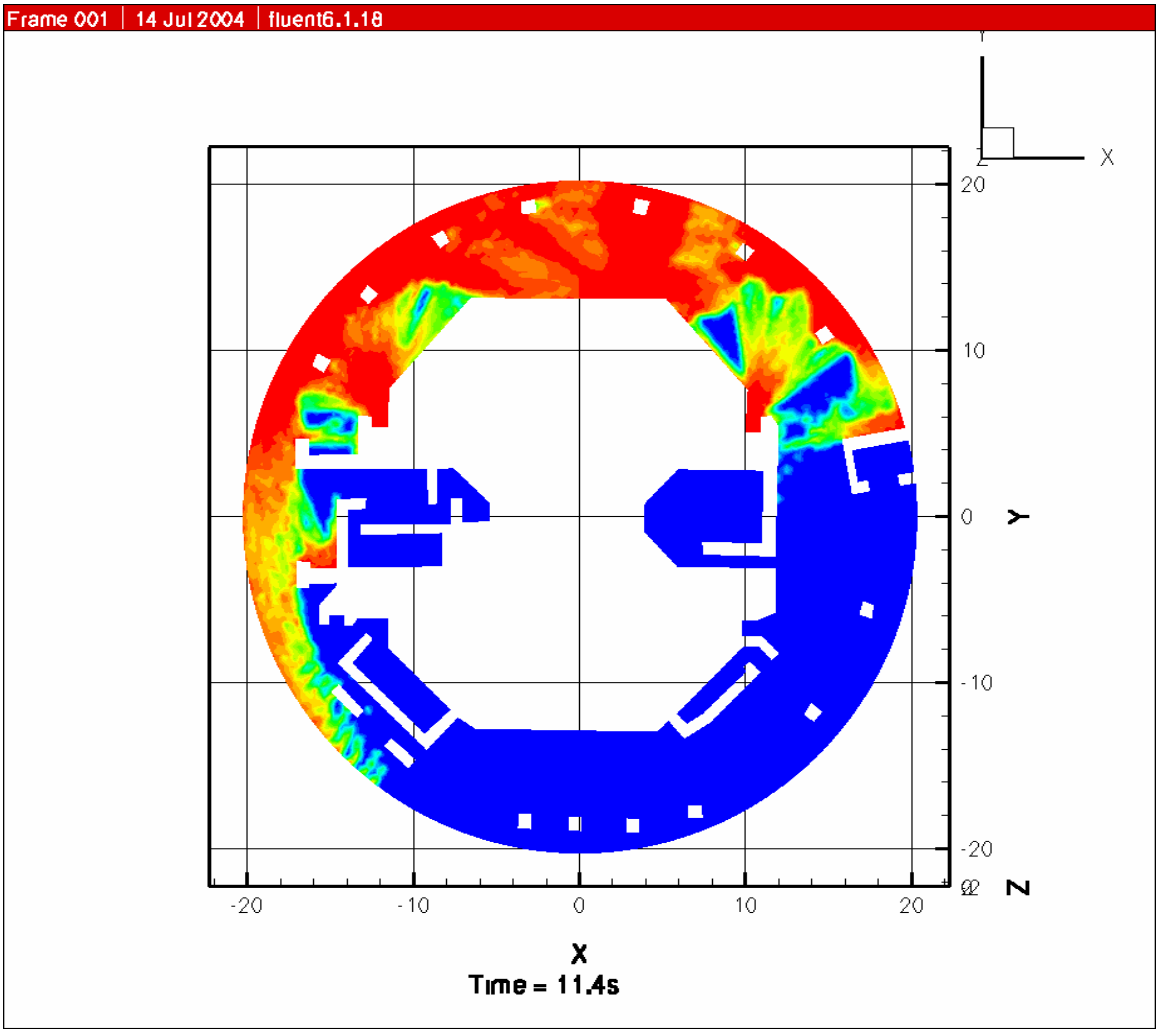

Figure III-6. Same as Figure III-4 for t = 11.4 Seconds

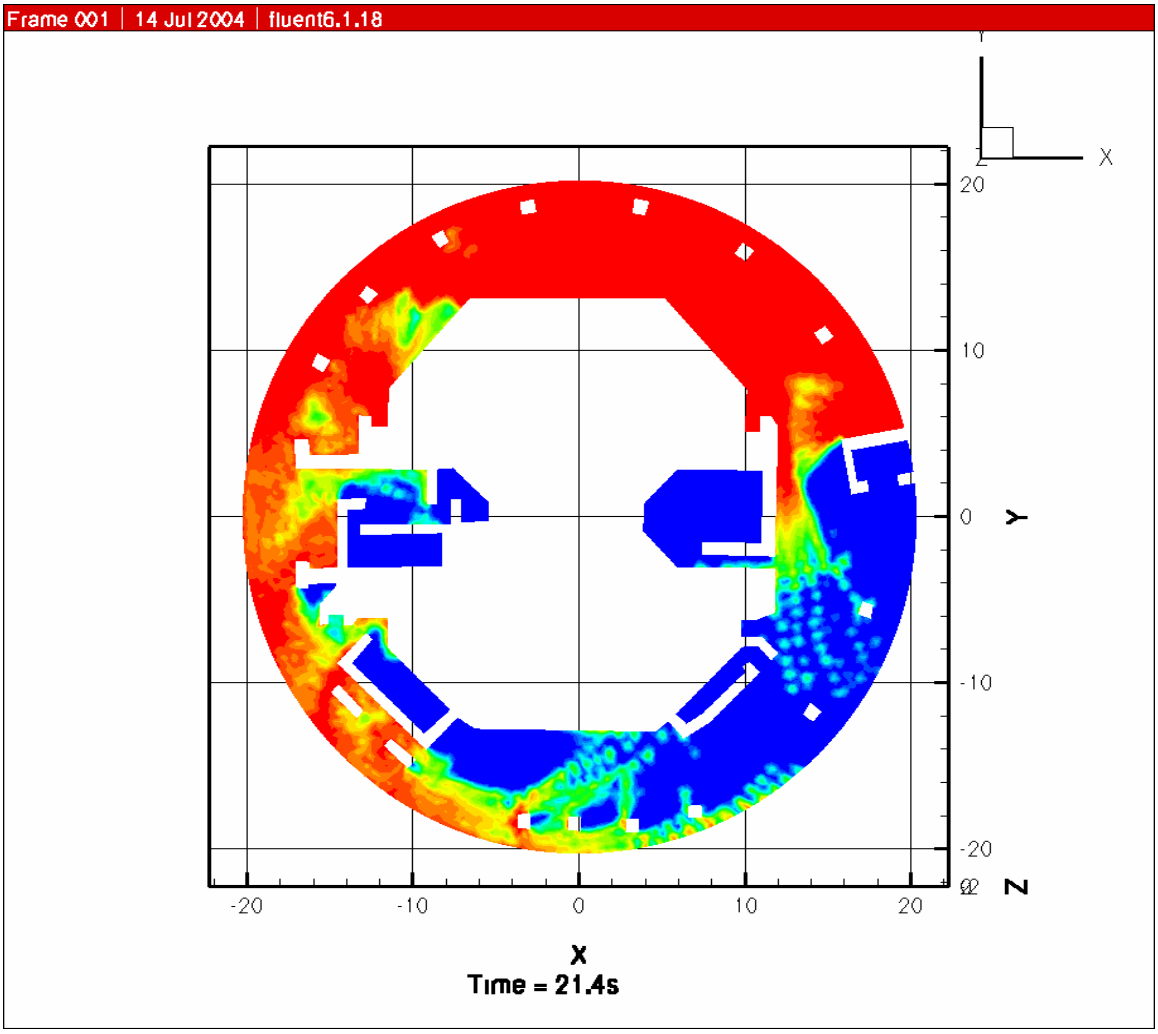

Figure III-7. Same as Figure III-4 for t = 21.4 Seconds

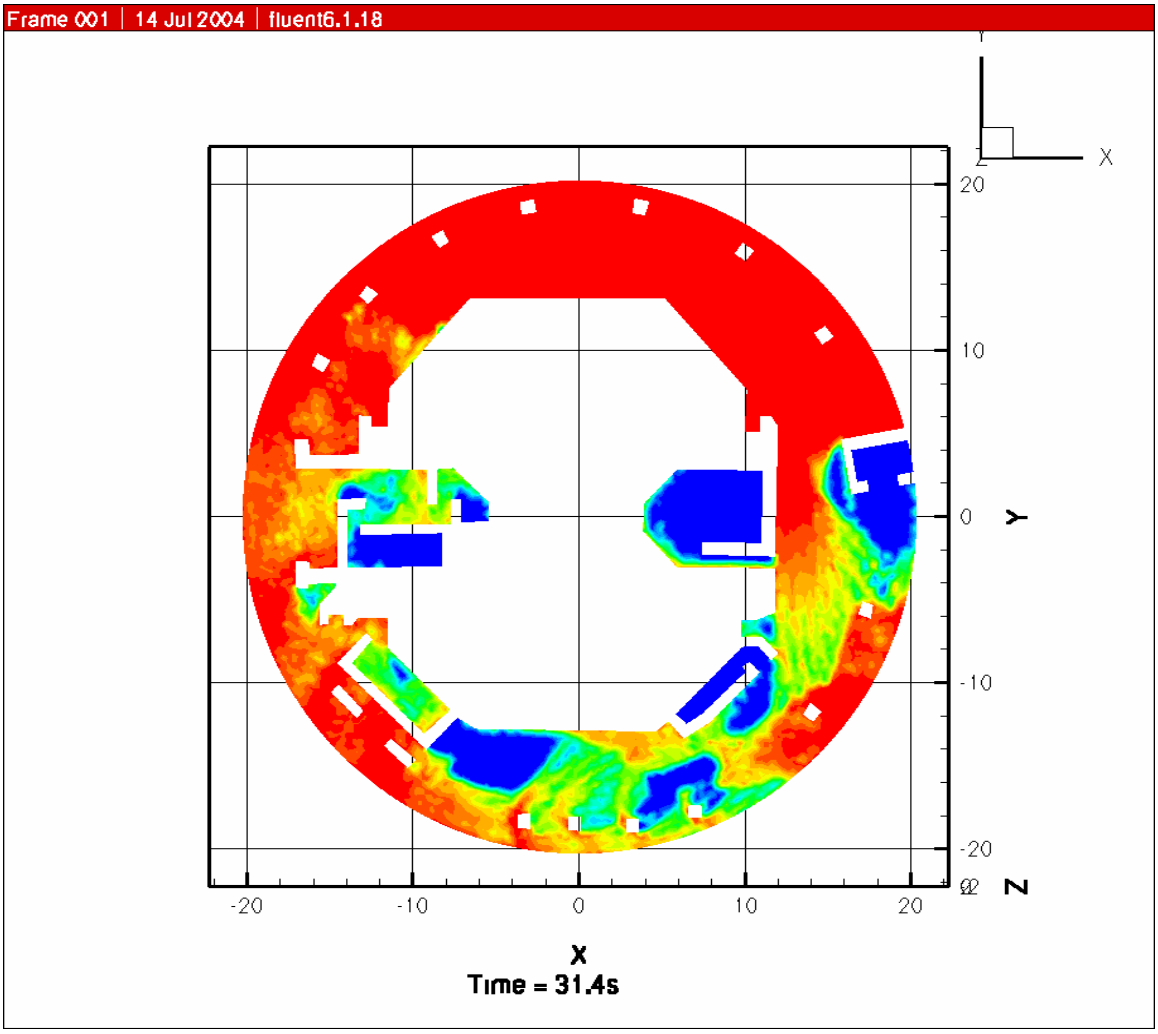

Figure III-8. Same as Figure III-4 for t = 31.4 Seconds

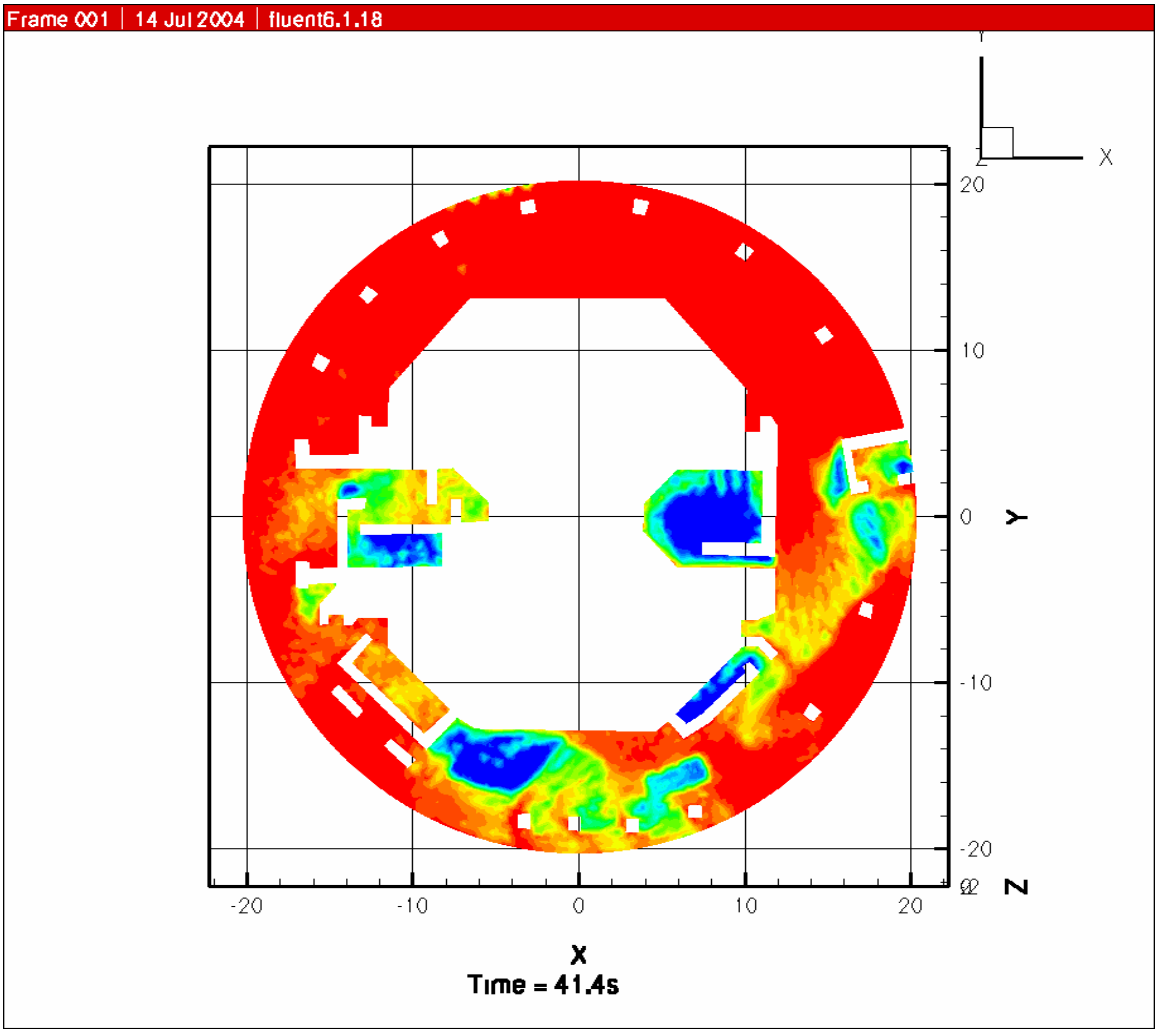

Figure III-9. Same as Figure III-4 for t = 41.4 Seconds

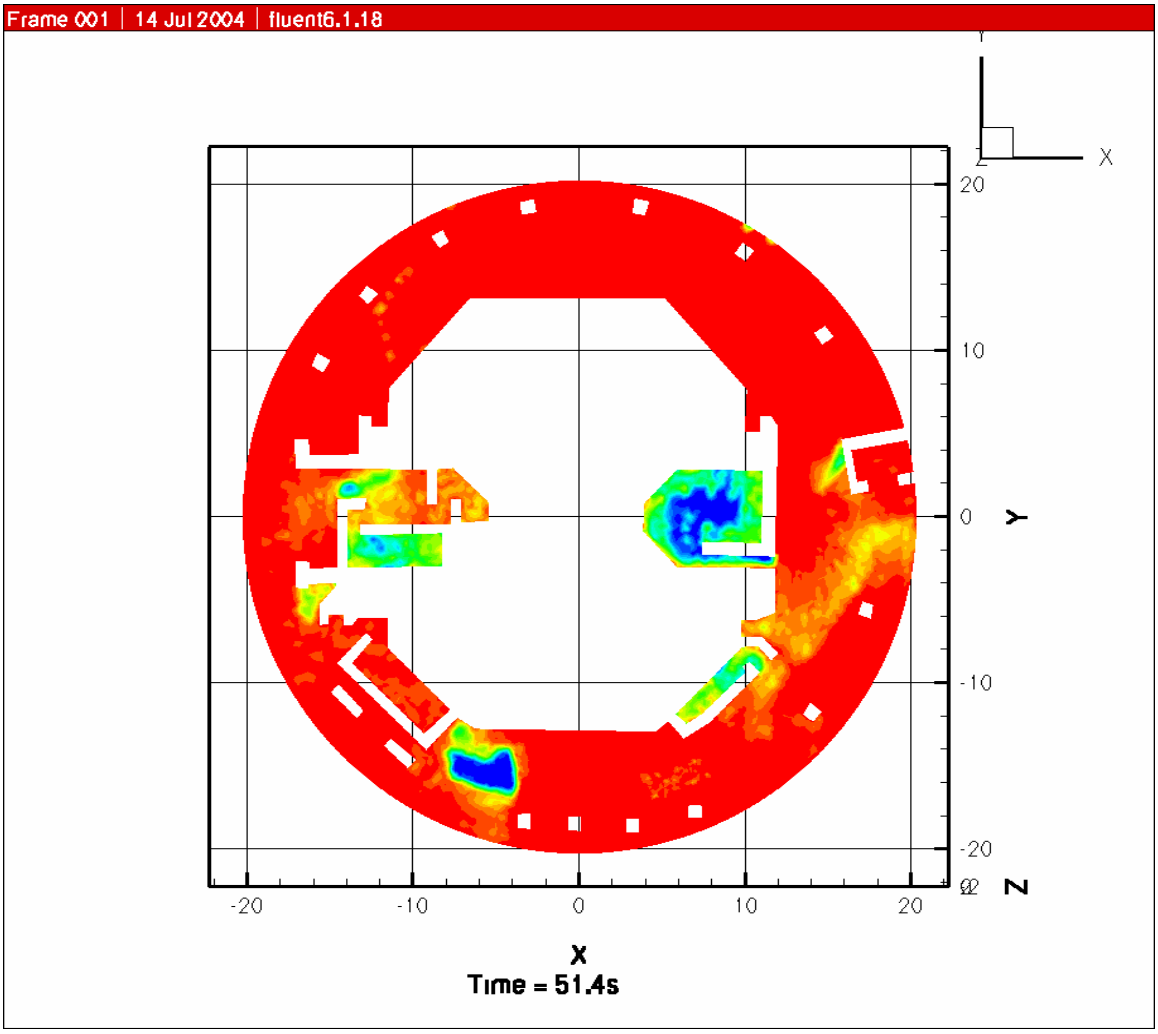

Figure III-10. Same as Figure III-4 for t = 51.4 Seconds

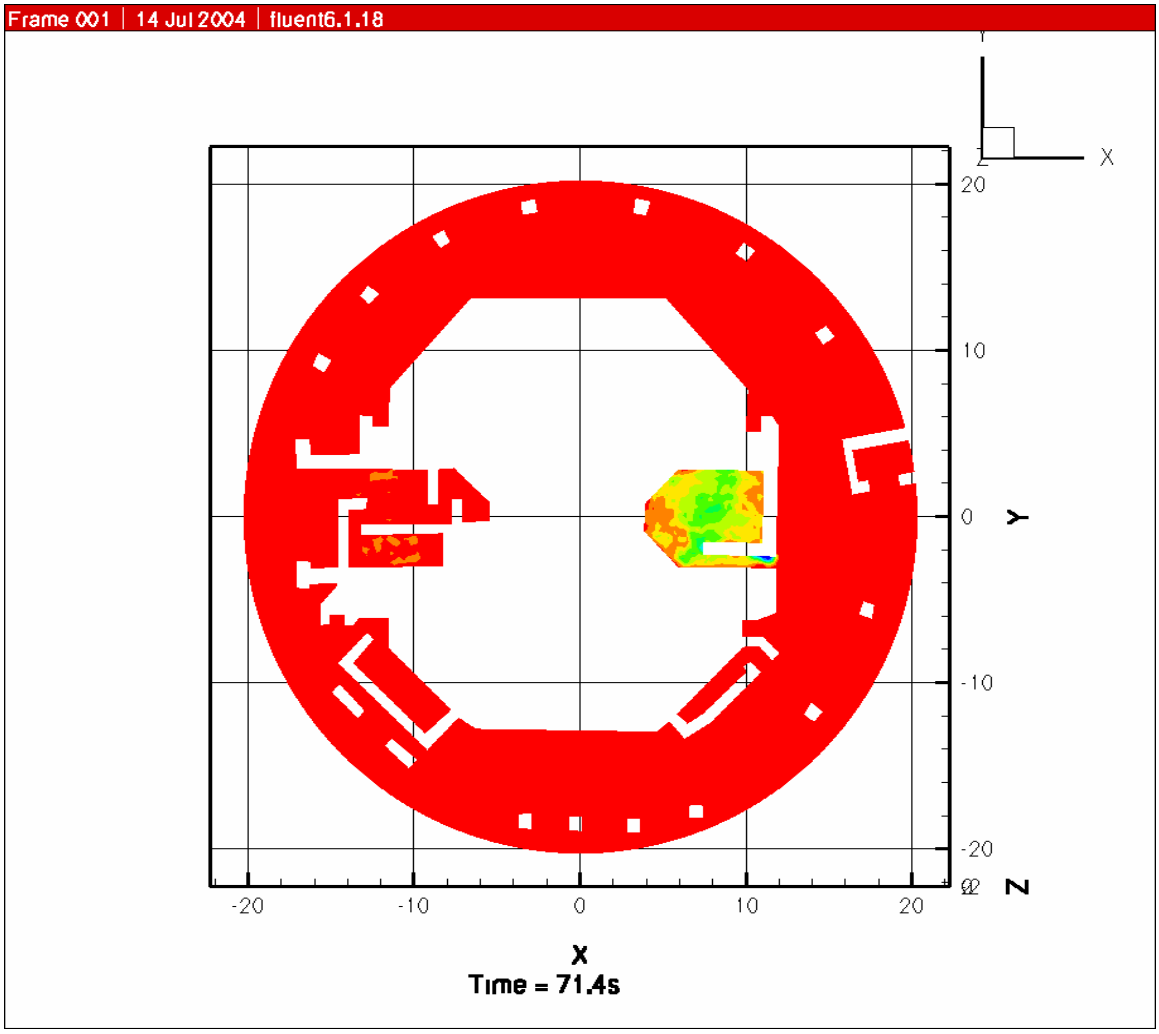

Figure III-11. Same as Figure III-4 for t = 71.4 Seconds

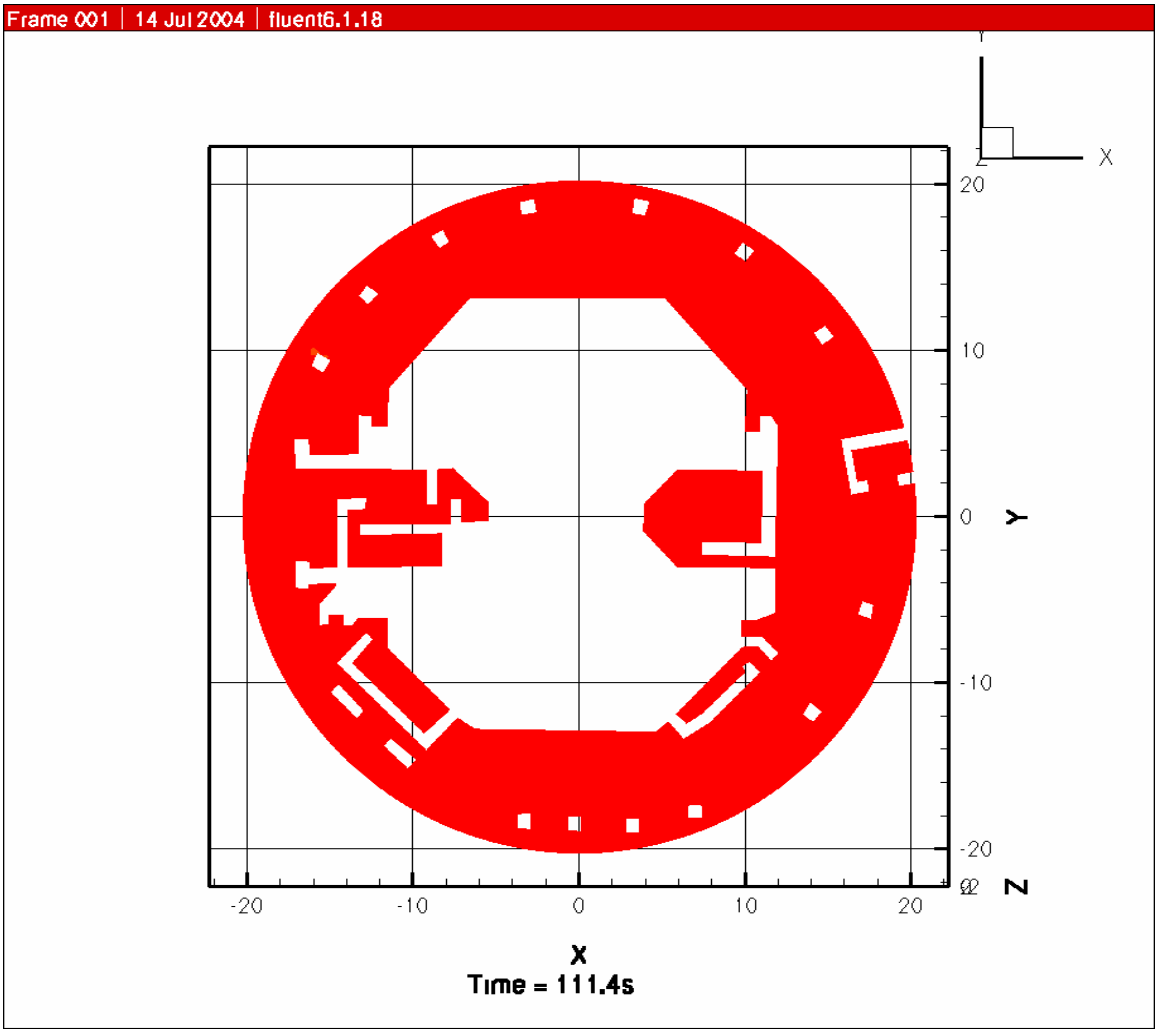

Figure III-12. Same as Figure III-4 for t = 111.4 Seconds

In Figure III-12, the solid red color indicates that the cells adjacent to the floor are full of water, not that the entire pool is full of water.

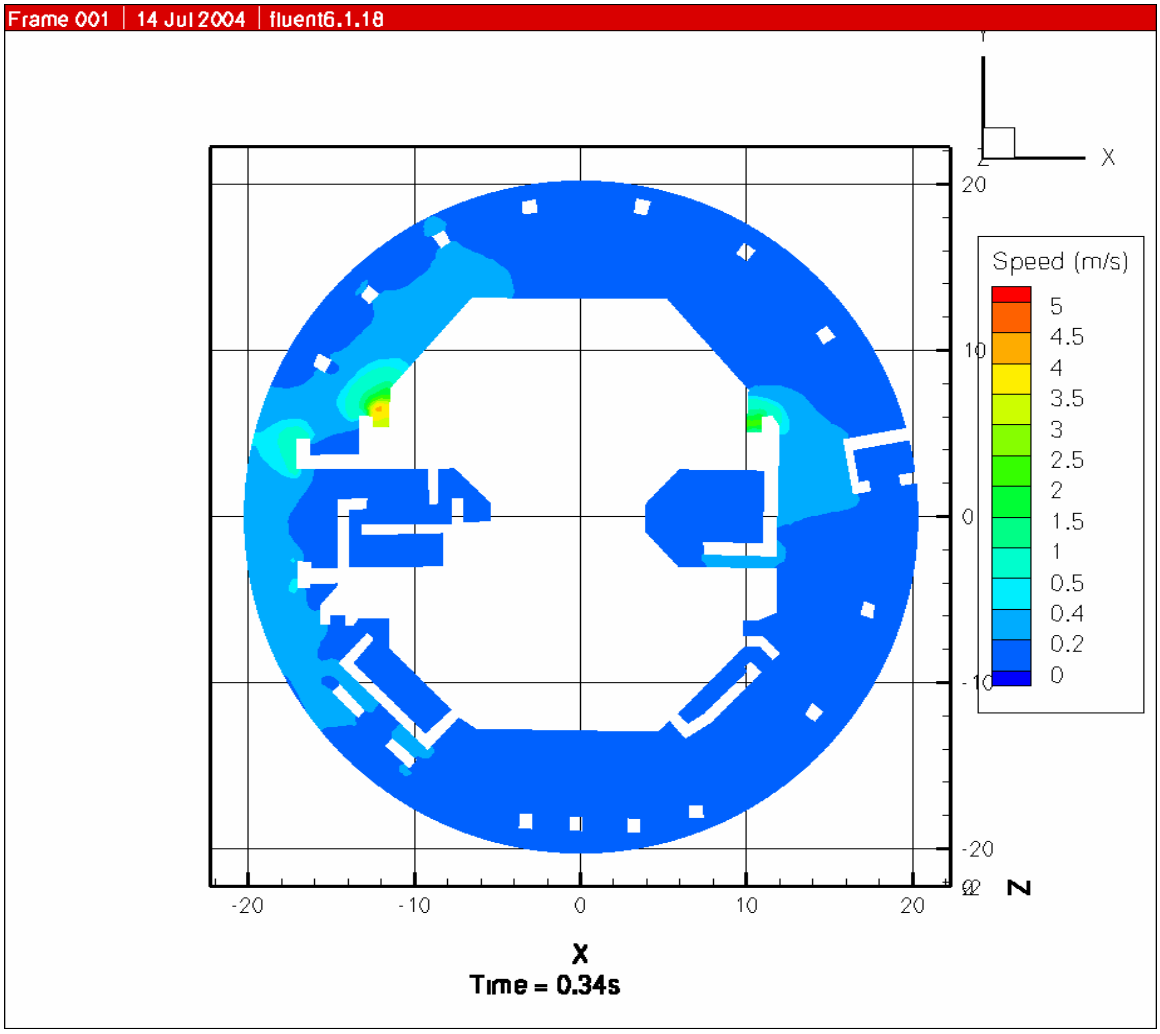

Figure III-13. Transient VOF Simulation of Containment Pool Fillup

Figure III-13 shows the contours of fluid velocity. The time snapshot shown in the figure is seconds after the breakflow is initiated. Note that the fluid velocity may be water or air; Figure III-4 to Figure III-12, showing the volume fraction of water, should be used to determine the actual water velocity.

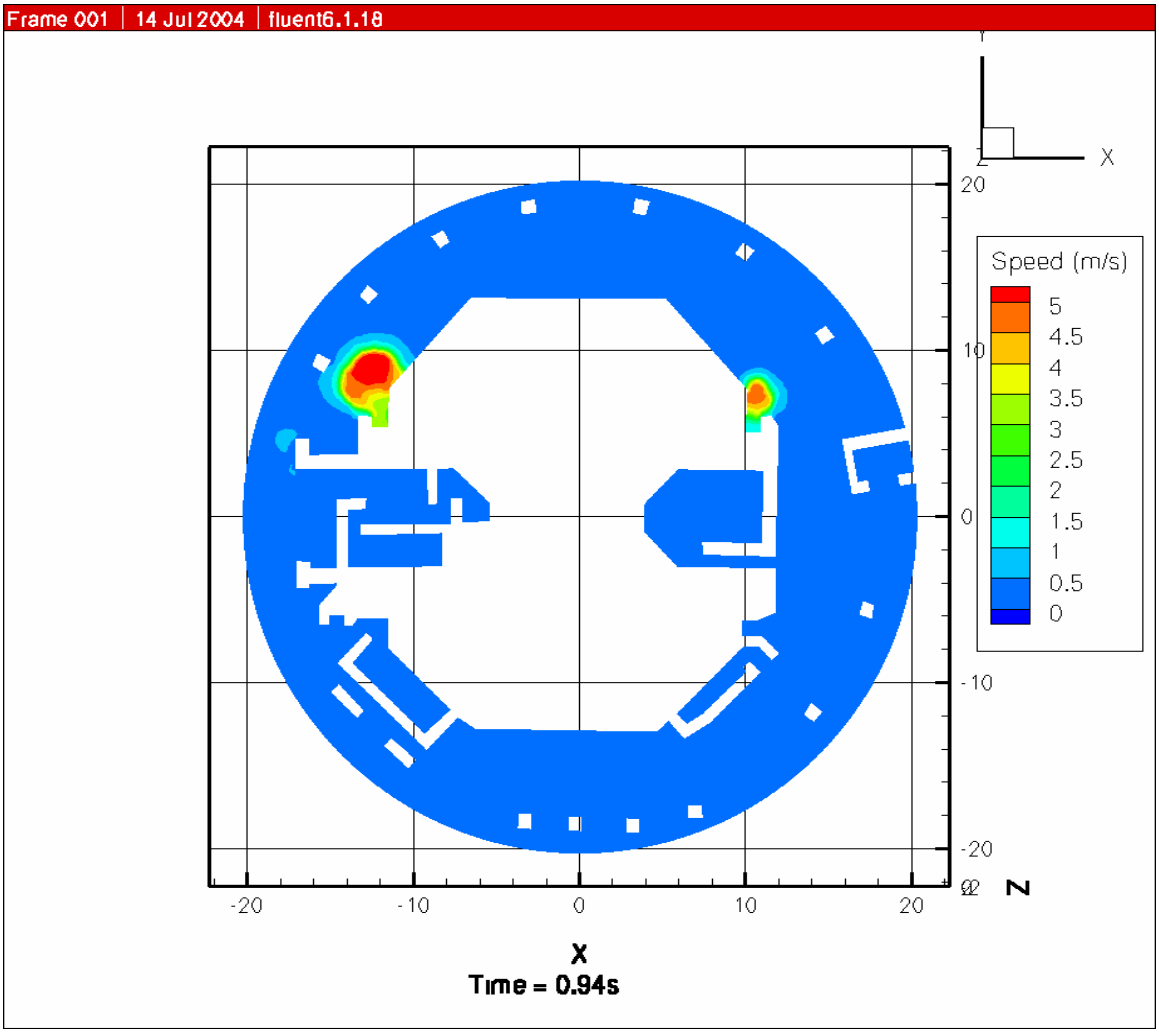

Figure III-14. Same as Figure III-13 for t = 0.94 Seconds

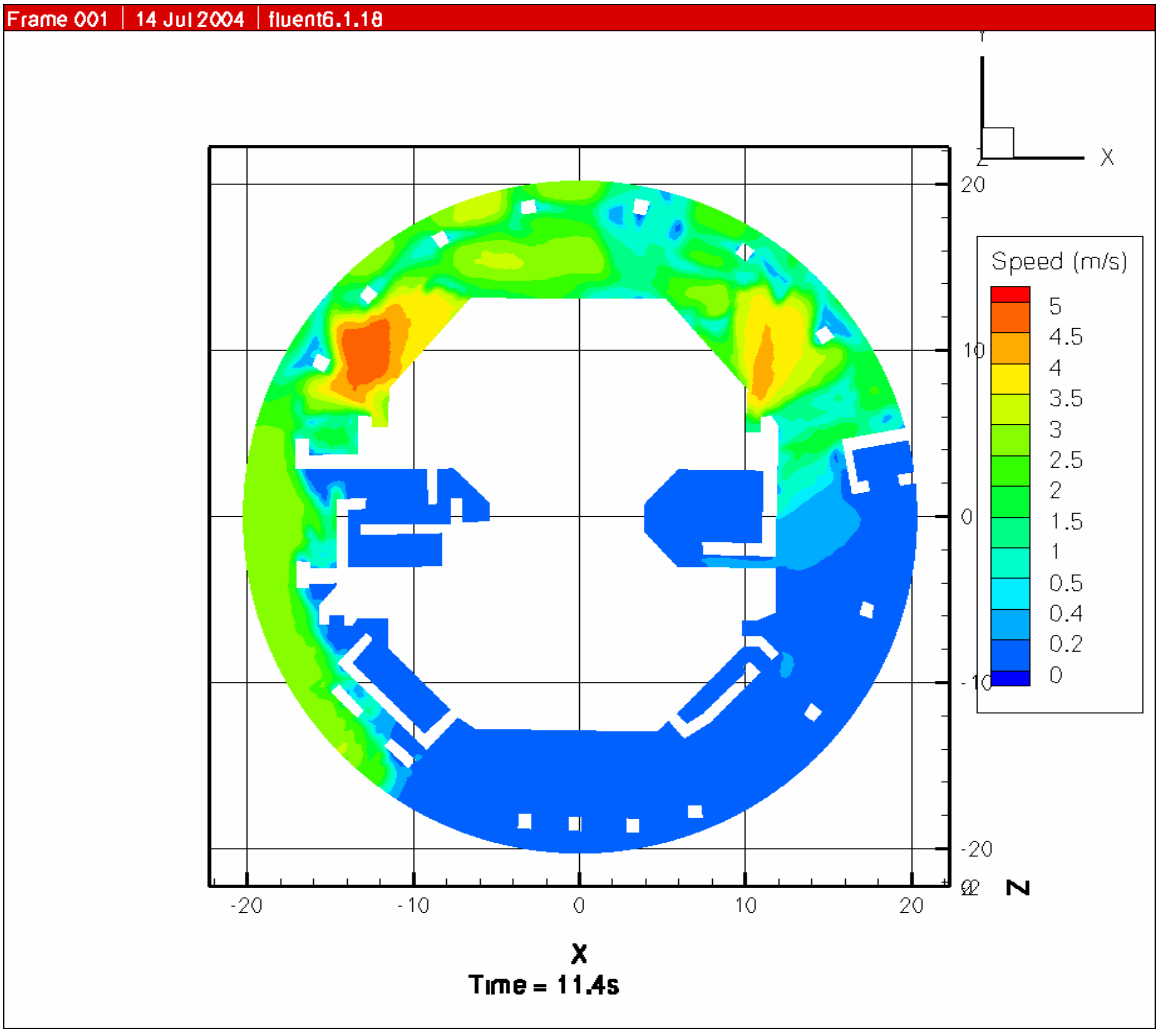

Figure III-15. Same as Figure III-13 for t = 11.4 Seconds

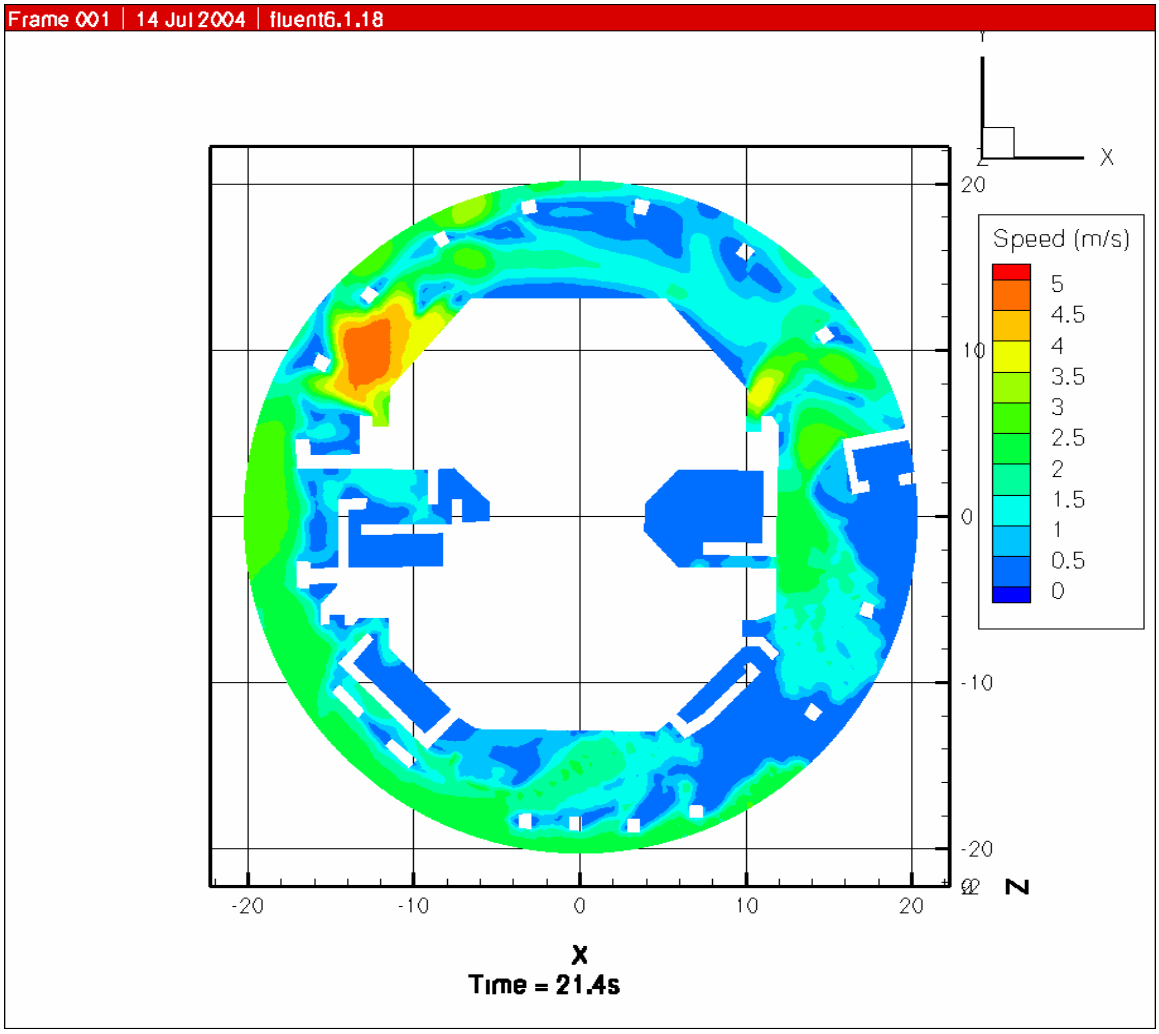

Figure III-16. Same as Figure III-13 for t = 21.4 Seconds

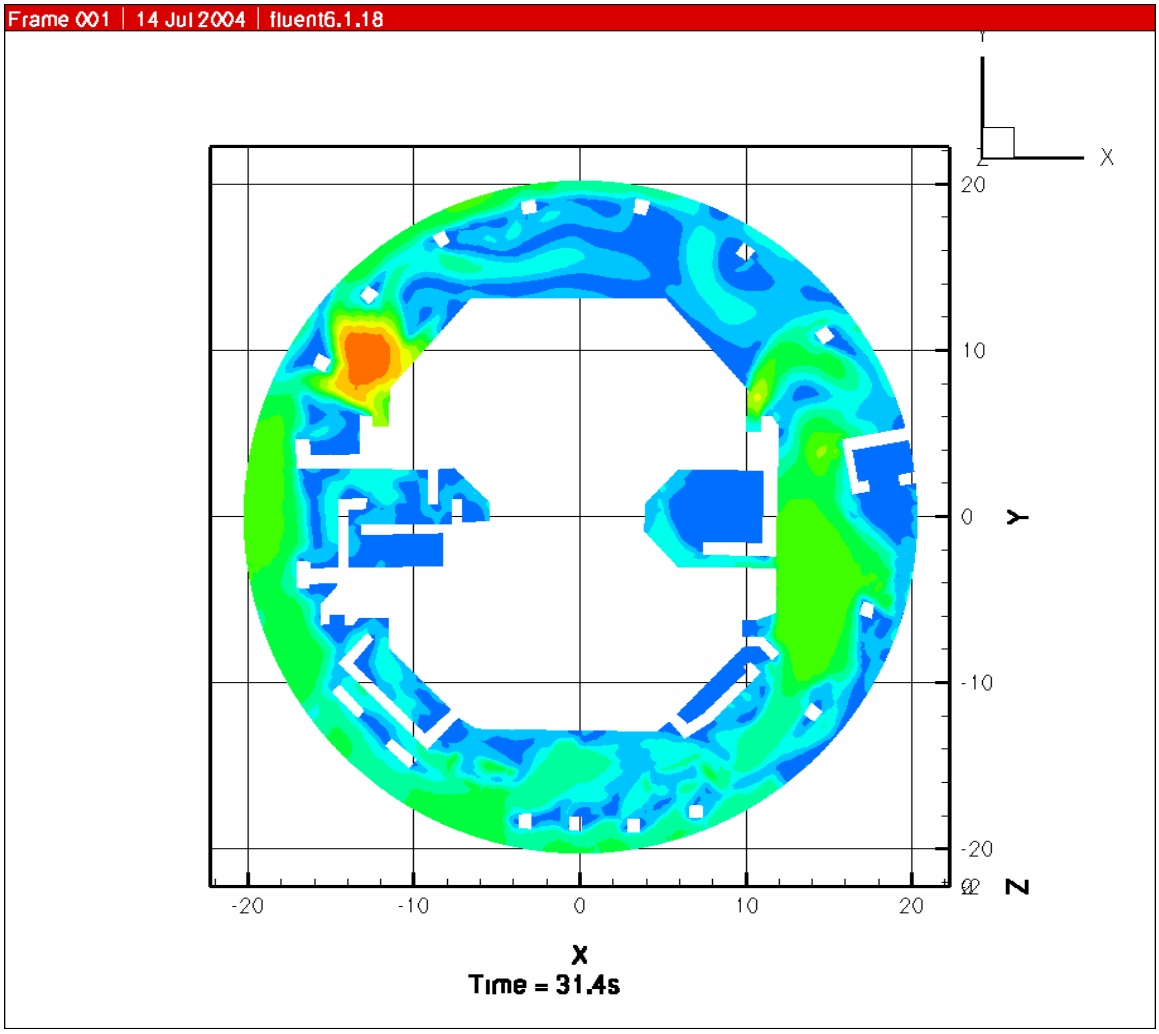

Figure III-17. Same as Figure III-13 for t = 31.4 Seconds

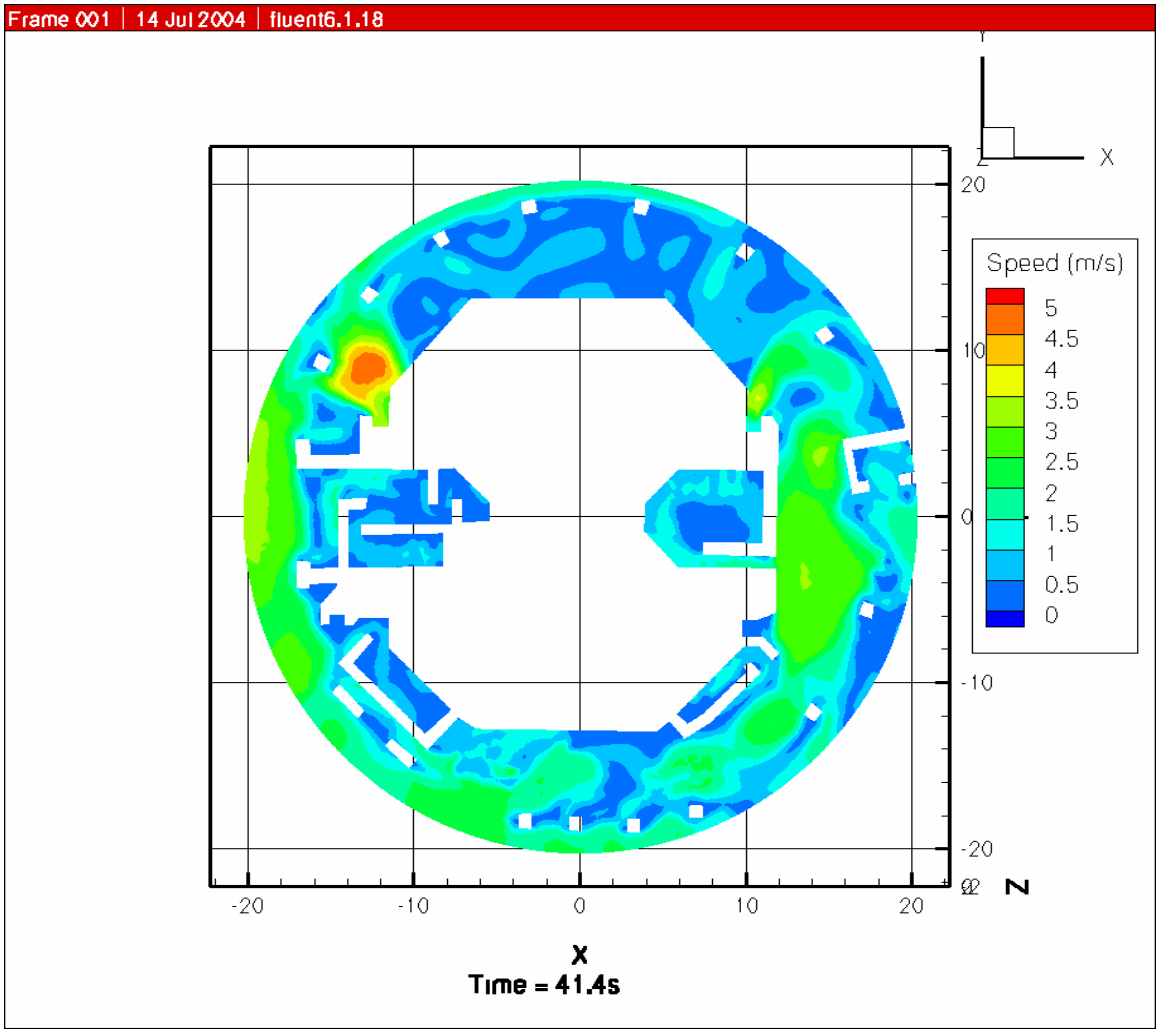

Figure III-18. Same as Figure III-13 for t = 41.4 Seconds

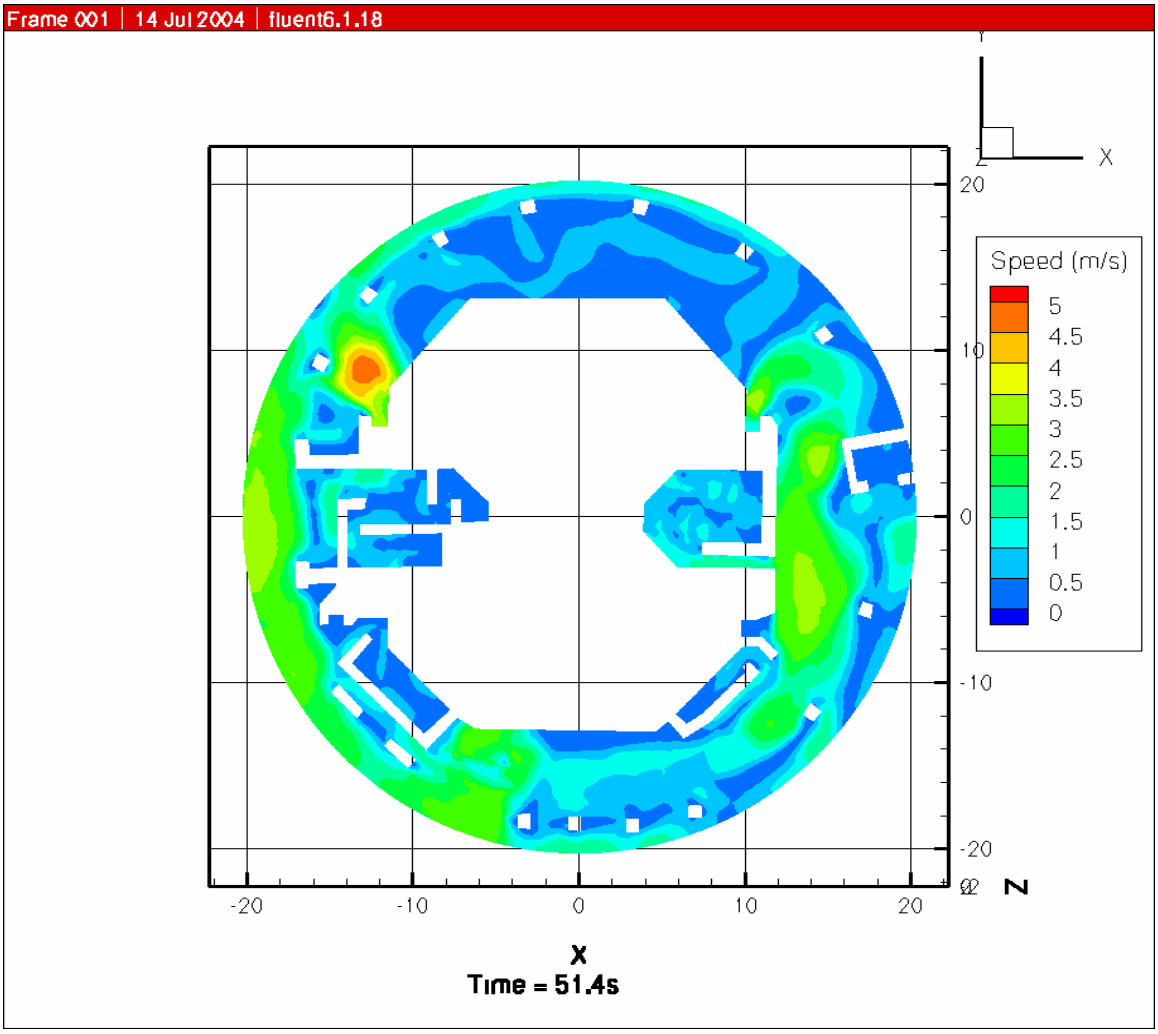

Figure III-19. Same as Figure III-13 for t = 51.4 Seconds

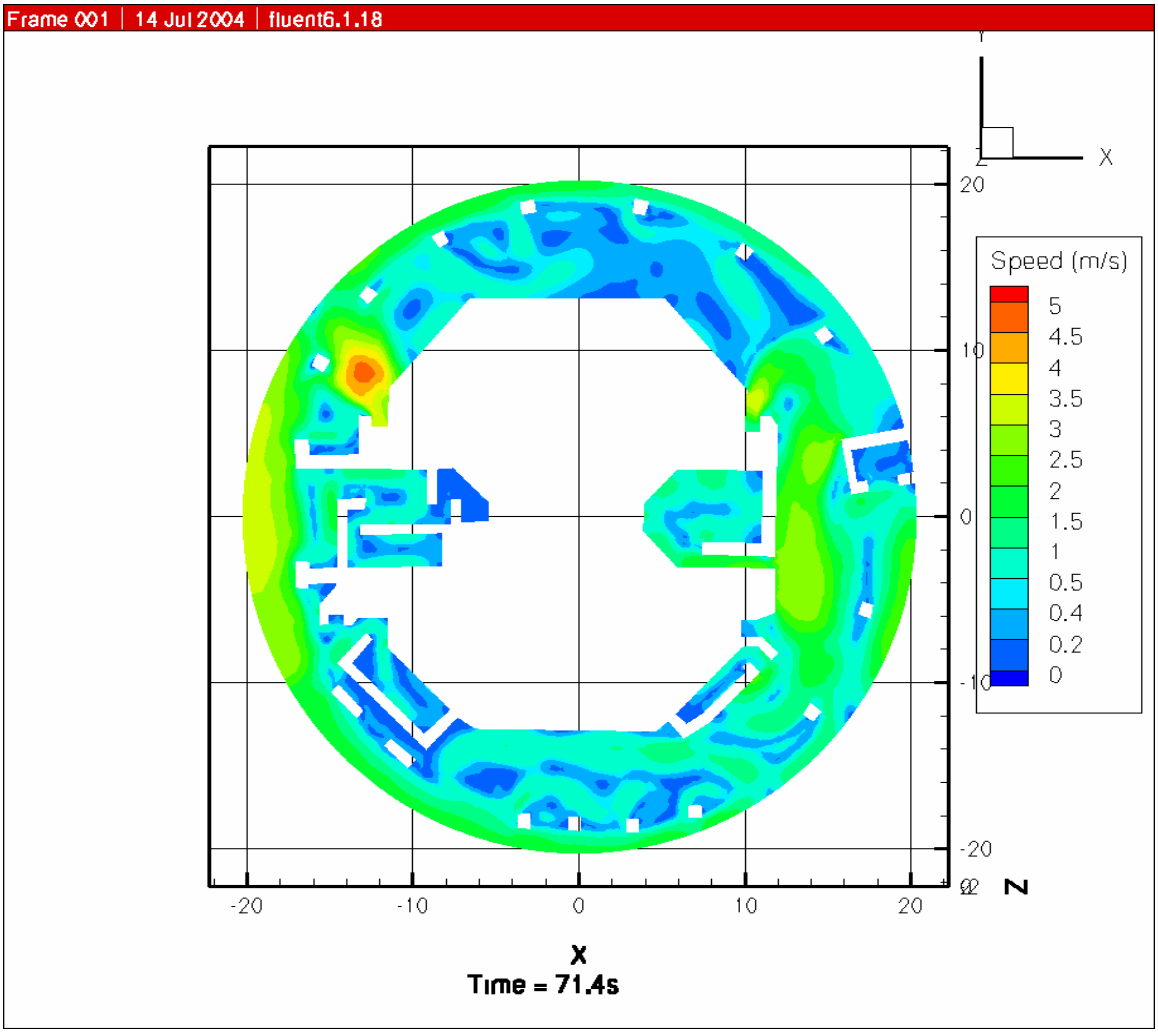

Figure III-20. Same as Figure III-13 for t = 71.4 Seconds

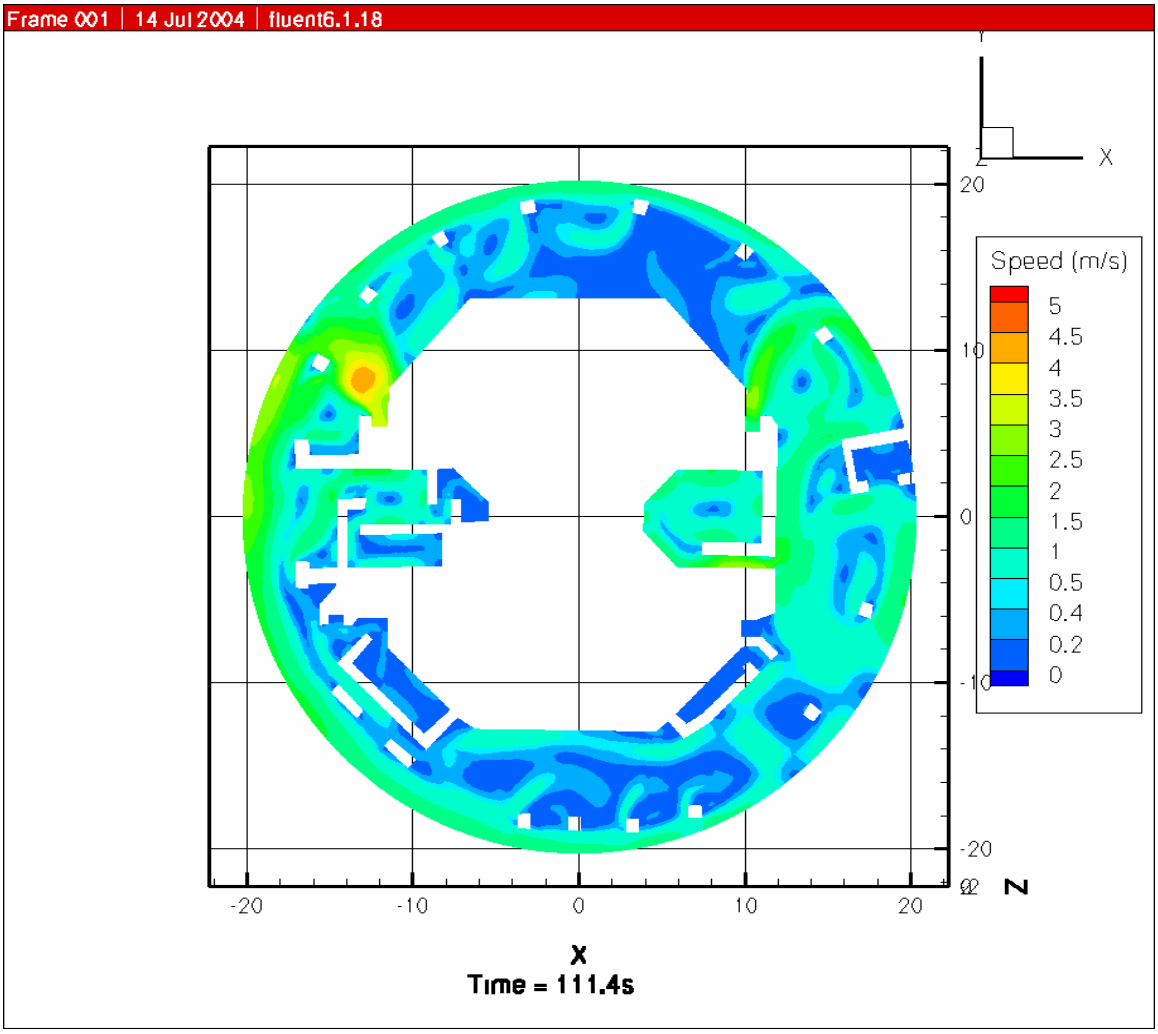

Figure III-21. Same as Figure III-13 for t = 111.4 Seconds

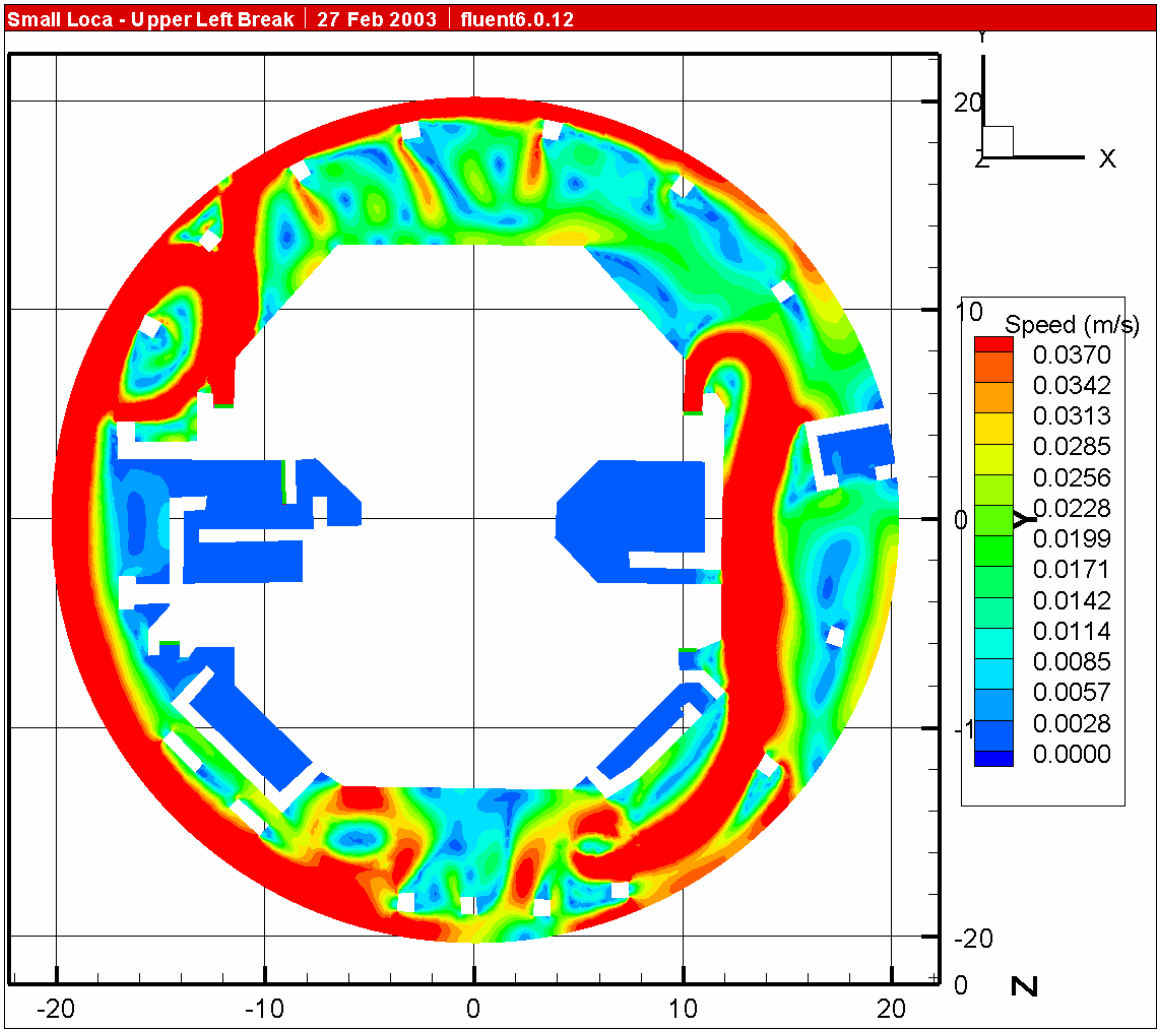

Figure III-22. Small LOCA Break Located in the Upper-Left Quadrant

In Figure III-22, speeds greater than or equal to the fiber threshold (0.037 m/s) are colored red.

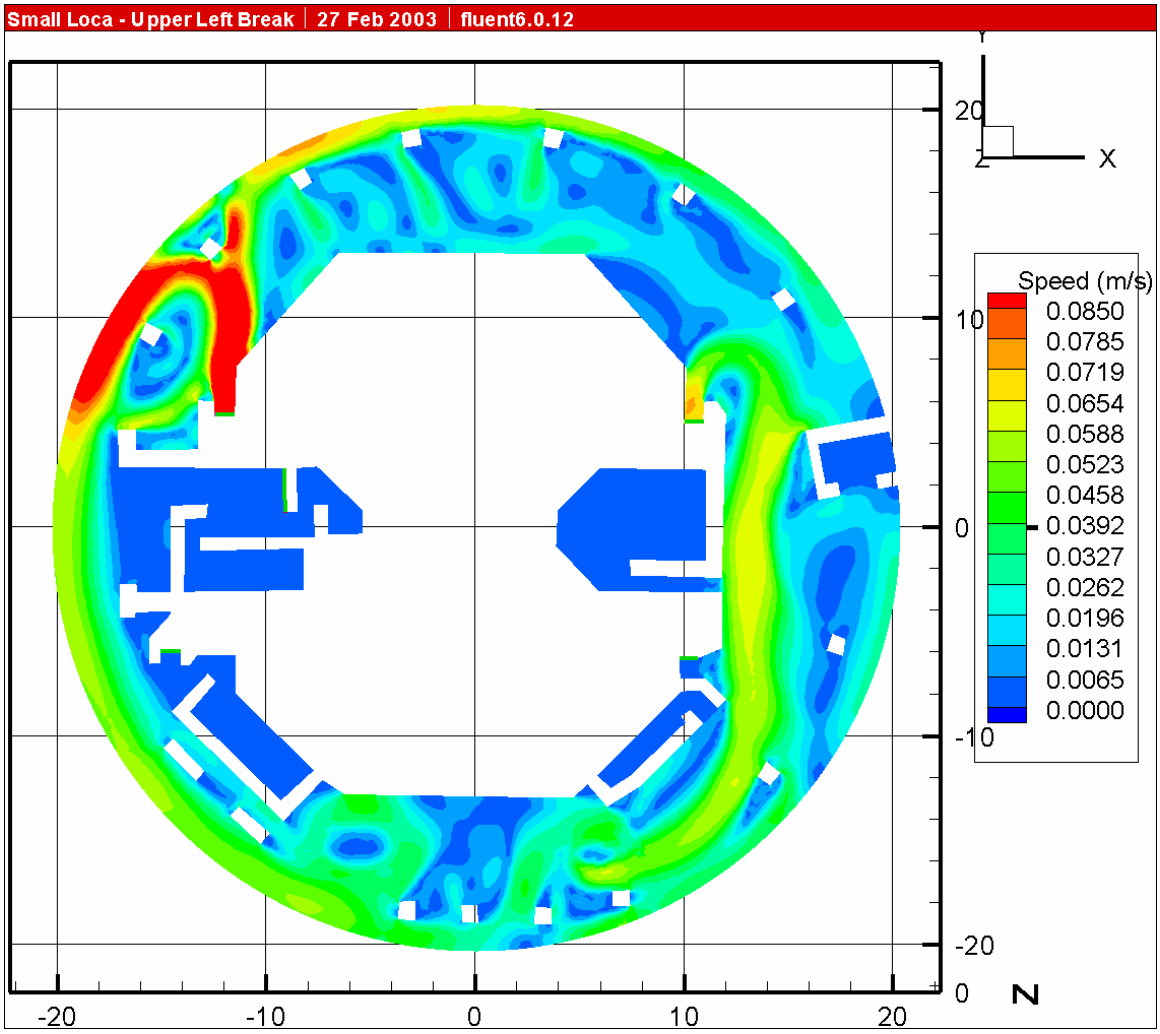

Figure III-23. Small LOCA Break Located in the Upper-Left Quadrant

In Figure III-23, speeds greater than or equal to the RMI threshold (0.085 m/s) are colored red.

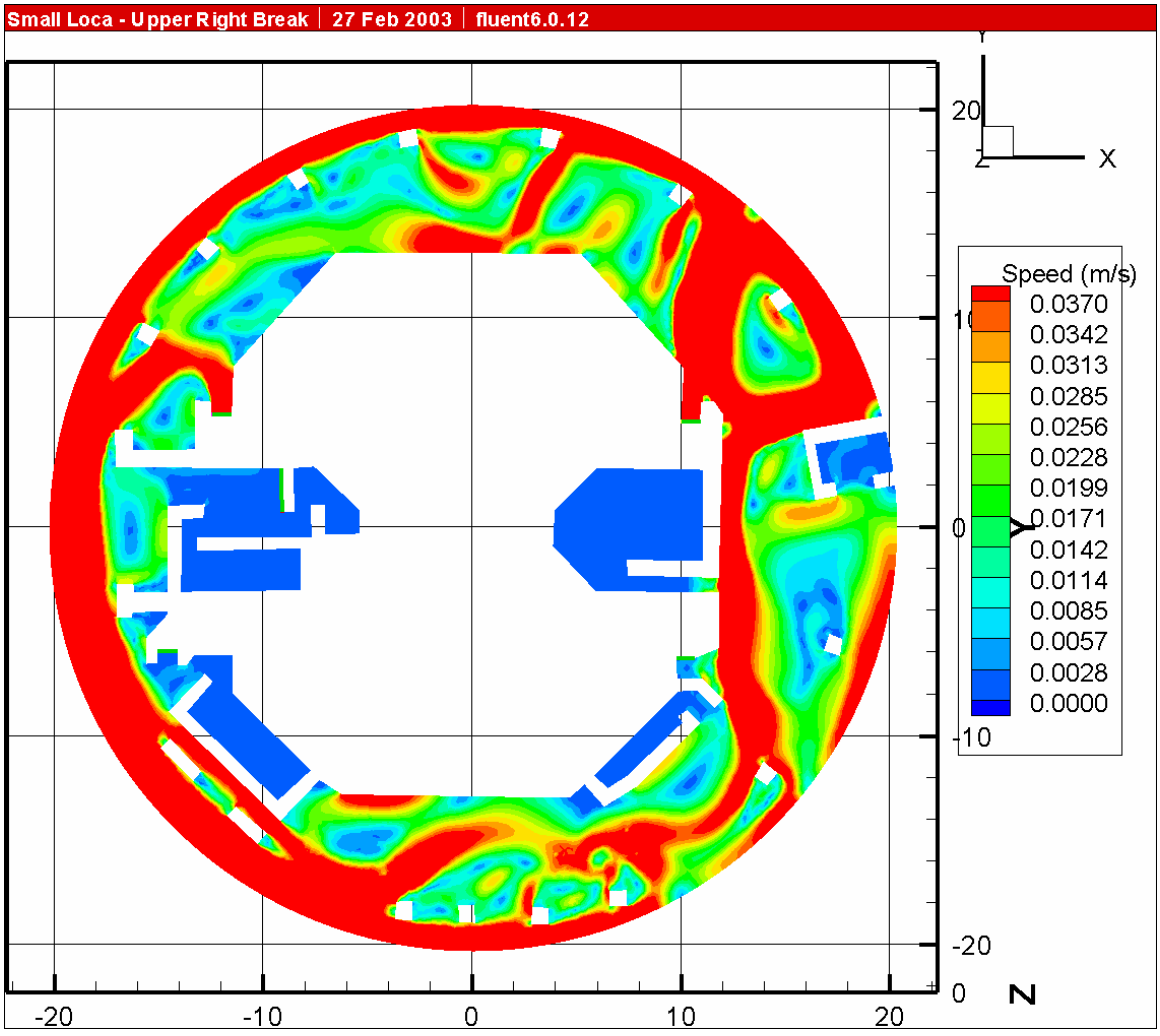

Figure III-24. Small LOCA Break Located in the Upper-Right Quadrant

In Figure III-24, speeds greater than or equal to the fiber threshold (0.037 m/s) are colored red.

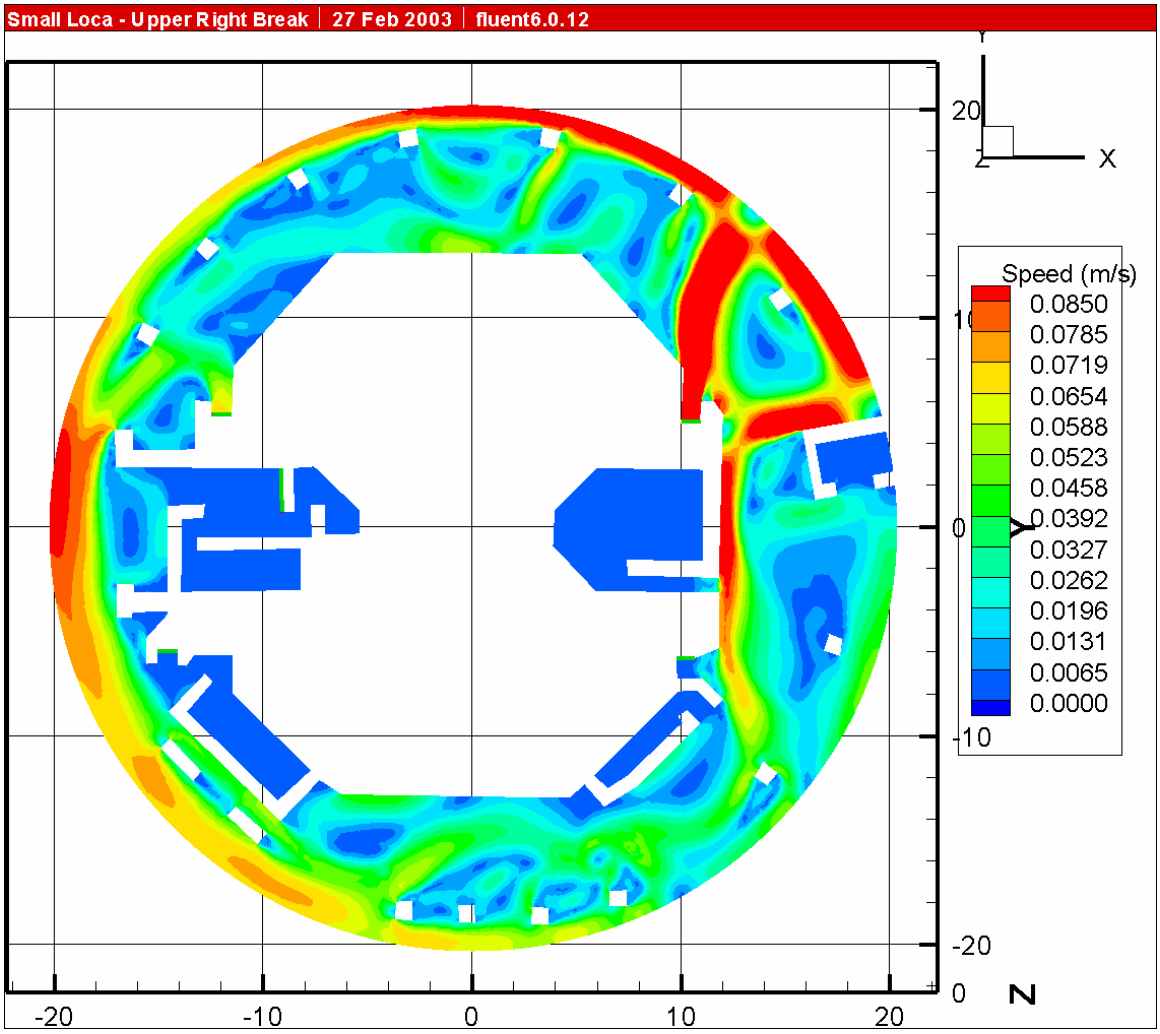

Figure III-25. Small LOCA Break Located in the Upper-Right Quadrant

In Figure III-25, speeds greater than or equal to the RMI threshold (0.085 m/s) are colored red.

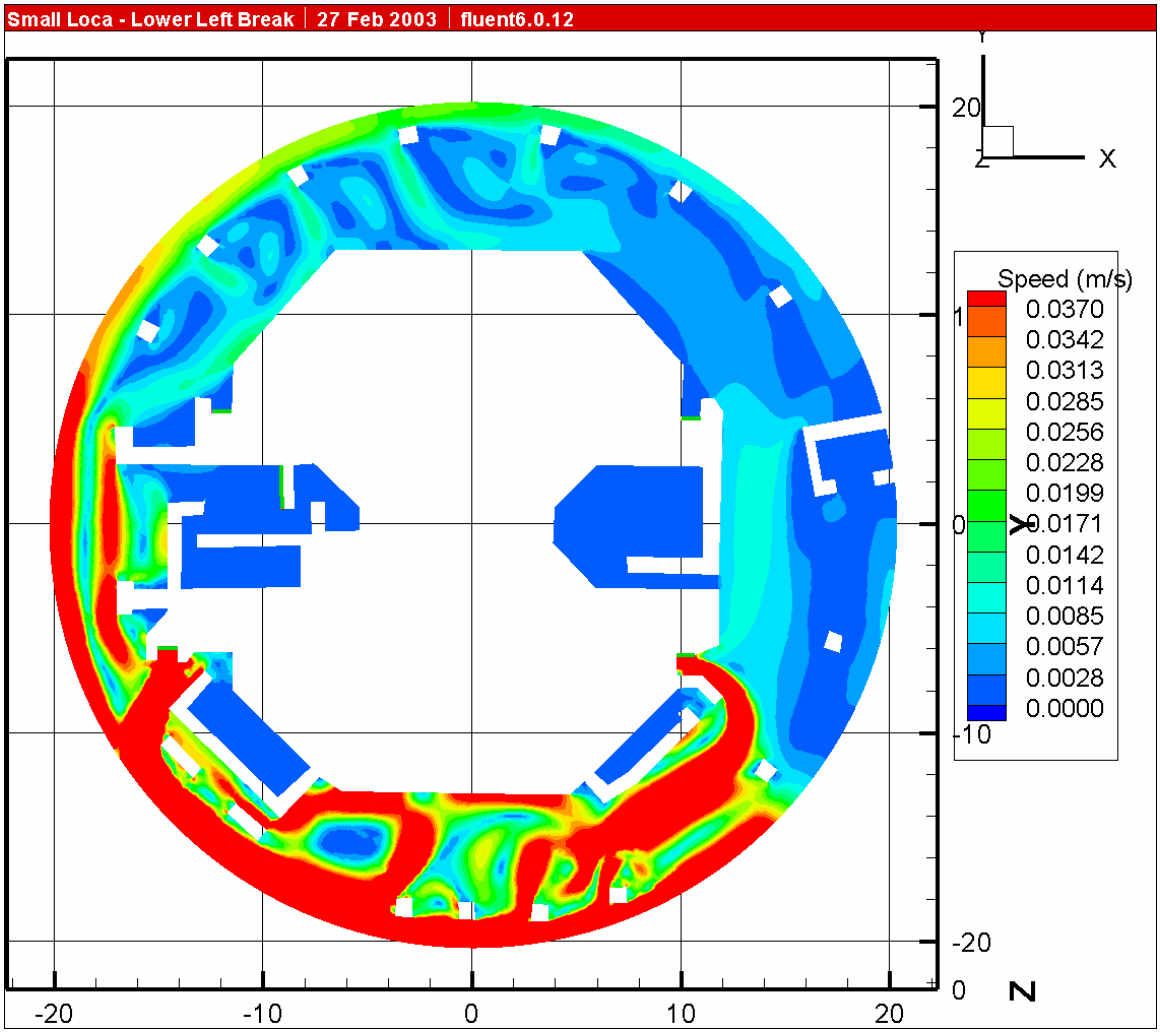

Figure III-26. Small LOCA Break Located in the Lower-Left Quadrant

In Figure III-26, speeds greater than or equal to the fiber threshold (0.037 m/s) are colored red.

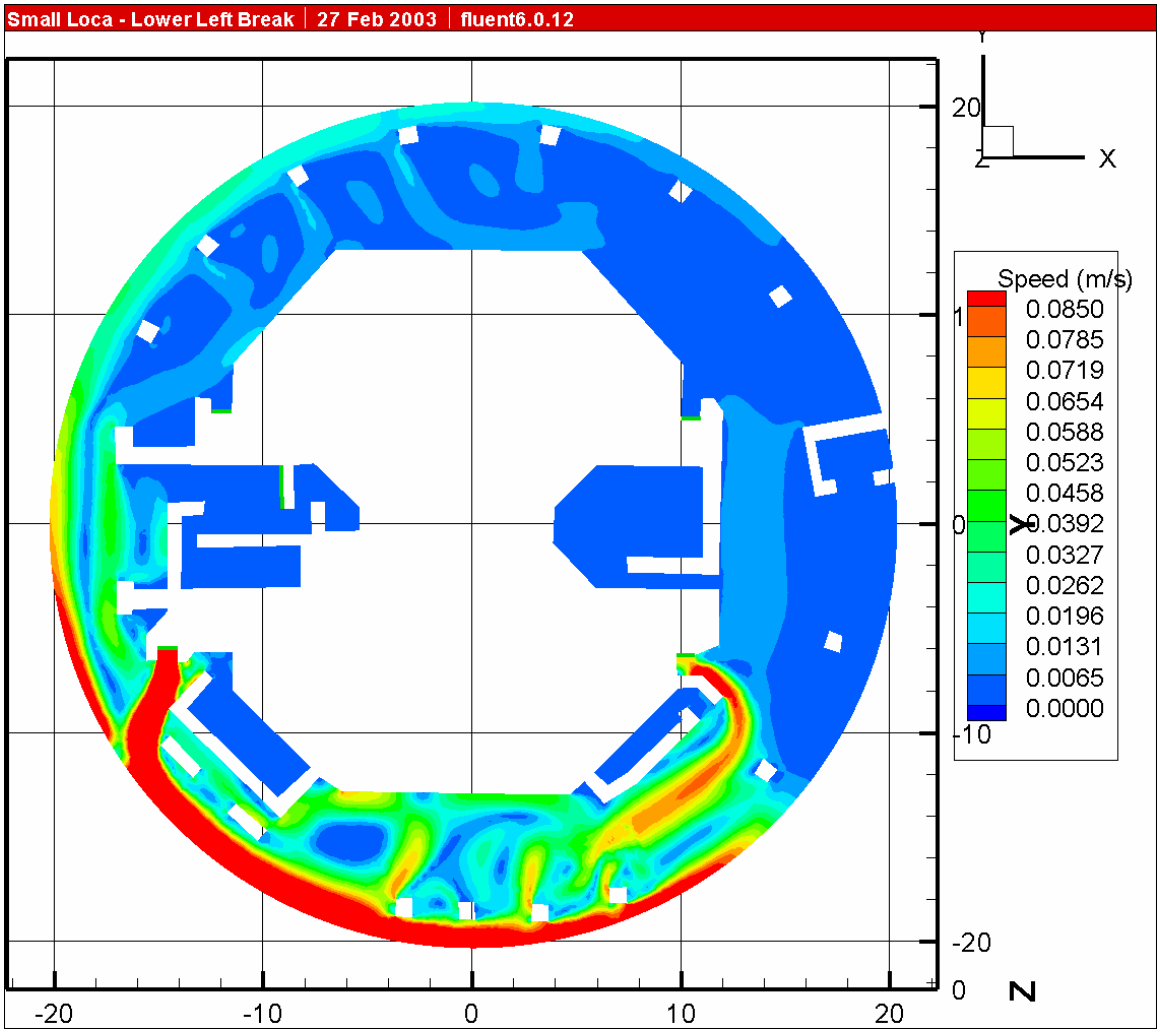

Figure III-27. Small LOCA Break Located in the Lower-Left Quadrant

In Figure III-27, speeds greater than or equal to the RMI threshold (0.085 m/s) are colored red.

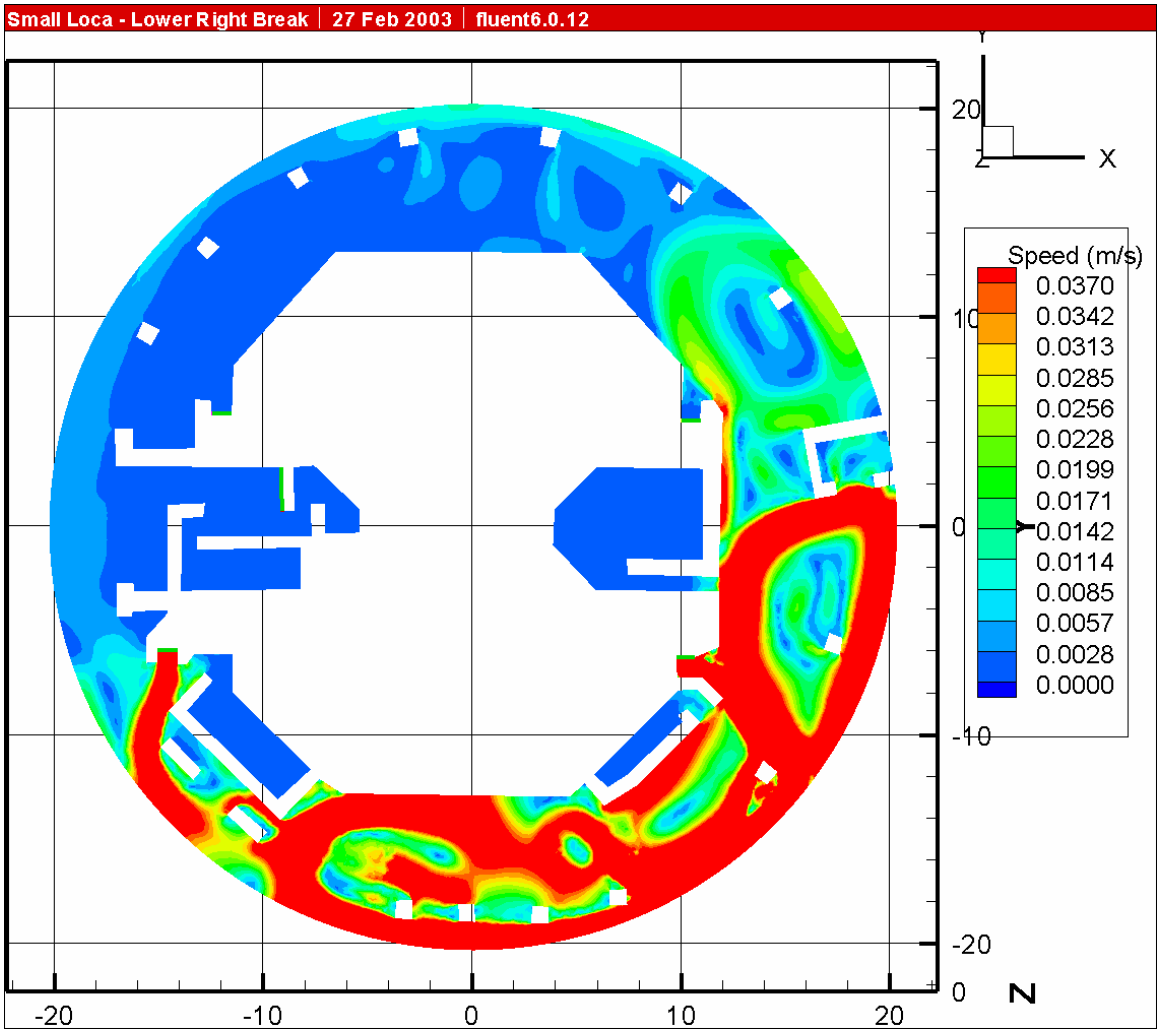

Figure III-28. Small LOCA Break Located in the Lower-Right Quadrant

In Figure III-28, speeds greater than or equal to the fiber threshold (0.037 m/s) are colored red.

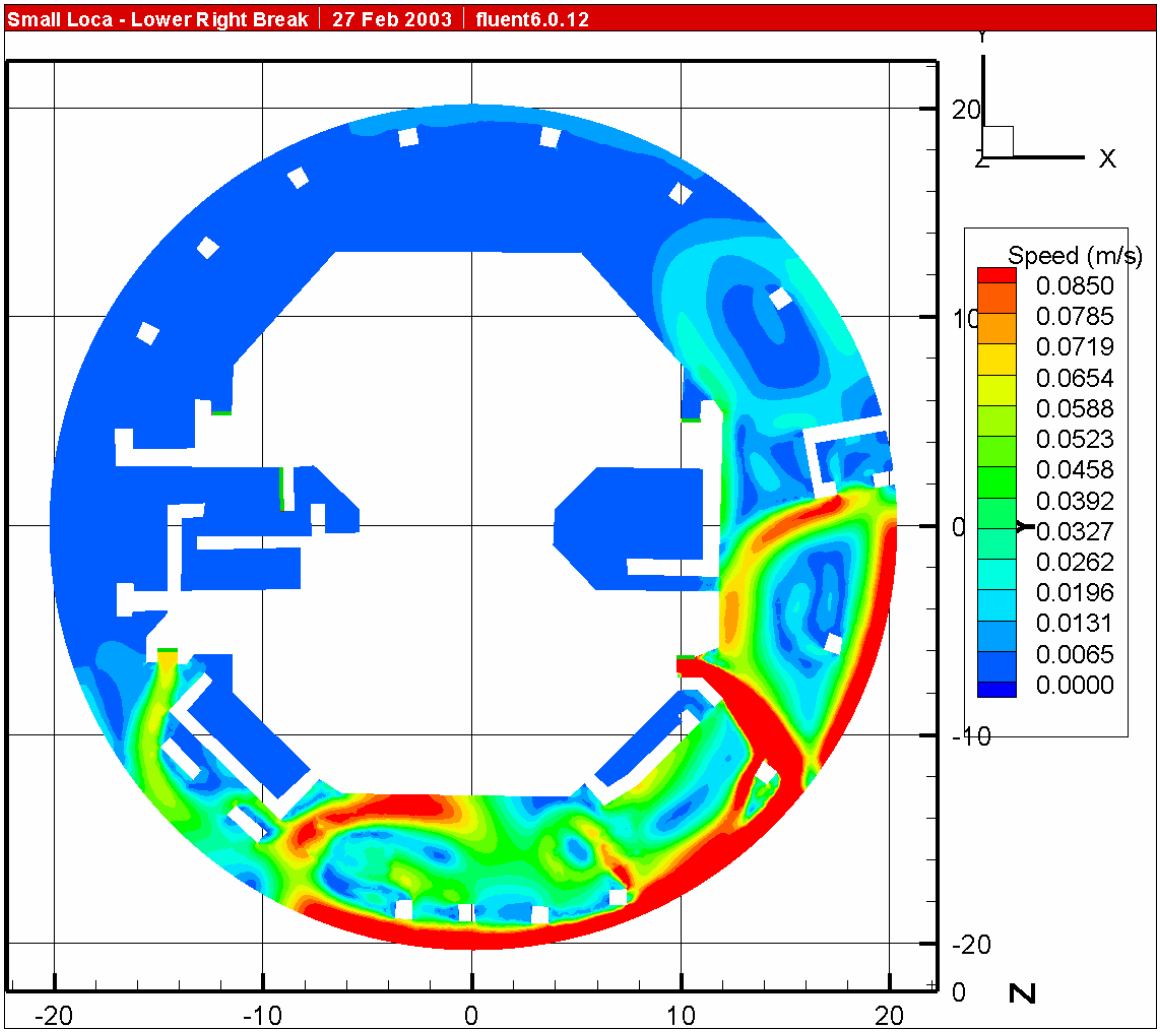

Figure III-29. Small LOCA Break Located in the Lower-Right Quadrant

In Figure III-29, speeds greater than or equal to the RMI threshold (0.085 m/s) are colored red.

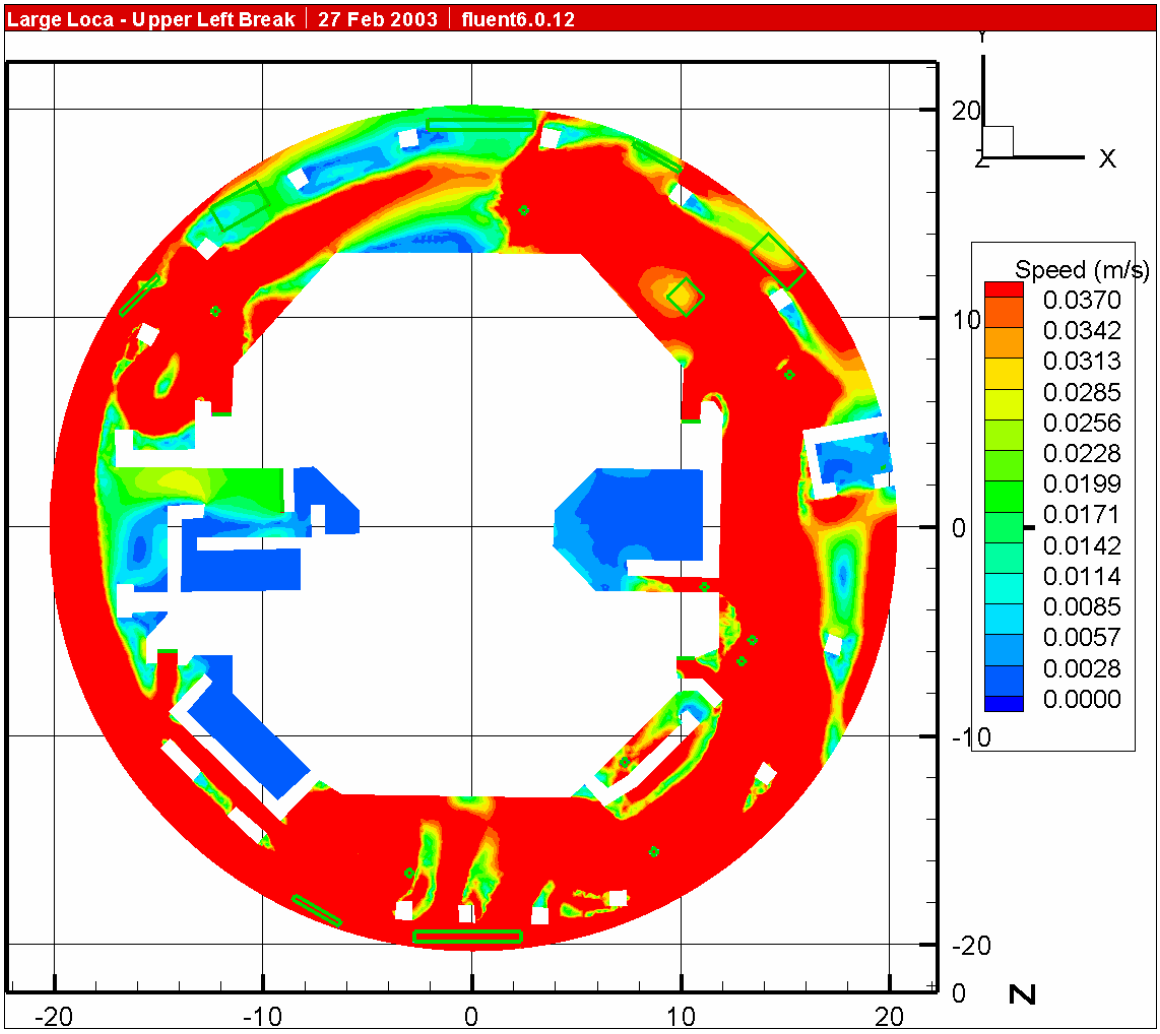

Figure III-30. Large LOCA Break Located in the Upper-Left Quadrant

In Figure III-30, speeds greater than or equal to the fiber threshold (0.037 m/s) are colored red.

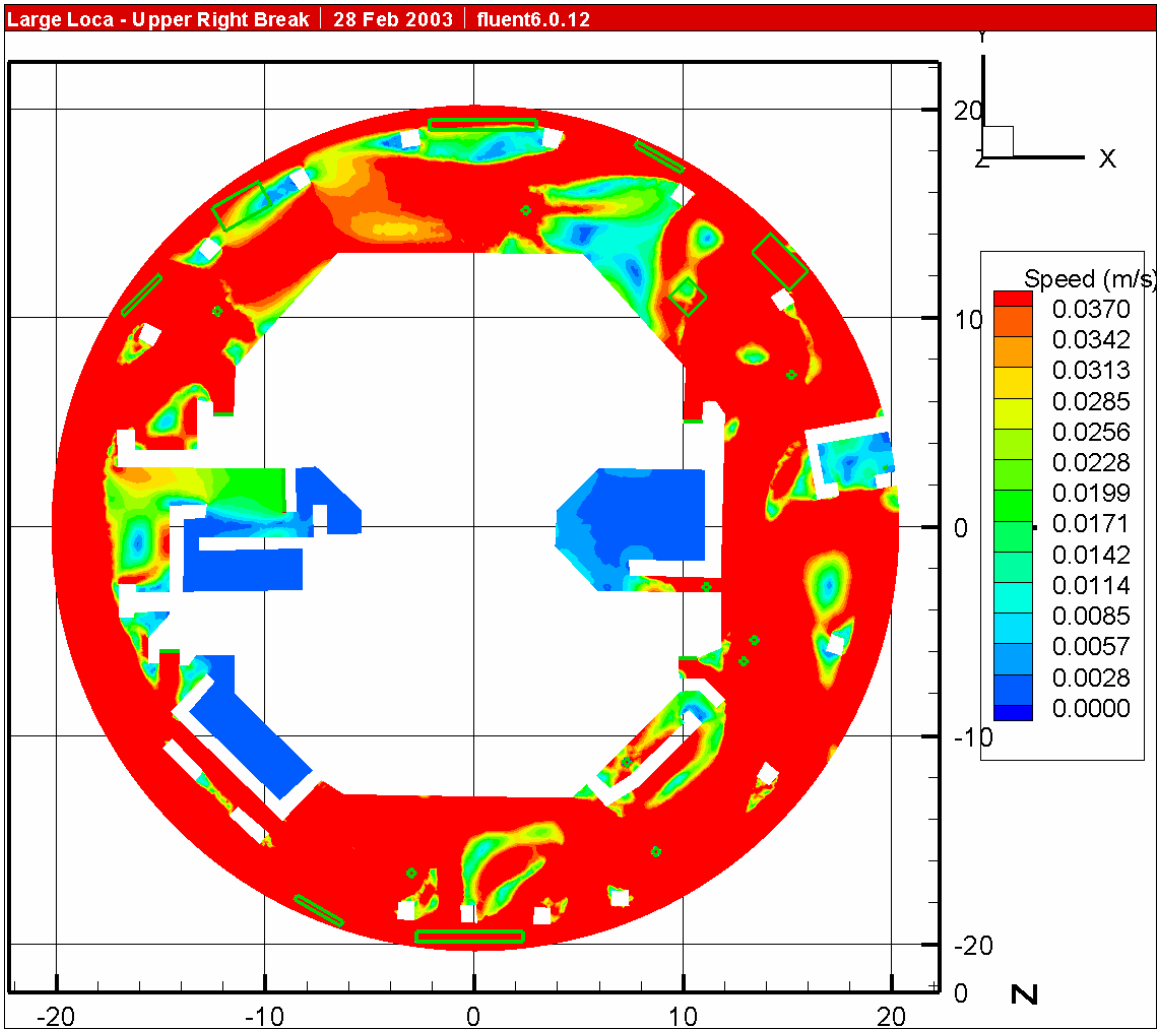

Figure III-31. Large LOCA Break Located in the Upper-Right Quadrant

In Figure III-31, speeds greater than or equal to the fiber threshold (0.037 m/s) are colored red.

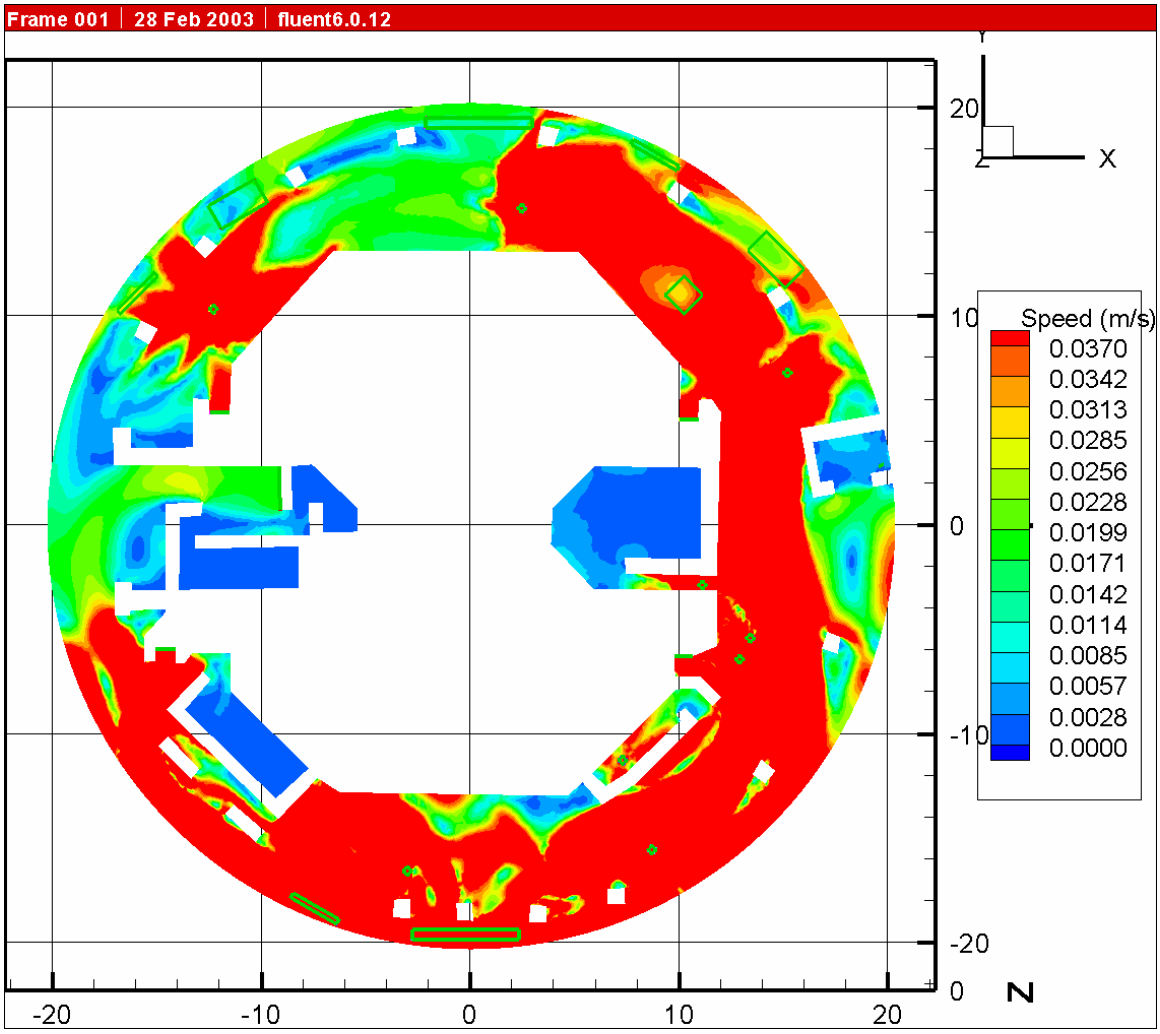

Figure III-32. Large LOCA Break Located in the Lower-Left Quadrant

In Figure III-32, speeds greater than or equal to the fiber threshold (0.037 m/s) are colored red.

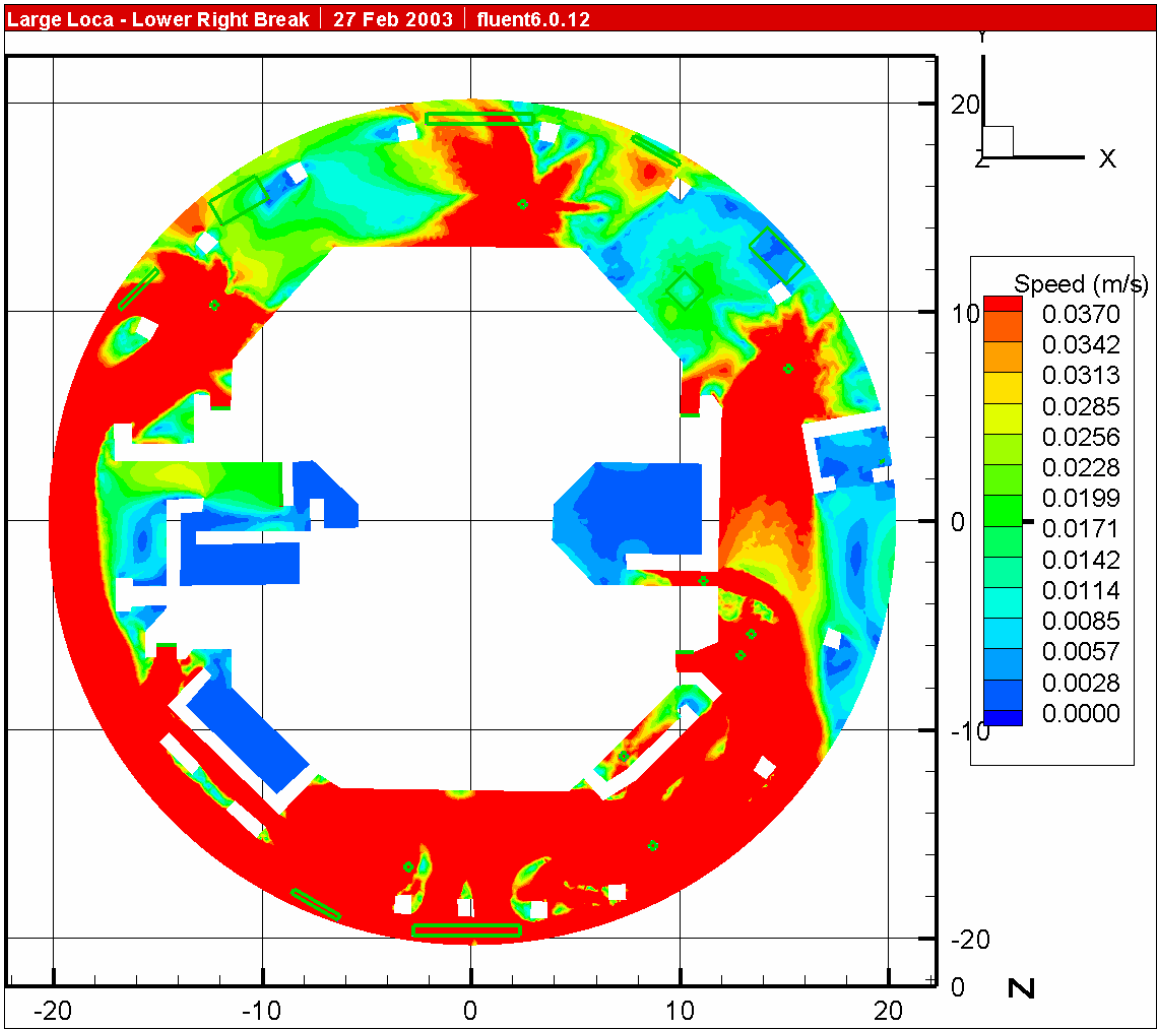

Figure III-33. Large LOCA Break Located in the Lower-Right Quadrant

In Figure III-33, speeds greater than or equal to the fiber threshold (0.037 m/s) are colored red.

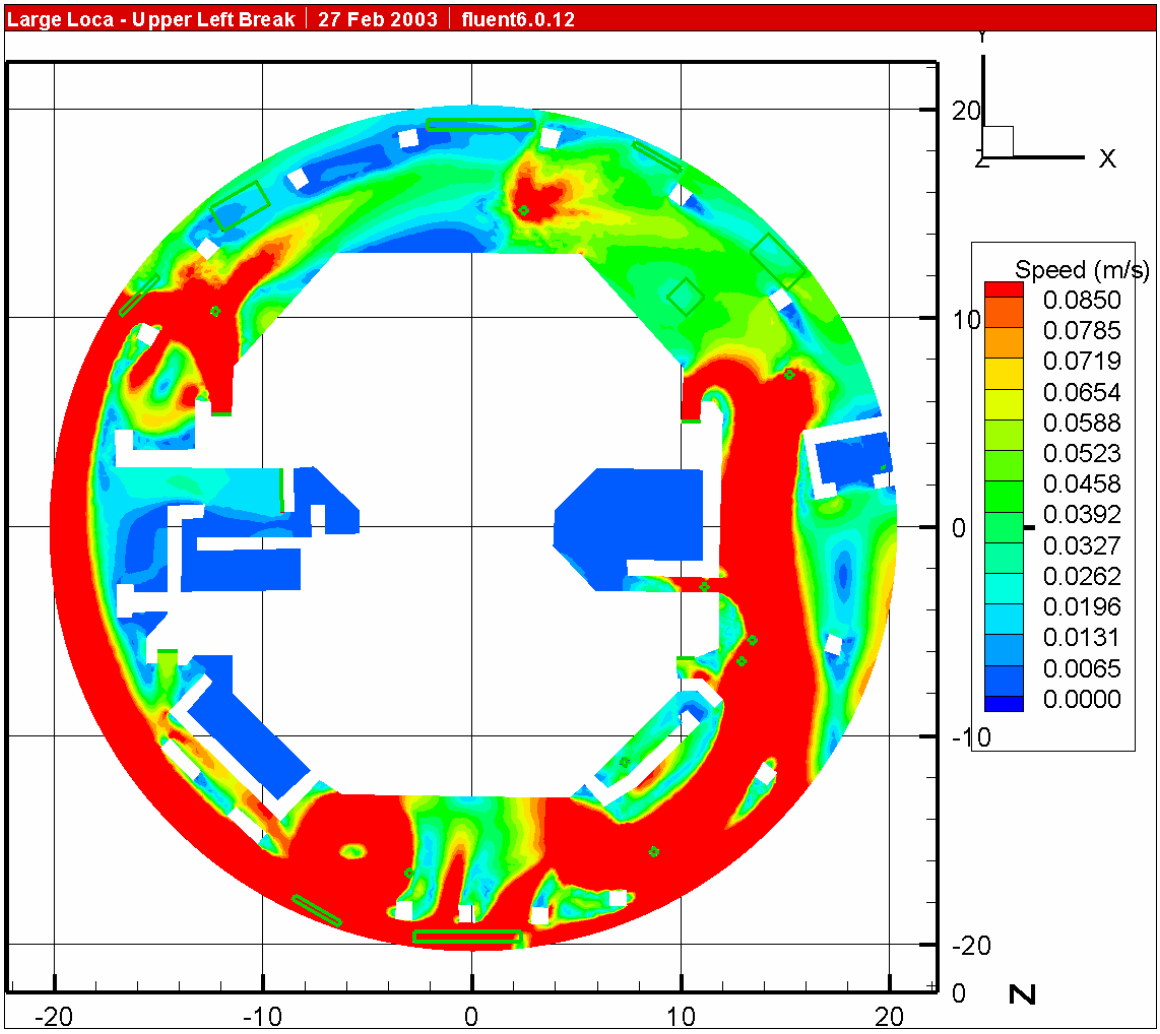

Figure III-34. Large LOCA Break Located in the Upper-Left Quadrant

In Figure III-34, speeds greater than or equal to the RMI threshold (0.085 m/s) are colored red.

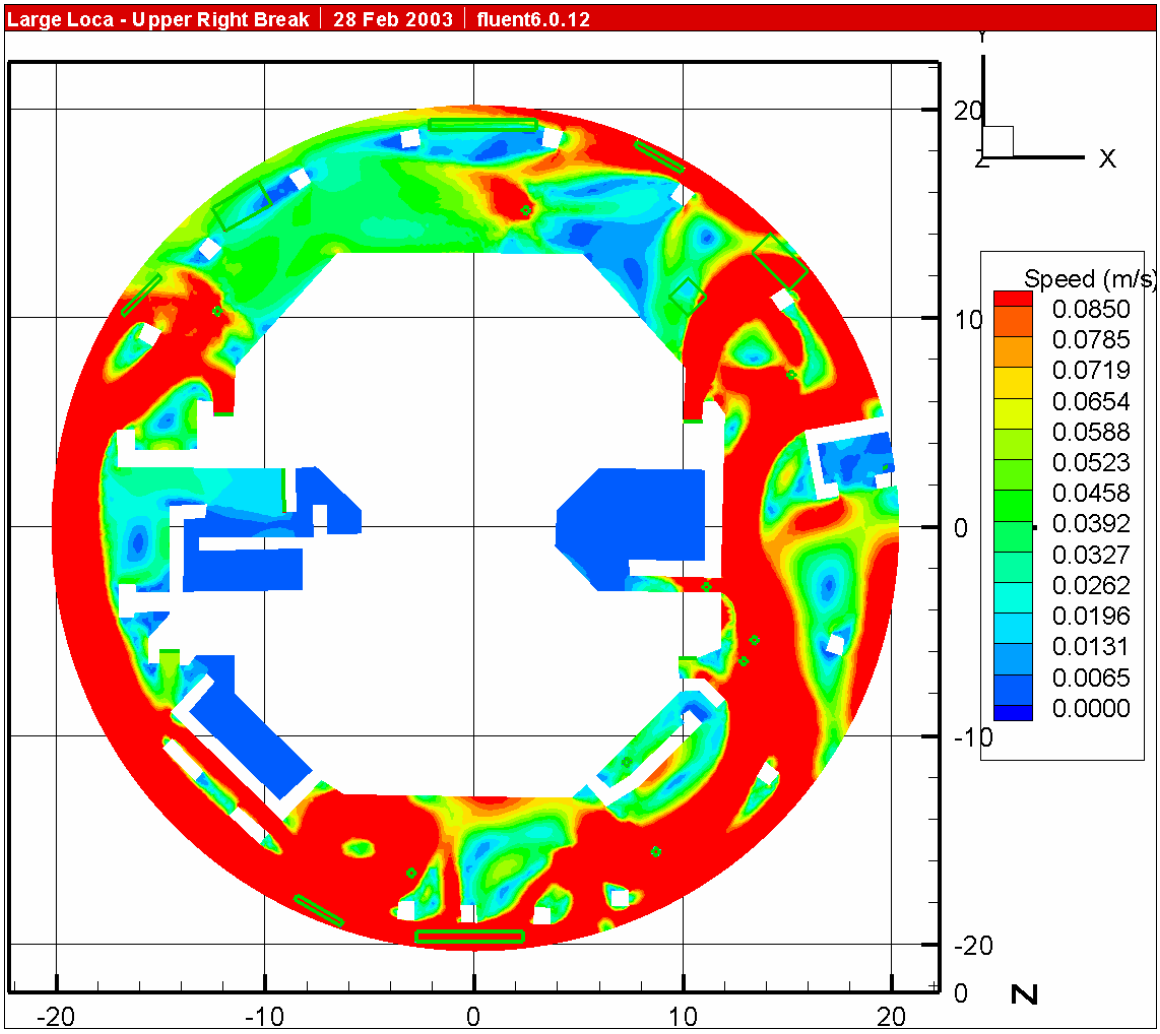

Figure III-35. Large LOCA Break Located in the Upper-Right Quadrant

In Figure III-35, speeds greater than or equal to the RMI threshold (0.085 m/s) are colored red.

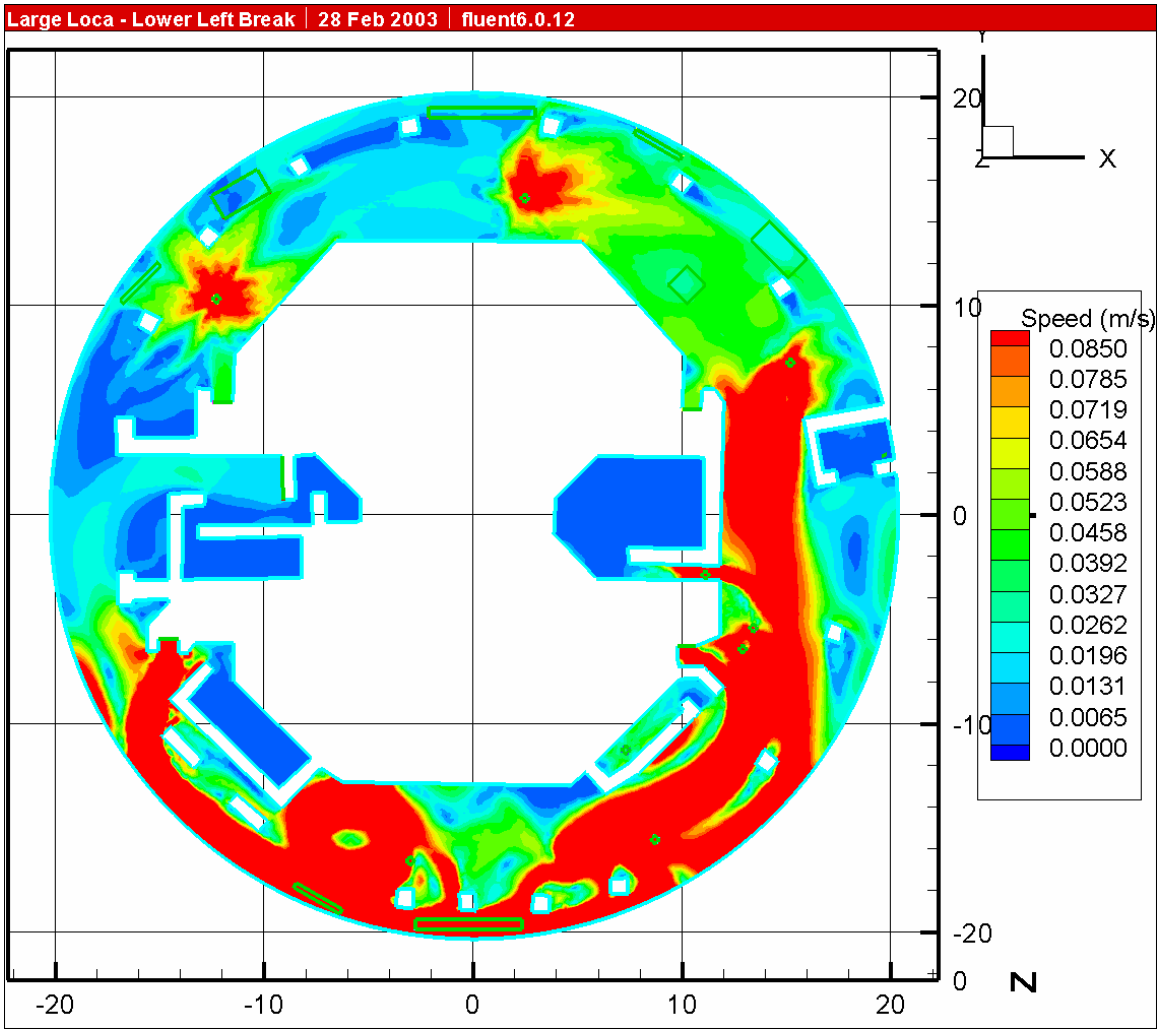

Figure III-36. Large LOCA Break Located in the Lower-Left Quadrant

In Figure III-36, speeds greater than or equal to the RMI threshold (0.085 m/s) are colored red.

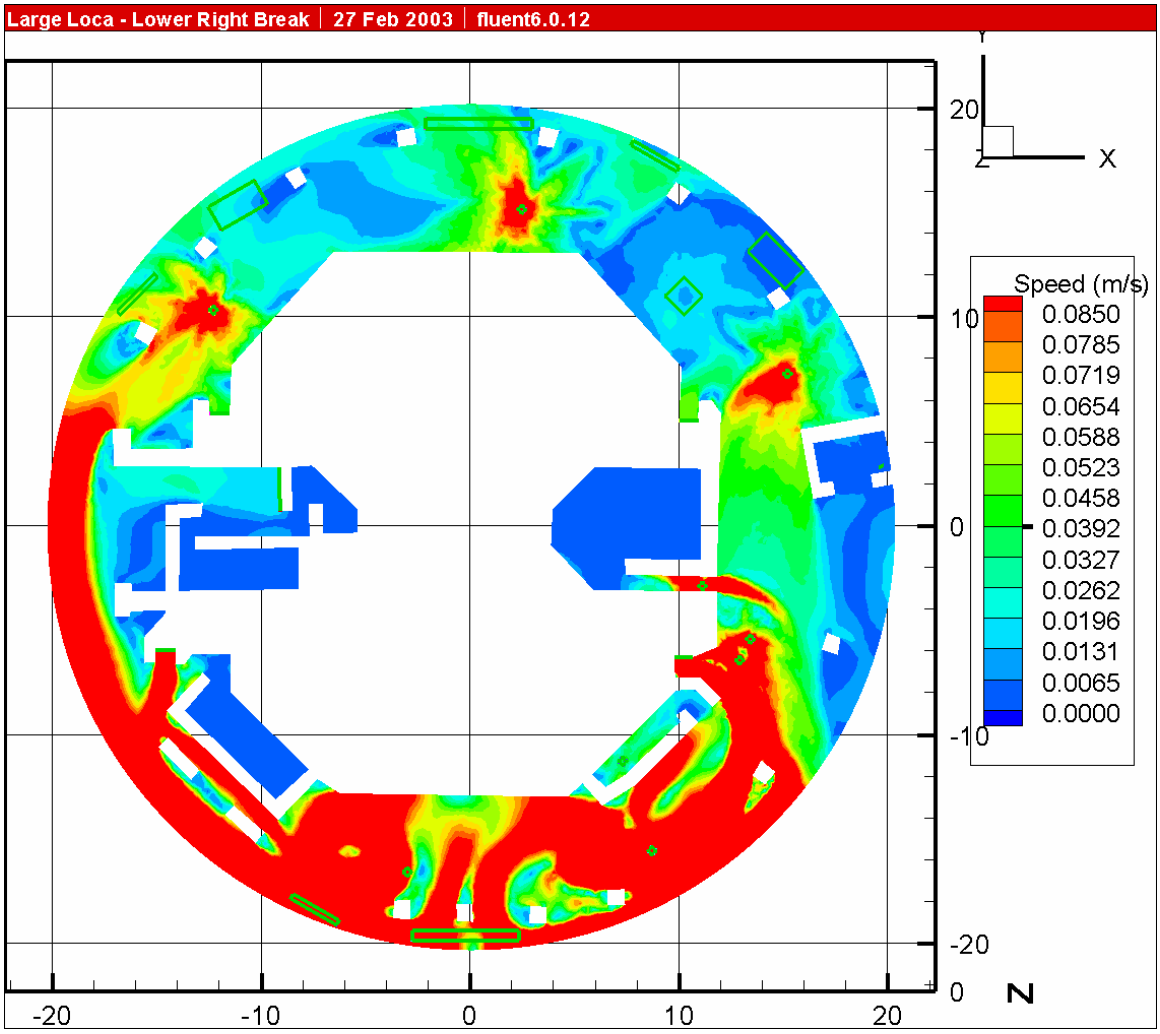

Figure III-37. Large LOCA Break Located in the Lower-Right Quadrant

In Figure III-37, speeds greater than or equal to the RMI threshold (0.085 m/s) are colored red.

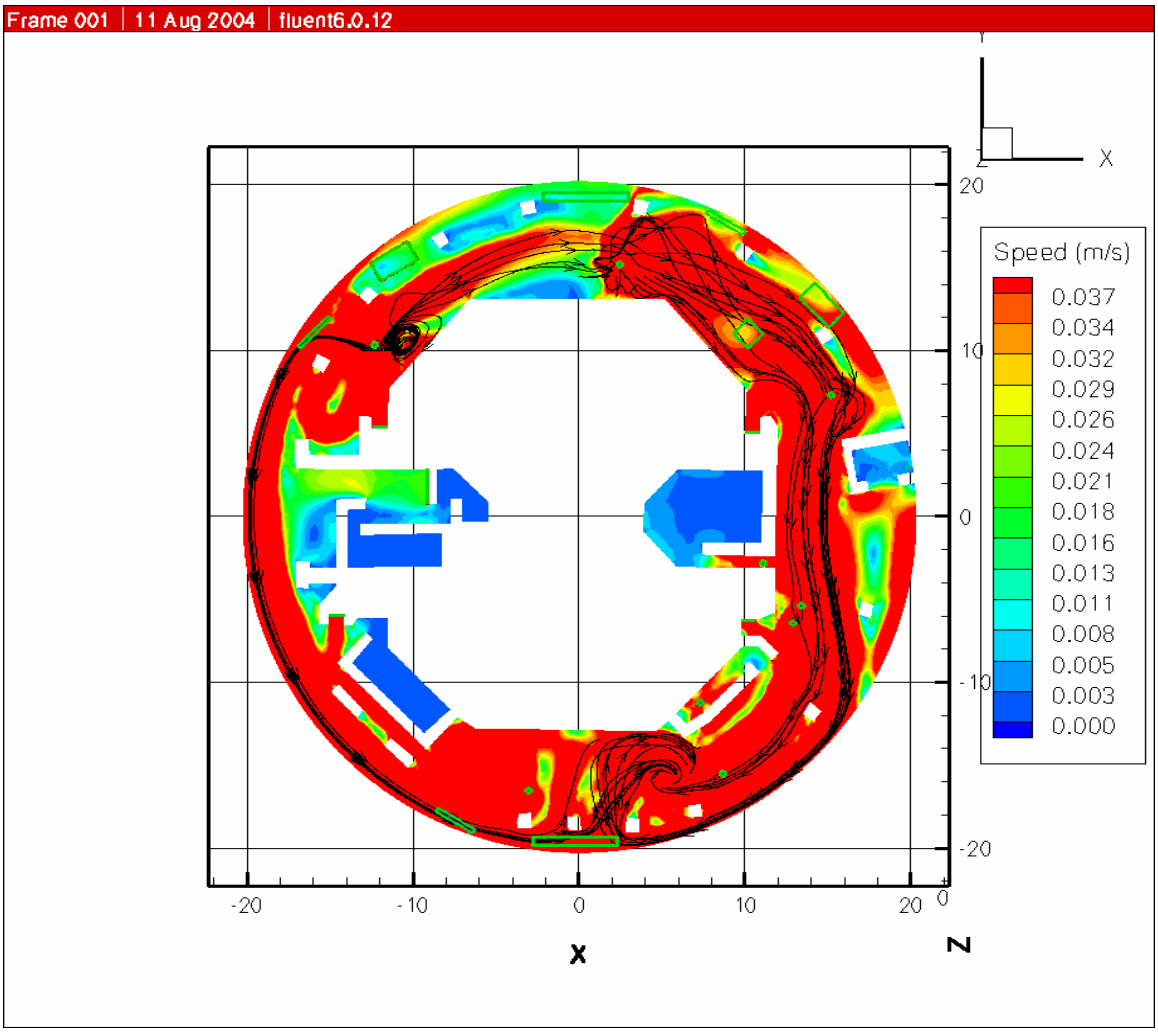

Figure III-38. Streamtraces across Two Splash Locations, Coordinates (-12,10) and (5,15), as Shown in the Figure, for a Large LOCA Break Located in the Upper-Left Quadrant

In Figure III-38, speeds greater than or equal to the fiber threshold (0.037 m/s) are colored red.

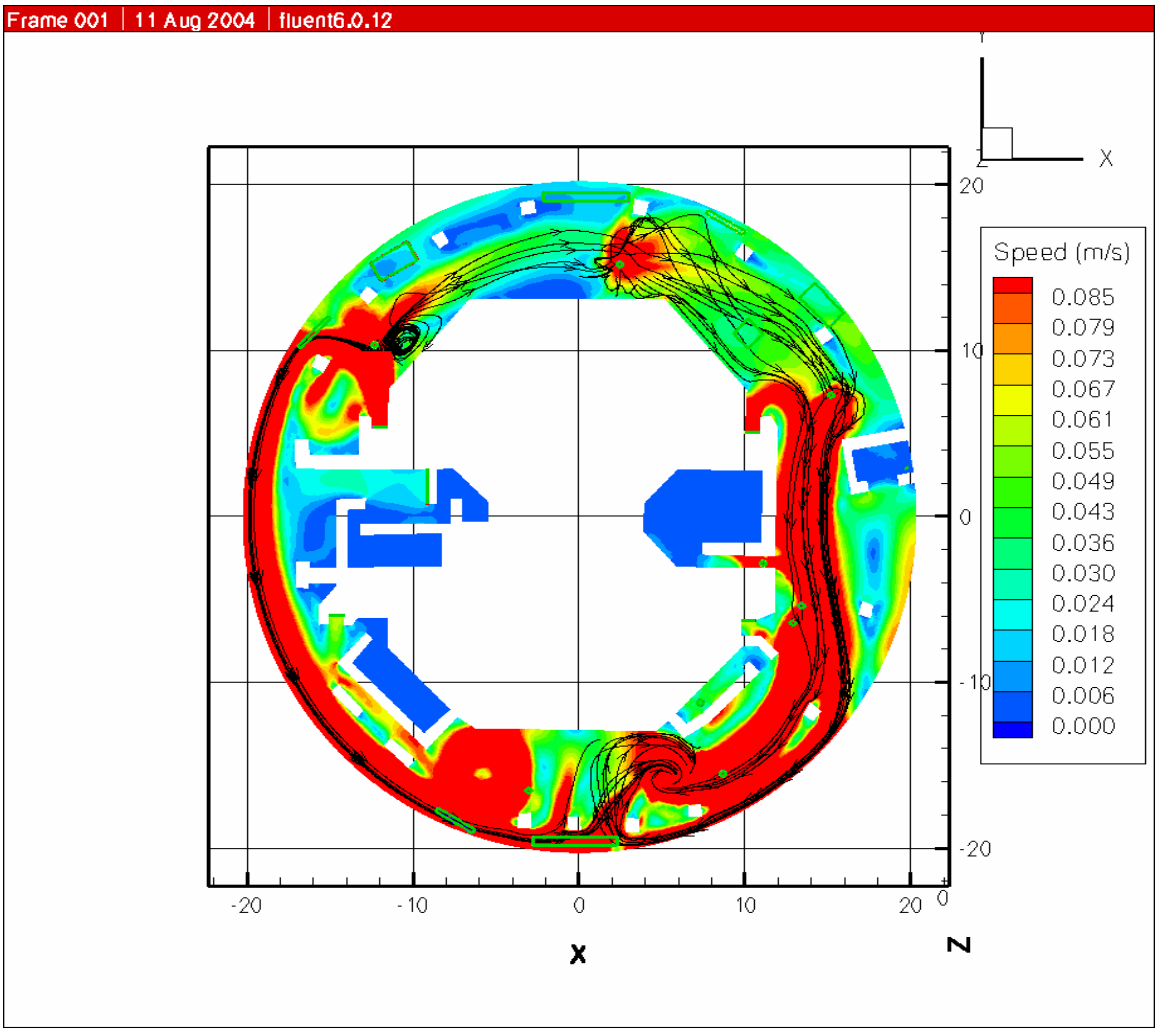

Figure III-39. Streamtraces across Two Splash Locations, Coordinates (-12,10) and (5,15), as Shown in the Figure, for a Large LOCA Break Located in the Upper-Left Quadrant

In Figure III-39, speeds greater than or equal to the RMI threshold (0.085 m/s) are colored red.

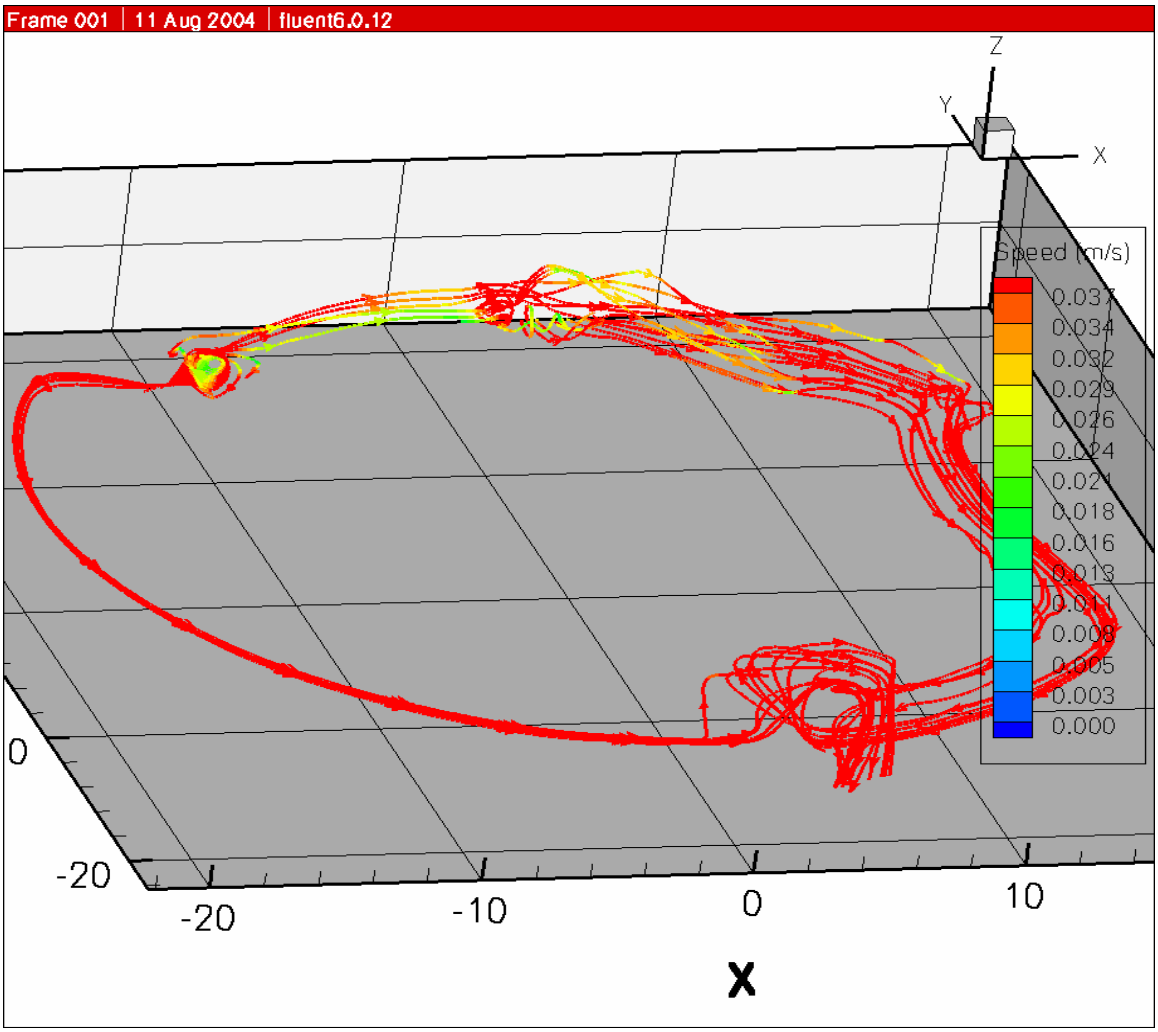

Figure III-40. Oblique View of the Streamtraces, as Shown in Figure III-38 for the Fiber Threshold Velocity

In Figure III-40, the traces are color coded to the local fluid velocity. Speeds greater than or equal to the fiber threshold (0.037 m/s) are colored red.

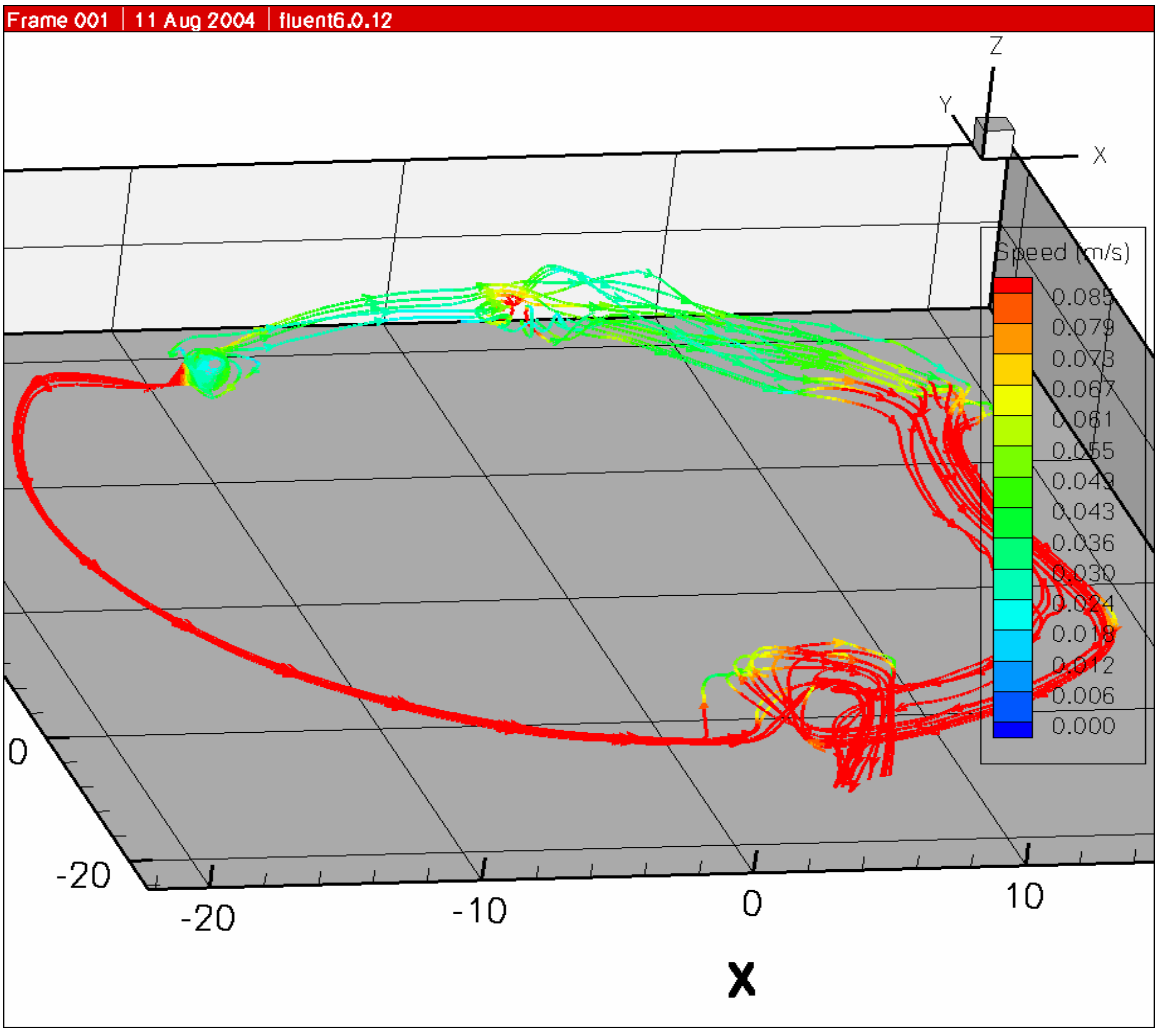

Figure III-41. Oblique View of the Streamtraces Shown in Figure III-39 for the RMI Threshold Velocity

In Figure III-41, the traces are color coded to the local fluid velocity. Speeds greater than or equal to the RMI threshold (0.085 m/s) are colored red.

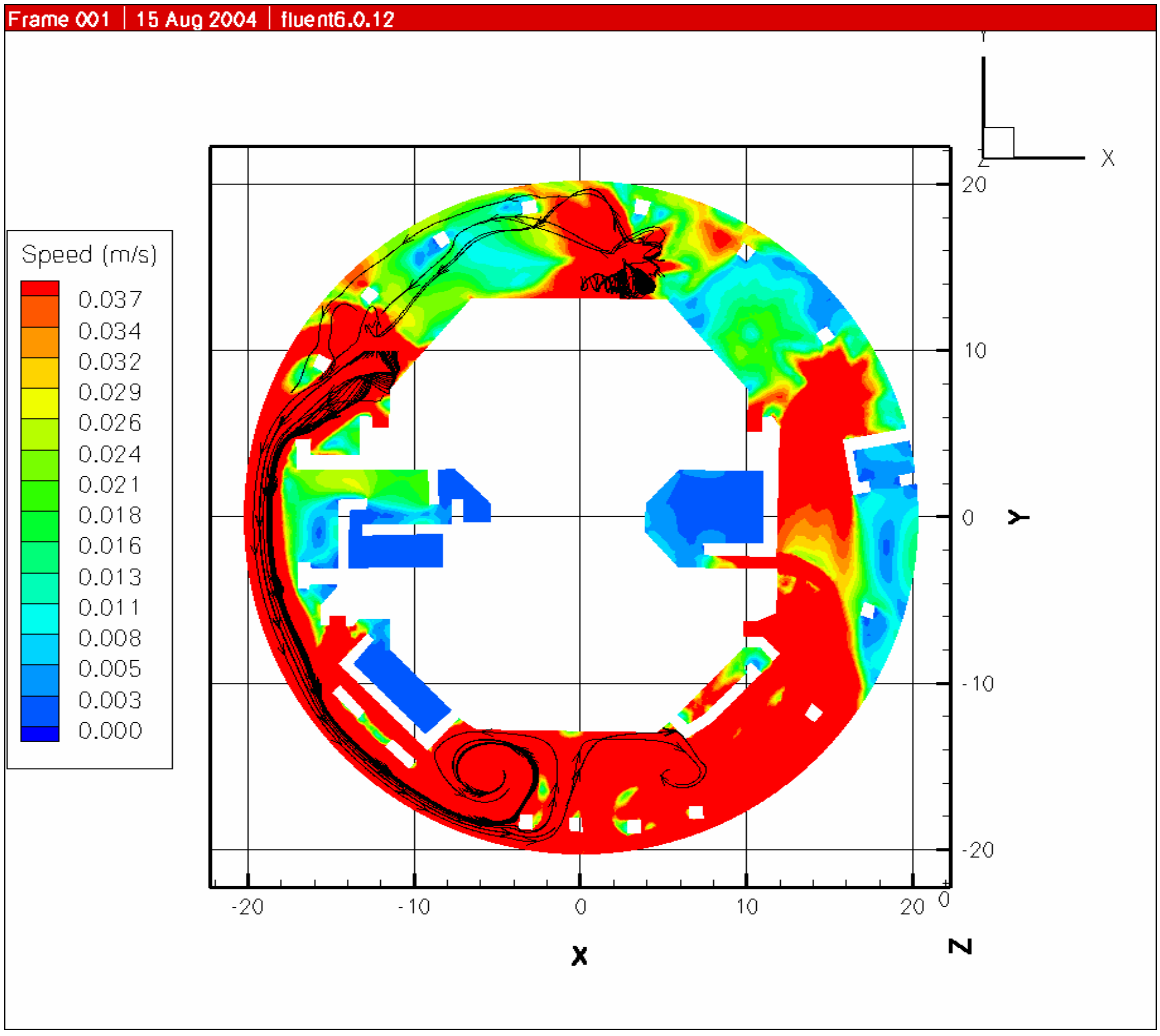

Figure III-42. Streamtraces across Two Splash Locations, Coordinates (-12,10) and (5,15) as Shown in the Figure, for a Large LOCA Break Located in the Lower-Right Quadrant

In Figure III-42, speeds greater than or equal to the fiber threshold (0.037 m/s) are colored red.

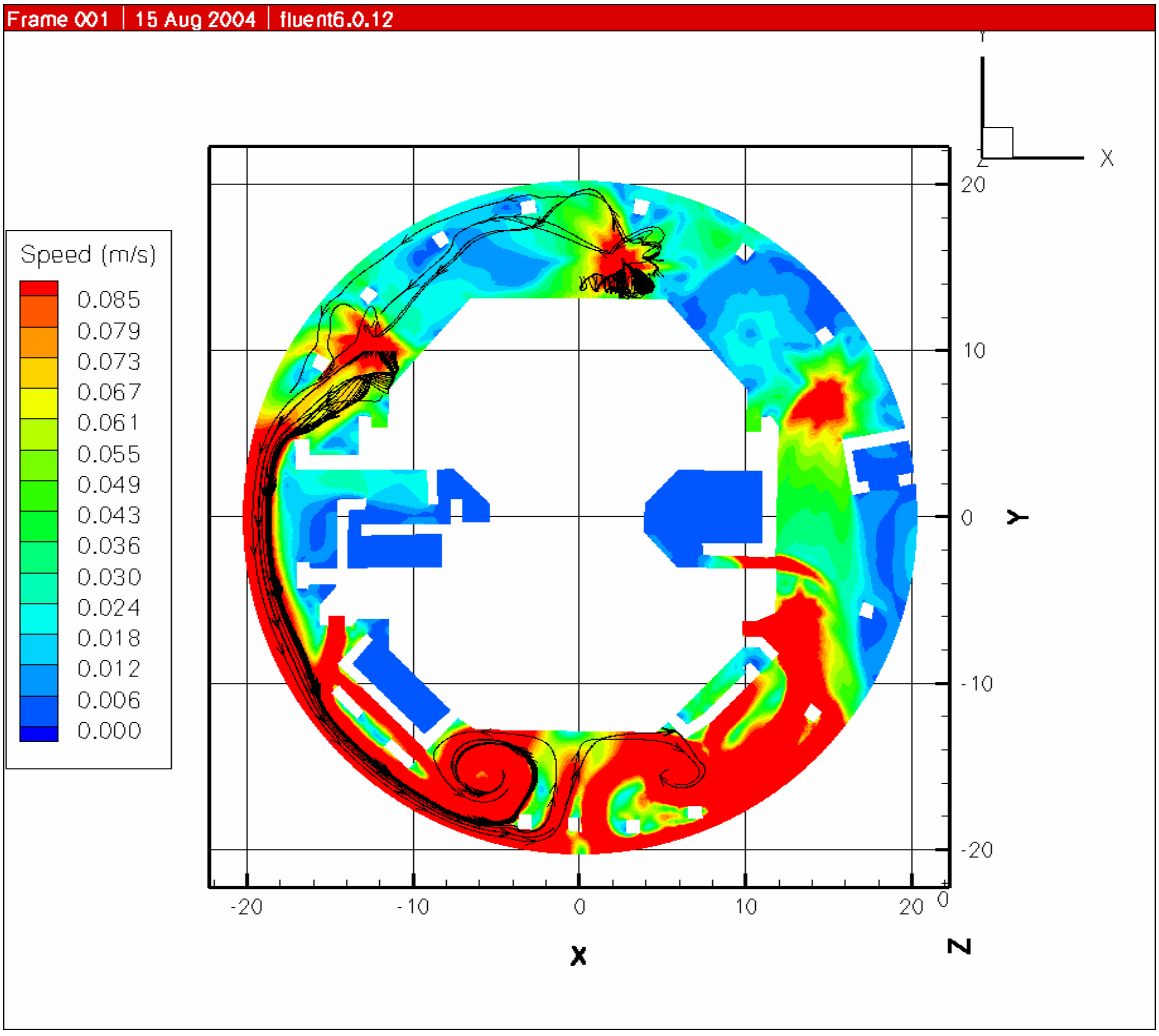

Figure III-43. Streamtraces across Two Splash Locations, Coordinates (-12,10) and (5,15), as Shown in the Figure, for a Large LOCA Break Located in the Lower-Right Quadrant

In Figure III-43, speeds greater than or equal to the RMI threshold (0.085 m/s) are colored red.

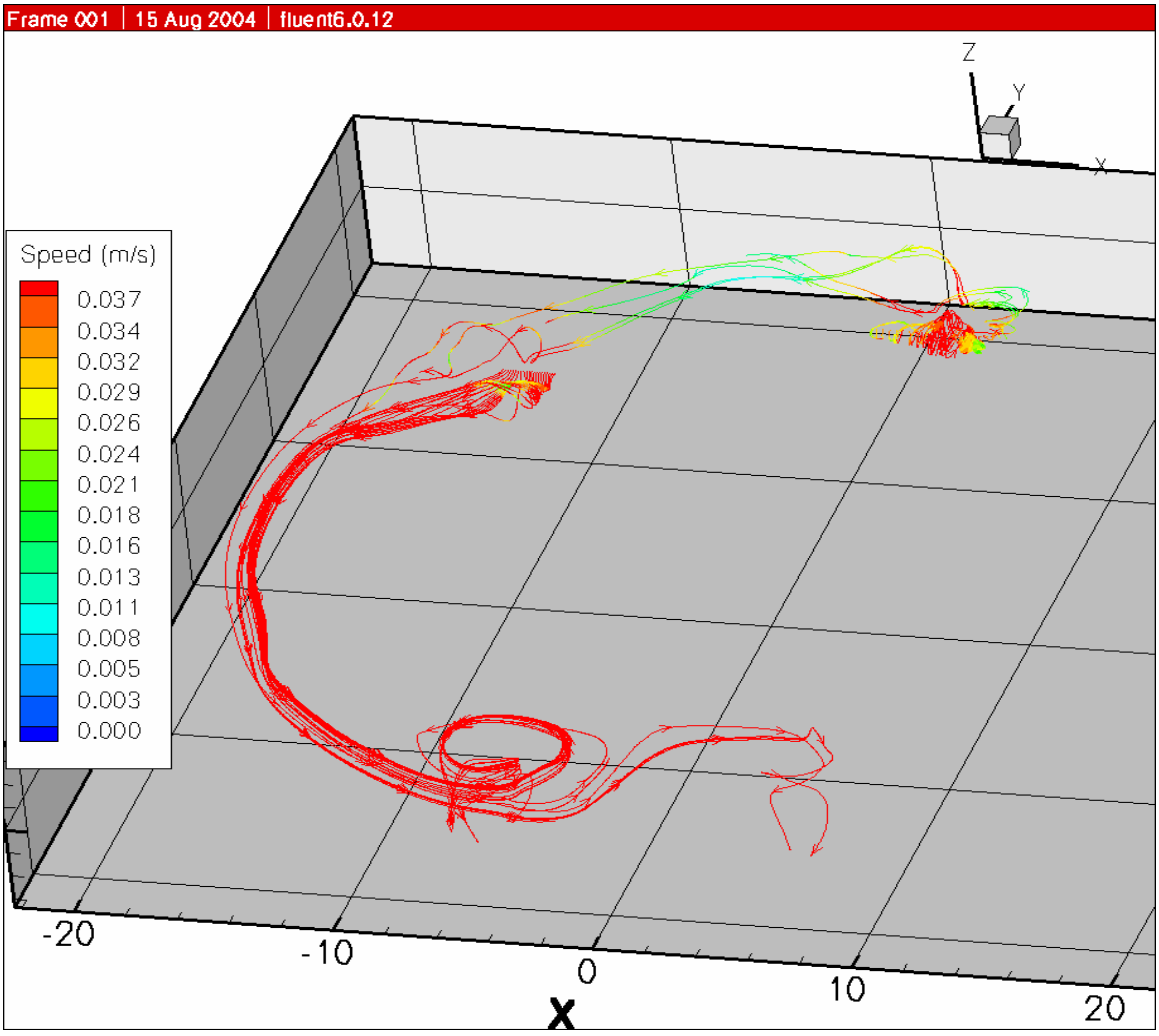

Figure III-44. Oblique View of the Streamtraces Shown in Figure III-42 for the Fiber Threshold Velocity

In Figure III-44, the traces are color coded to the local fluid velocity. Speeds greater than or equal to the fiber threshold (0.037 m/s) are colored red.

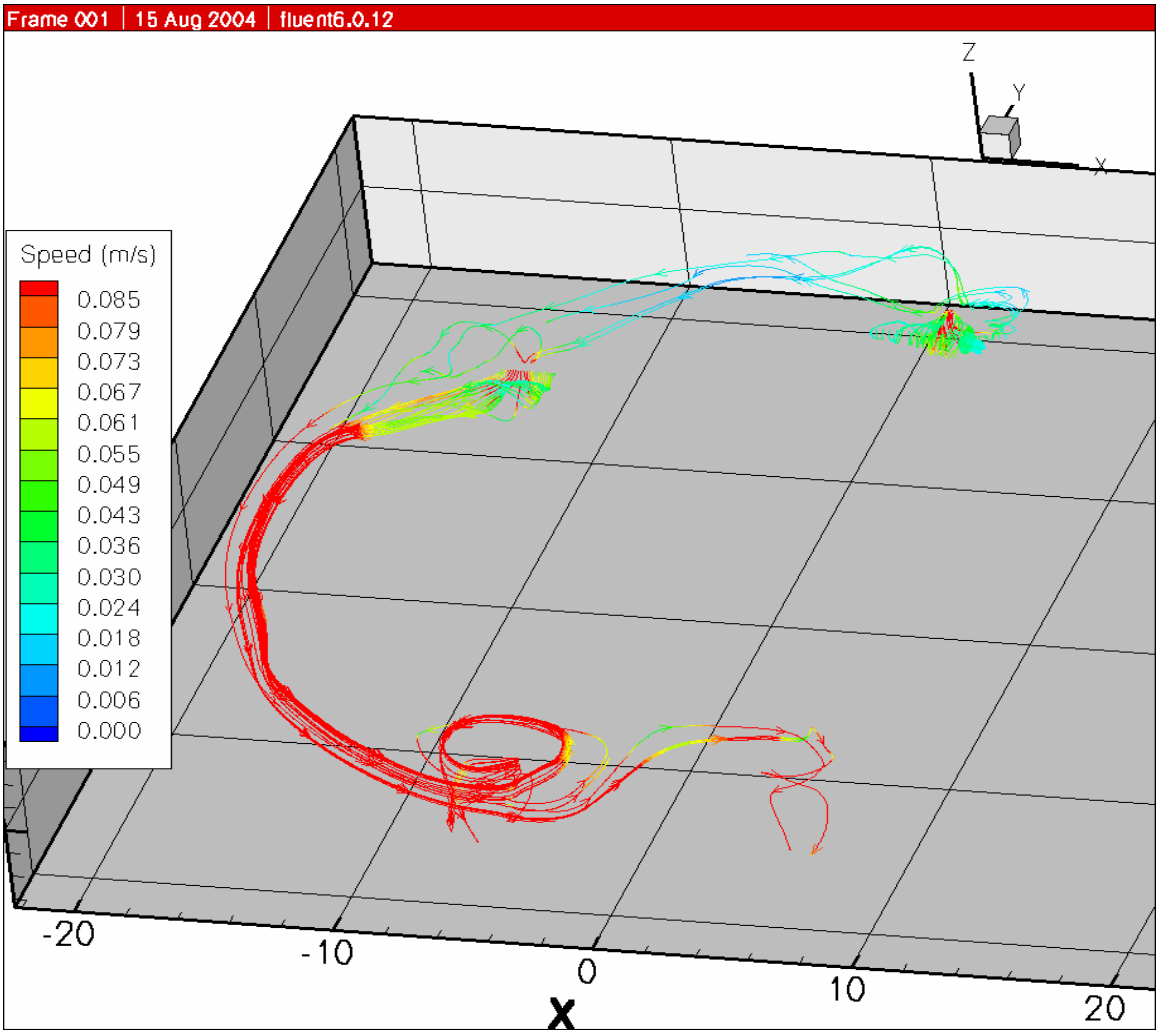

Figure III-45. Oblique View of the Streamtraces Shown in Figure III-43 for the Fiber Threshold Velocity

In Figure III-45, the traces are color coded to the local fluid velocity. Speeds greater than or equal to the RMI threshold (0.085 m/s) are colored red.

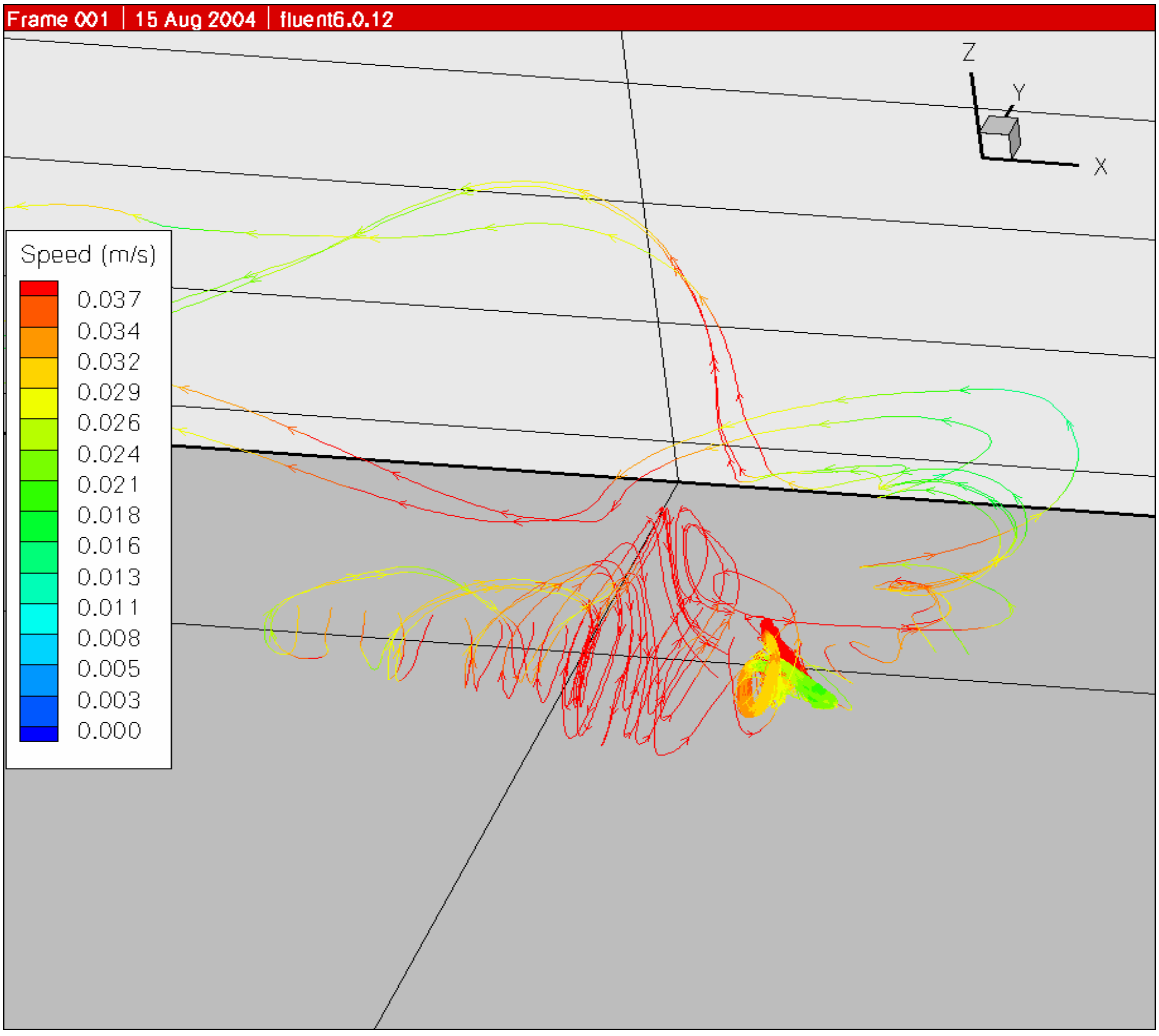

Figure III-46. Large LOCA Lower-Right Break, Zoom in at Upper-Right Splash Location Shown in Figure III-42 and Figure III-43

In Figure III-46, the traces are color coded to the local fluid velocity. Speeds greater than or equal to the fiber threshold (0.037 m/s) are colored red.

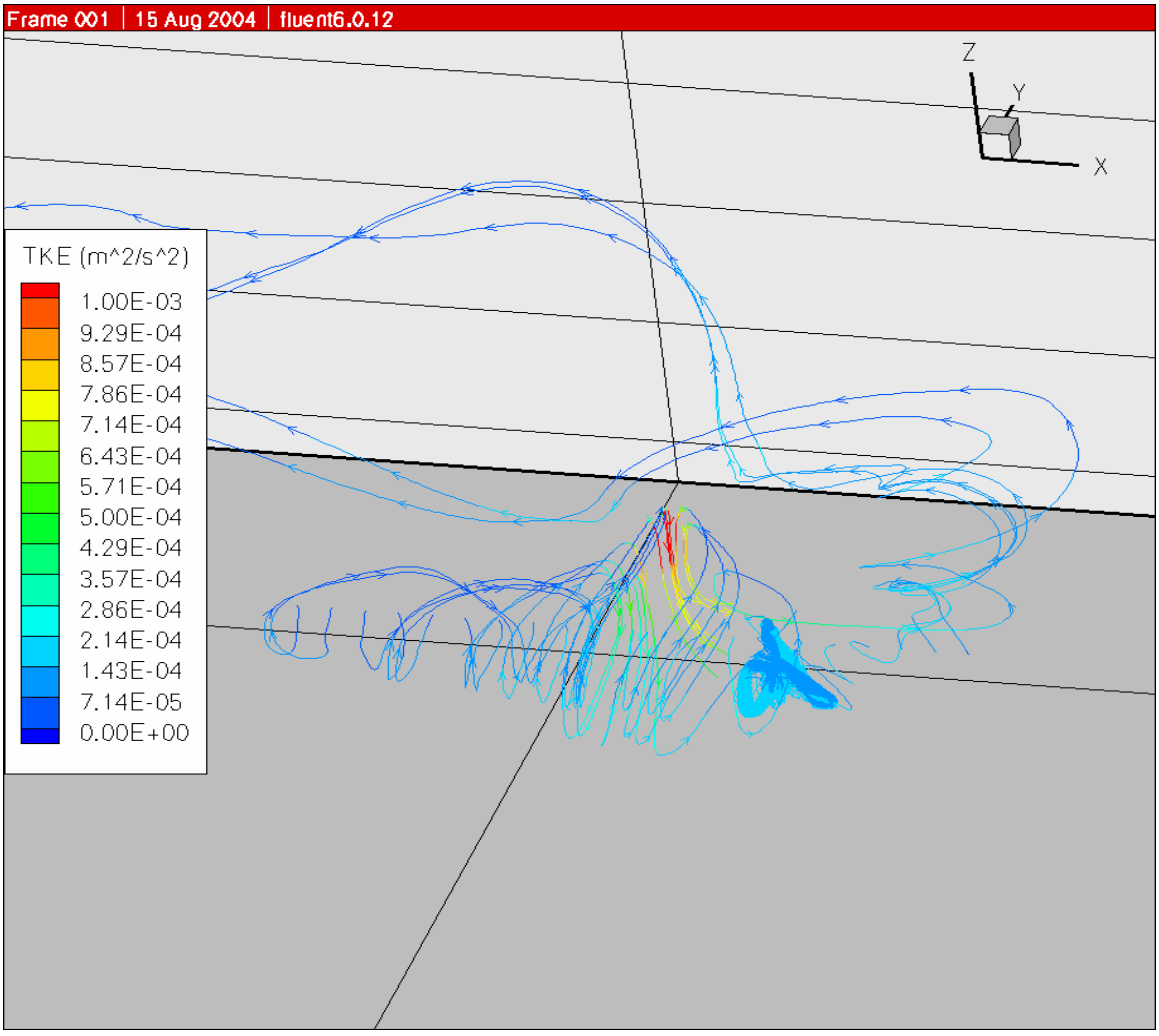

Figure III-47. Same as Figure III-46, with Streamlines Color Coded by TKE

III.3 Sump Pool Debris Transport

The CFD analyses characterized the flow conditions in the sump for a selection of LOCA accident scenarios. These conditions include flow velocity patterns, pool turbulence, and flow streamlines. The pool velocity and turbulence characteristics determine areas of the pool where debris entrapment may occur. The flow streamlines can be used to determine whether debris entering the pool at a discrete location would be likely to pass through one of the potential entrapment locations. The debris transport process was broken down using a logic chart approach to facilitate the individual transport steps—steps that could be determined analytically or experimentally, or simply judged. The subsequent quantification of the chart then provided an estimate of the overall sump pool debris transport.

III.3.1 Debris Transport Logic Chart Methodology

When and where the debris enters the pool is key to the evaluation of sump pool debris transport. The debris enters the pool either when directly deposited onto the sump floor

during the blowdown phase or with the subsequent drainage of the containment sprays. To put the timing in perspective, the reactor cavity would likely fill in less than 12 minutes (e.g., a large LOCA break flow rate of 7,400 gpm would fill the reactor cavity volume, estimated by the plant to be less than 12,000 ft^3, in less than 12 minutes neglecting the contribution from the containment sprays), and the sump pool should reach a reasonable steady state in about 30 minutes. The entrance location for blowdown-deposited debris is a debris distribution on the floor that likely favors deposition nearer the location of the break.

Where the debris enters the pool depends on whether the debris is blown onto the break room floor (SG compartment housing the break) or the remainder of the sump floor, which is the lower level annulus floor. Debris transported into the pool via the spray drainage would enter at the primary drainage locations. The debris transport analysis requires a distribution for where the washdown debris enters the sump pool. The spray drainage analysis in Appendix VI provides a distribution for drainage flows entering the sump pool. These analyses assume that the distribution of washdown debris entering the pool mimics that of the spray water distribution for debris deposited outside the break compartment. The blowdown deposition analyses determined substantial debris deposition within the break compartment that would subsequently wash directly to the break compartment floor; this deposition was considered in the debris introduction to the pool. The drainage from the containment sprays entered into the sump pool at many locations, including floor drains, stairwells, an equipment hatch, the containment liner, refueling pool drains, and containment spray trains located at the sump level. The drainage flowed over from upper levels into the annular gap, or spray fell directly into the SG compartments. To simplify the analysis, the multiple drainage entrance locations into the sump pool were grouped into seven groups around the sump annulus. Figure III-48 shows this distribution in an event chart format. One of these charts applies to each size category of each type of insulation. The chart includes the following distributions (moving from left to right):

- the blowdown transport deposition distribution that splits the total debris among debris deposited in the upper level floors, the break compartment floor, and the remainder of the lower level (sump) floor
- the washdown transport distributions of whether the debris deposited in the upper levels would likely transport to the sump pool or remain in the upper levels
- the distribution of the locations where debris entrained in the containment spray drainage would enter the sump pool
- the distributions associated with sump pool formation debris transport
- the distributions associated with pool recirculation debris transport
- the distributions associated with potential debris erosion

Each transport path is assumed to transport debris to one of three destinations, which include (1) accumulation on the sump screens, (2) entrapment within the inactive pools, and (3) entrapment at other locations along the transport pathways. The fraction of the debris predicted to accumulate on the screens is then the transport fraction for the size and type of debris. The overall transport fraction by insulation type is obtained by applying the debris-size distributions to the size-specific transport fractions.

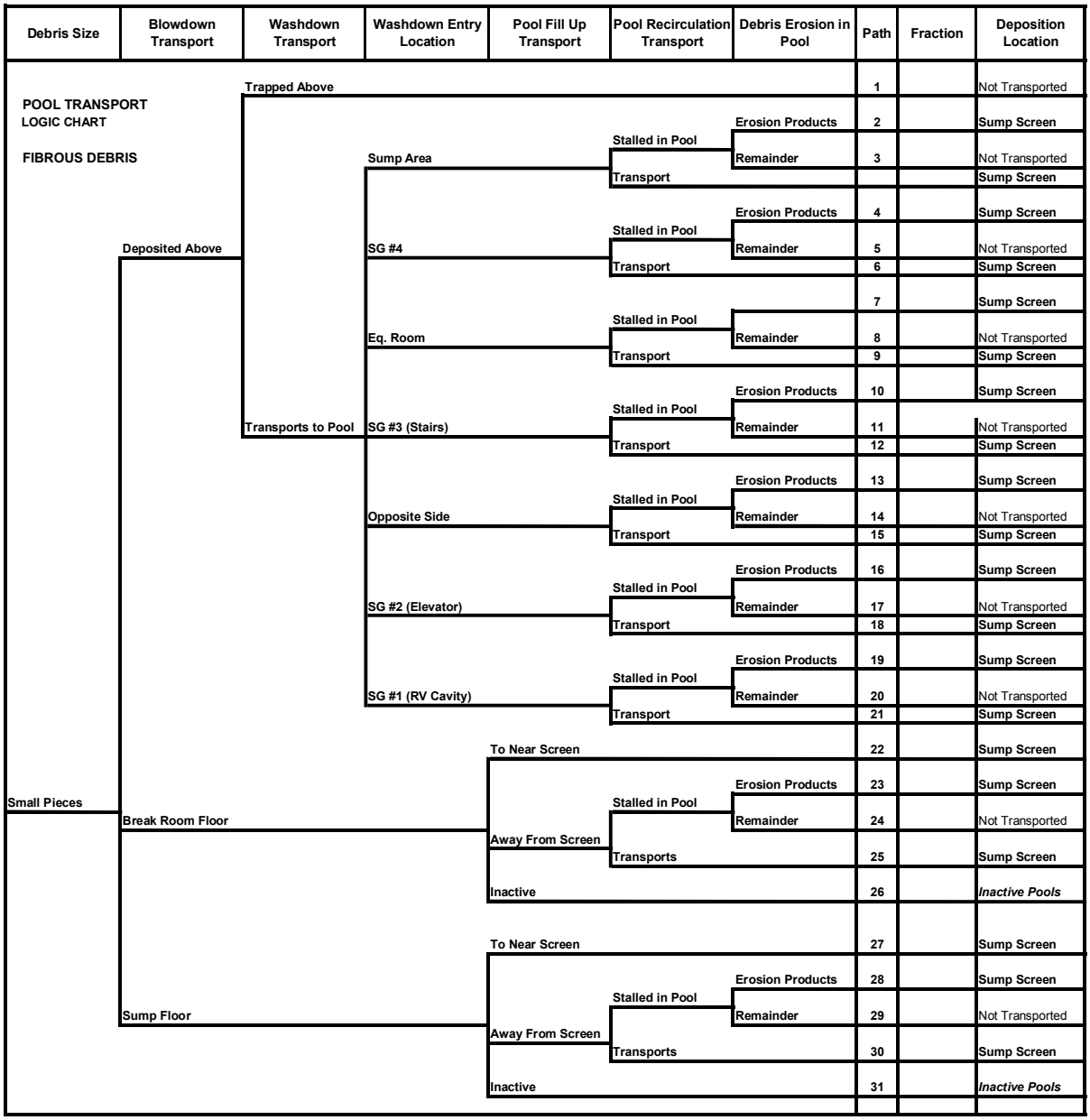

Figure III-48. Sump Pool Debris Transport Chart

III.3.2 Blowdown/Washdown Debris Entry into the Sump Pool

The details of the volunteer-plant blowdown/washdown debris transport analyses documented in Appendix VI provided the distributions for the blowdown and washdown phases of the transport analysis. Table III-2 shows these distributions.

The volunteer-plant fibrous debris was categorized as (1) fines, (2) small pieces, (3) large pieces, and (4) intact pieces. The fines and small pieces represent debris capable of passing through a typical grating during blowdown. The fines are generally the individual fibers that remain suspended in the sump pool, whereas the small-piece

fibrous debris typically would readily sink to the pool floor in hot water. Thus, the fines and small pieces must be evaluated differently. The large-piece and intact-piece debris represents debris too large to pass through a grating, which is a process fundamental to blowdown debris transport evaluations. The difference between the large- and intact-piece debris is whether the fibrous insulation continues to be protected by covering material. With large-piece debris, the fibrous insulation is subject to erosion, whereas the intact-piece debris insulation is not. Another distinction is that the covering materials on the intact debris, which include nearly intact blankets, are more likely to snag onto structures, including gratings, during blowdown transport such that the debris is less likely to fall back to a floor or wash off with the sprays. The guidance report (GR) baseline small-fines category corresponds to the combination of the fines and small-piece debris in the volunteer-plant analyses, and the GR large-piece debris corresponds to the large- and intact-piece debris in the volunteer-plant analyses.

Table III-2. Blowdown/Washdown Debris Transport Fractions

Debris Size and Type	Debris Transport Fractions				
	Blowdown Transport			Washdown Transport	
	Deposited in Upper Levels	Deposited on Break Room Floor	Deposited on Sump Floor	Remains Trapped Above	Transports to Sump Pool
Fibrous Debris					
Fines	0.92	0.05	0.03	0.07	0.93
Small Pieces	0.92	0.05	0.03	0.37	0.63
Large Pieces	0.57	0.39	0.04	0.81	0.19
Intact Pieces	0.69	0.30	0.01	0.78	0.22
RMI Debris					
< 2 in.	0.47	0.50	0.03	0.38	0.62
2 to 6 in.	0.35	0.61	0.04	0.69	0.31
> 6 in.	0.22	0.77	0.01	0.68	0.32

The volunteer-plant RMI debris was categorized as (1) debris pieces smaller than 2 in., (2) pieces between 2 and 6 in., and (3) pieces larger than 6 in. The GR RMI size groups were subdivided at 4 in. rather than the 2 and 6 in. used for the volunteer-plant analysis. However, the combination of the volunteer-plant analysis categories less than 6 in. is a reasonable representation of the GR small-fines category, leaving the pieces larger than 6 in. to represent the large-piece debris.

The debris washing down from the upper levels was assumed to enter the sump pool with the same distribution as the spray drainage. However, blowdown debris that was preferentially deposited in the SG compartment where the break occurred (SG1) and its adjacent SG compartment (SG4) would wash directly to the floors of these compartments, regardless of the spray drainage fractions. For the volunteer plant, the spray drainage analysis documented in Appendix VI provided the spray drainage distribution, as shown in Table III-3. Table III-4 and Table III-5 provide the location distributions for debris washing down from the upper levels by debris size category for

fibrous and RMI debris, respectively. Because the larger debris was preferentially trapped in SG1 and SG4, these washdown location fractions are larger.

Table III-3. Spray Drainage Distribution into the Sump Pool

No.	Location in Annular Sump	Spray Drainage Water Sources	Drainage Fraction
1	Annulus Section Containing Recirculation Sumps	Floor drains and annular gap sources.	0.14
2	Vicinity of SG4 Access (SG Adjoining Break Room)	SG4 personnel access doorway and liner flow. Includes flow from a 6-in. refueling pool drain.	0.08
3	Vicinity of Interior Equipment Room Access (~90° from Sumps)	Refueling pool water drains into equipment room below refueling pools, then exits doorway into sump and liner flow.	0.06
4	Vicinity of SG3 Access	SG3 personnel access doorway, annular gap sources, and stairwell. Includes flow from a 6-in. refueling pool drain.	0.18
5	Annulus Section Directly Opposite Recirculation Sumps	Floor drains and annular gap sources.	0.09
6	Vicinity of SG2 Access	SG2 personnel access doorway, floor drains, upper level equipment hatch, annular gap sources, and stairwell. Includes flow from a 6-in. refueling pool drain.	0.25
7	Vicinity of SG1 Access (Compartment with Break)	SG1 personnel access doorway, floor drains, and annular gap sources. Includes flow from a 6-in. refueling pool drain.	0.20

Table III-4. Fibrous Debris Entrance Distributions to Sump Pool

No.	Location in Annular Sump	Drainage Fraction	Fines Debris	Small-Piece Debris	Large-Piece Debris	Intact-Piece Debris
1	Sumps	0.14	0.09	0.09	0.01	0.01
2	SG4	0.08	0.17	0.17	0.28	0.22
3	Eq. Room	0.06	0.04	0.04	0	0
4	SG3	0.18	0.12	0.12	0.07	0.07
5	Opposite	0.09	0.06	0.06	0.01	0.01
6	SG2	0.25	0.16	0.16	0.07	0.07
7	SG1	0.20	0.36	0.36	0.56	0.62

Table III-5. RMI Debris Entrance Distributions to Sump Pool

No.	Location in Annular Sump	Drainage Fraction	<2-in. Debris	2- to 6-in. Debris	>6-in. Debris
1	Sumps	0.14	0.06	0.01	0.01
2	SG4	0.08	0.24	0.28	0.22
3	Eq. Room	0.06	0.02	0	0
4	SG3	0.18	0.06	0.07	0.07
5	Opposite	0.09	0.04	0.01	0.01
6	SG2	0.25	0.09	0.07	0.07
7	SG1	0.20	0.49	0.56	0.62

III.3.3 Sump Pool Debris Transport Estimates

The following three phases represent debris transport in the sump pool:

(1) transport of floor-deposited debris during the formation (fillup) of the sump pool

(2) debris transport in an established sump during recirculation mode

(3) long-term erosion of exposed fibrous debris in the sump pool

III.3.3.1 Pool Formation Debris Transport

As observed during the integrated debris transport tests (NUREG/CR-6773, 2002), the primary driver for moving debris during pool formation, especially for the large debris, is the sheeting flow as the initial water from the break spreads across the sump floor. Debris initially deposited on the floor is pushed along with the wave front. Thus, the movement of the debris has significant momentum that can carry the debris past the openings into interior spaces. Once the water depth becomes significant, further transport occurs because of the drag forces of the flow of water, and for larger debris, that transport becomes substantially less dynamic than the sheeting flow transport. Individual fibers will move as suspended debris following the waterflow.

In the volunteer plant, most of the debris initially deposited on the floor of the compartment containing the break (SG compartment 1 in this evaluation) would likely transport from that compartment onto the annular sump floor through either the personnel access door for SG1 or the door for SG4. Because the break is in SG1, considerably more flow would exit the door to SG1 than to SG4. In the scenario evaluated here, the larger portion of the break room flow and therefore the debris (perhaps 75 percent) would flow through the personnel access door into the annulus on the side nearer the access for the reactor cavity (Section III.2.1 discusses the flow distribution assumption). A smaller portion of the debris would exit the SG compartment through the access door into SG compartment 2. In the volunteer plant, nearly all of the essentially inactive pool is the water below the sump floor in the reactor cavity. All other quiescent regions would have sufficient water circulation so that suspended fibers over time would circulate from those regions. When debris exits an SG compartment through a personnel access door because of the initial sheeting flow, the flow splits, with part going toward the recirculation sumps and part going in the opposite direction. In the

scenario analyzed, the part going away from the sump screens flowed past the narrow passageway into the room leading to the reactor cavity access hatch. For debris to follow water into this passageway, it must essentially make a 90-degree bend in a short distance. Therefore, the conclusion is that only a small fraction of debris moving with the dynamic wave front, especially larger debris, will make the 90-degree turn into the reactor cavity passageway.

With these concepts as a basis, the pool transport distributions were judged as shown in Table III-6. Starting with the fines, it is assumed that 75 percent of the flow exits the SG1 compartment on the reactor cavity side; then, 60 percent of that flows in the direction of the reactor cavity; then, 50 percent of the flow makes the turn into the reactor cavity passageway. Thus, perhaps 25 percent of the fines initially on the break room floor go into the reactor cavity on initial formation of the pool. Because these fibers are suspended, the remaining pool formation could increase this number to, for example, a conservative 40 percent. Then, the remaining amount is split 50 percent–50 percent toward the recirculation sump and away from the sump. With each fibrous debris category of increasing size, the fraction entering the reactor cavity decreases somewhat, with the even split maintained between the flow toward and the flow away from the screen. With the heavier metallic debris, even the smaller pieces would transport less readily than the fiber pieces.

Of the debris initially deposited on the annular sump floor, a significant fraction could be located such that flow from the break compartment to the reactor cavity would not greatly affect it because the exit from the break compartment is near the entrance to the reactor cavity. However, larger debris deposition would also be more likely near the break compartment door. For lack of a better justification, the same distributions judged for debris initially deposited on the break room floor are assumed for debris initially deposited on the annular sump floor. In any case, only a few percent of the total debris is estimated to be deposited on the annular sump floor because of the relatively small doorway areas as compared with the upward area of the SG compartments.

Table III-6. Pool Formation Debris Transport Distributions

Debris Size and Type	Pool Formation Debris Transport Distributions					
	Floor of Break Room			Floor of Sump Pool		
	Toward Screen	Away from Screen	Into Inactive Pools	Toward Screen	Away from Screen	Into Inactive Pools
Fibrous Debris						
Fines	0.30	0.30	0.40	0.30	0.30	0.40
Small Pieces	0.35	0.35	0.30	0.35	0.35	0.30
Large Pieces	0.40	0.40	0.20	0.40	0.40	0.20
Intact Pieces	0.40	0.40	0.20	0.40	0.40	0.20
RMI Debris						
<2 in.	0.35	0.35	0.30	0.35	0.35	0.30
2 to 6 in.	0.40	0.40	0.20	0.40	0.40	0.20
>6 in.	0.50	0.50	0.00	0.50	0.50	0.00

III.3.3.2 Recirculation Pool Debris Transport

Important aspects of the transport of sump pool debris were observed during the integrated debris transport tests (NUREG/CR-6773, 2002). For low-density fiberglass debris, the fines (e.g., individual fibers) remain suspended and move with the flow of water, whereas larger debris pieces readily saturate with water at the water temperatures typical of LOCA accidents and then sink to the pool floor, where further transport depends on the flow velocity and turbulence near the floor. All RMI debris sinks to the floor of the pool, with the occasional exception of a piece of debris that encapsulates an air pocket, keeping that piece buoyant.

The CFD analyses provide realistic descriptions of the floor-level flow conditions, which Section III.2 describes as contours established so that the velocities higher than the experimental measured threshold are clearly indicated. The velocity contours illustrate the portion of the pool where debris would most likely move readily with the flow. In addition to velocity contours, the streamline plots provide a reasonable connecting pathway whereby a piece of debris would likely travel from its original location in the pool to the recirculation sumps. If a transport pathway passes through a slower portion of the pool, then debris moving along that pathway could stall and not transport to the recirculation sump. Otherwise, the transport is very likely.

The effects of pool turbulence are more difficult to quantify. Test observations have shown the occasional reentrainment of debris once stalled in relatively quiescent water. Water within quiescent regions typically tends to rotate, sending debris into the center of the vortex, where it becomes semi-trapped. However, an occasional pulsation can kick a piece of debris out of the vortex and back into the main stream. Although this behavior cannot be reasonably quantified, transport estimates should be enhanced to consider these effects.

A detailed transport analysis using the CFD predicted flow contours and flow streamlines would subdivide the sump pool floor into relatively fine subdivisions, with each subdivision having a source term for debris depositing onto the pool floor at that location. Then, the transport of the debris from each specific subdivision would be evaluated independently using a streamline generated from that subdivision to the recirculation sumps to illustrate where that debris would likely reside after movement ceases. Quantification of all the subdivision transport results would provide an overall sump pool transport fraction for each debris category. The transport results should then be adjusted to account for pool turbulence effects on debris (i.e., the threshold transport tumbling velocities reported in NUREG/CR-6772 were measured in very uniform and turbulence-dampened flows, but turbulence is capable of moving debris where bulk flow will not). One method of accounting for turbulence effects would be to decrease the threshold velocities for transport.

This analysis simplified the preceding detailed model description to include only seven subdivisions for the sump floor. Even then, the available CFD streamlines did not form a complete set. Thus, the individual pool transport fractions used to populate the transport charts were basically engineering judgments based on the velocity profiles. Table III-7 provides the individual transport estimates. Figure III-33 and Figure III-37 show the CFD flow velocity contour maps used to make these judgments for fibrous and RMI debris, respectively. Figure III-42 and Figure III-43 show a sampling of corresponding flow streamline plots for fibrous and RMI debris, respectively. The transport fractions range

from 100-percent transport for the suspended fibers and debris located nearer the recirculation sumps to 0-percent transport for the largest debris located on the opposite side of the containment.

Table III-7. Recirculation Pool (Steady-State) Debris Transport Fractions

Location Where Debris Enters Sump Pool	Fraction of Debris Transported to Sump Screen						
	Fibrous Debris				RMI Debris		
	Fines	Small Pieces	Large Pieces	Intact Pieces	<2 in.	2 to 6 in.	>6 in.
Debris Entering Annular Sump Pool by Containment Spray Drainage (Debris Assumed to Enter Established Sump Pool)							
Annulus Section Containing Recirculation Sumps	1	1	1	1	1	1	1
Vicinity of SG4 Access (SG Adjoining Break Room)	1	1	1	1	1	1	1
Vicinity of Interior Equipment Room Access (~90° from Sumps)	1	1	1	1	1	1	1
Vicinity of SG3 Access (Includes Inter-Level Stairwell)	1	0.5	0.4	0.3	0.3	0.2	0.1
Annulus Section Directly Opposite Recirculation Sumps	1	0.2	0.1	0	0.1	0	0
Vicinity of SG2 Access (Includes Inter-Level Stairwell and Hatch)	1	0.5	0.4	0.3	0.3	0.2	0.1
Vicinity of SG1 Access (Compartment with Break, Includes Multiple Floor Drains)	1	0.7	0.6	0.5	0.5	0.4	0.3
Debris Directly Blowdown Deposited onto Sump Floor but Subsequently Relocated Away from Recirculation Sumps during Pool Formation (Section III.3.3.1)							
Initially on Break Room Floor, Relocated Away from Recirculation Sumps	1	0.3	0.2	0.1	0.2	0.1	0
Initially Spread Around Annular Sump Floor, Relocated Away from Recirculation Sumps	1	0.3	0.2	0.1	0.2	0.1	0

III.3.3.3 Sump Pool Debris Erosion

The only source of data for the erosion of fibrous debris in a sump pool was the integrated debris transport tests documented in NUREG/CR-6773. This test program included four longer term tests (3- to 5-hour durations) where debris accumulation on the simulated sump screen was collected every 30 minutes.

The three sources of fibrous debris contributing to this accumulation are (1) small-piece debris tumbling or sliding along the floor, (2) suspended fibers initially introduced into the tank, and (3) fibers that had eroded from the small-piece debris residing on the floor of the tank. Late in these tests, most of the small-piece debris had already either been transported to the screen or had come to relative rest in some quiescent location on the tank floor; therefore, the contribution of the small-piece debris should have been minimal near the end of the tests. Also late in the tests, water recirculation should have substantially reduced the initially suspended fibers so that continued accumulation would fall off quite noticeably. Sufficient time had elapsed in each test for the water in the tank to be replaced (tank water volume divided by the simulated break flow) from 19 to 46 times during the course of the test. Because the continued accumulation tended to hold at a somewhat sustainable rate, it is likely that continued erosion was supporting the continued debris accumulation.

Table III-8 shows the end of test debris accumulation rates for these longer term tests. Although these tests ran for several hours, as indicated in the table, the tests were of short duration compared with LOCA long-term recirculation times. One of the four tests was conducted with a shallower pool of 9-in. depth compared with the usual depth of 16 in The accumulation was about eight times more rapid for the shallow pool test than for the deeper tests. In addition, during the shallow pool test, the water recirculation in terms of water replacements (46) was significantly more frequent for the 9-in. test than for the 16-in. tests; thus, the initial suspended debris would have been more readily filtered from the tank. Therefore, most of the longer term debris accumulation should have resulted from the continued erosion of fibrous debris in the tank. Further, the erosion rate was greater in the shallow depth pool, most likely because of the greater turbulence in the shallow pool relative to the deeper pools.

Table III-8. Late-Term Debris Accumulation in Integrated Debris Transport Tests

Test ID	Pool Depth (in.)	Test Duration (Hours)	Accumulation Rate near the End of the Test (Percent of Debris in Tank/hr)	Approximate Number of Water Replacements During the Test
LT1	16	4	0.4	26
LT2	9	4	2	46
LT3	16	3	0.3	19
LT4	16	5	0.3	32

In conclusion, the only applicable test data for long-term debris erosion in a sump pool strongly indicate a sustainable rate of erosion that is affected by the relative turbulence in the pool. The small-piece debris residing on the floor of the pool, late term, was generally found in quiescent locations, not necessarily directly under the simulated break

flow. The turbulence associated with the spray drainage was not simulated. Because the 16-in. depth more closely resembles the fully established volunteer-plant pool, this analysis adopts the erosion rate of 0.3 percent of the current tank debris/hour.

In the debris transport charts, the overall fraction of debris on the sump floor that erodes into fines is required. Using the long-term recirculation mission time of 30 days, analysis indicates that nearly 90 percent of the initial debris mass would become eroded if this erosion rate remained constant throughout the 30 days. This calculation took into account the steadily decreasing mass of debris in the pool using the following equation:

$$f_{eroded} = 1 - (1 - rate)^{Number\ ofHours}$$

Therefore, in the debris transport charts, 90 percent of the small- and large-piece debris predicted to reside on the sump floor is assumed to erode into suspended fibers unless the debris is still enclosed in a protective cover.

This calculation has the following substantial sources of uncertainty:

- The integral debris transport tests lasted 3 to 5 hours. Therefore, the question remains whether the erosion rate tapers off with time. In addition, it is not certain that all of the end-of-test debris accumulation was the result of erosion products.
- The test results include the usual variances in test data, such as flow and depth control and debris collection.
- Although the test series was designed to approximate the flow and turbulence characteristics of the volunteer-plant sump pool, the tank characteristics may have been significantly different than those at the plant. The difference in the erosion rates between the 9-in. and 16-in. pool depths in the integrated tests clearly illustrates the effect of pool turbulence on fibrous debris erosion.
- The geometry of the volunteer-plant sump pool is larger and more complex than that of the test tank used in the integrated tests.
- The long-term tests did not study large-piece debris.

The 90-percent debris eroded value is used for both the small- and large-piece debris, despite the uncertainties. With such limited data, the use of the 90-percent value is necessary to ensure conservatism in the overall transport results. This number can possibly be reduced, once better erosion data are available.

III.3.4 Quantification Results

The blowdown/washdown/pool transport estimates presented in Sections III.3.2 and III.3.3 were entered into debris transport charts (shown generically in Figure III-48) and quantified to obtain overall transport fractions. A separate chart was created for each size category and for each type of debris. Figure III-49, Figure III-50, Figure III-51, and Figure III-52 illustrate the transport processes for the fibrous debris categories of fines, small pieces, large pieces, and intact pieces, respectively. Figure III-53, Figure III-54,

and Figure III-55 illustrate the transport processes for RMI debris categories of pieces less than 2 in., 2 to 6 in., and greater than 6 in., respectively.

Debris Size	Blowdown Transport	Washdown Transport	Washdown Entry Location	Pool Fill Up Transport	Pool Recirculation Transport	Debris Erosion in Pool	Path	Fraction	Deposition Location
POOL TRANSPORT LOGIC CHART FIBROUS DEBRIS		Trapped Above 0.07					1	6.440E-02	Not Transported
						Erosion Products	2	0.000E+00	Sump Screen
					Stalled in Pool 0.00	1.00 Remainder	3	0.000E+00	Not Transported
			Sump Area 0.09		Transport 1.00	0.00		7.700E-02	Sump Screen
						Erosion Products	4	0.000E+00	Sump Screen
					Stalled in Pool 0.00	1.00 Remainder	5	0.000E+00	Not Transported
	Deposited Above 0.92		SG #4 0.17		Transport 1.00	0.00	6	1.455E-01	Sump Screen
							7	0.000E+00	Sump Screen
					Stalled in Pool 0.00	1.00 Remainder	8	0.000E+00	Not Transported
			Eq. Room 0.04		Transport 1.00	0.00	9	3.422E-02	Sump Screen
						Erosion Products	10	0.000E+00	Sump Screen
					Stalled in Pool 0.00	1.00 Remainder	11	0.000E+00	Not Transported
		Transports to Pool 0.93	SG #3 (Stairs) 0.12		Transport 1.00	0.00	12	1.027E-01	Sump Screen
						Erosion Products	13	0.000E+00	Sump Screen
					Stalled in Pool 0.00	1.00 Remainder	14	0.000E+00	Not Transported
			Opposite Side 0.06		Transport 1.00	0.00	15	5.134E-02	Sump Screen
						Erosion Products	16	0.000E+00	Sump Screen
					Stalled in Pool 0.00	1.00 Remainder	17	0.000E+00	Not Transported
			SG #2 (Elevator) 0.16		Transport 1.00	0.00	18	1.369E-01	Sump Screen
						Erosion Products	19	0.000E+00	Sump Screen
					Stalled in Pool 0.00	1.00 Remainder	20	0.000E+00	Not Transported
			SG #1 (RV Cavity) 0.36		Transport 1.00	0.00	21	3.080E-01	Sump Screen
				To Near Screen 0.30			22	1.500E-02	Sump Screen
						Erosion Products	23	0.000E+00	Sump Screen
Fines 1.00					Stalled in Pool 0.00	1.00 Remainder	24	0.000E+00	Not Transported
	Break Room Floor 0.05			Away From Screen 0.30	Transports 1.00	0.00	25	1.500E-02	Sump Screen
				Inactive 0.40			26	2.000E-02	*Inactive Pools*
				To Near Screen 0.30			27	9.000E-03	Sump Screen
						Erosion Products	28	0.000E+00	Sump Screen
					Stalled in Pool 0.00	1.00 Remainder	29	0.000E+00	Not Transported
	Sump Floor 0.03			Away From Screen 0.30	Transports 1.00	0.00	30	9.000E-03	Sump Screen
				Inactive 0.40			31	1.200E-02	*Inactive Pools*
								1.0000000	
								0.06440	Not Transported
								0.03200	*Inactive Pools*
								0.90360	Sump Screen

Figure III-49. Sump Pool Debris Transport Chart for Fine Fibrous Debris

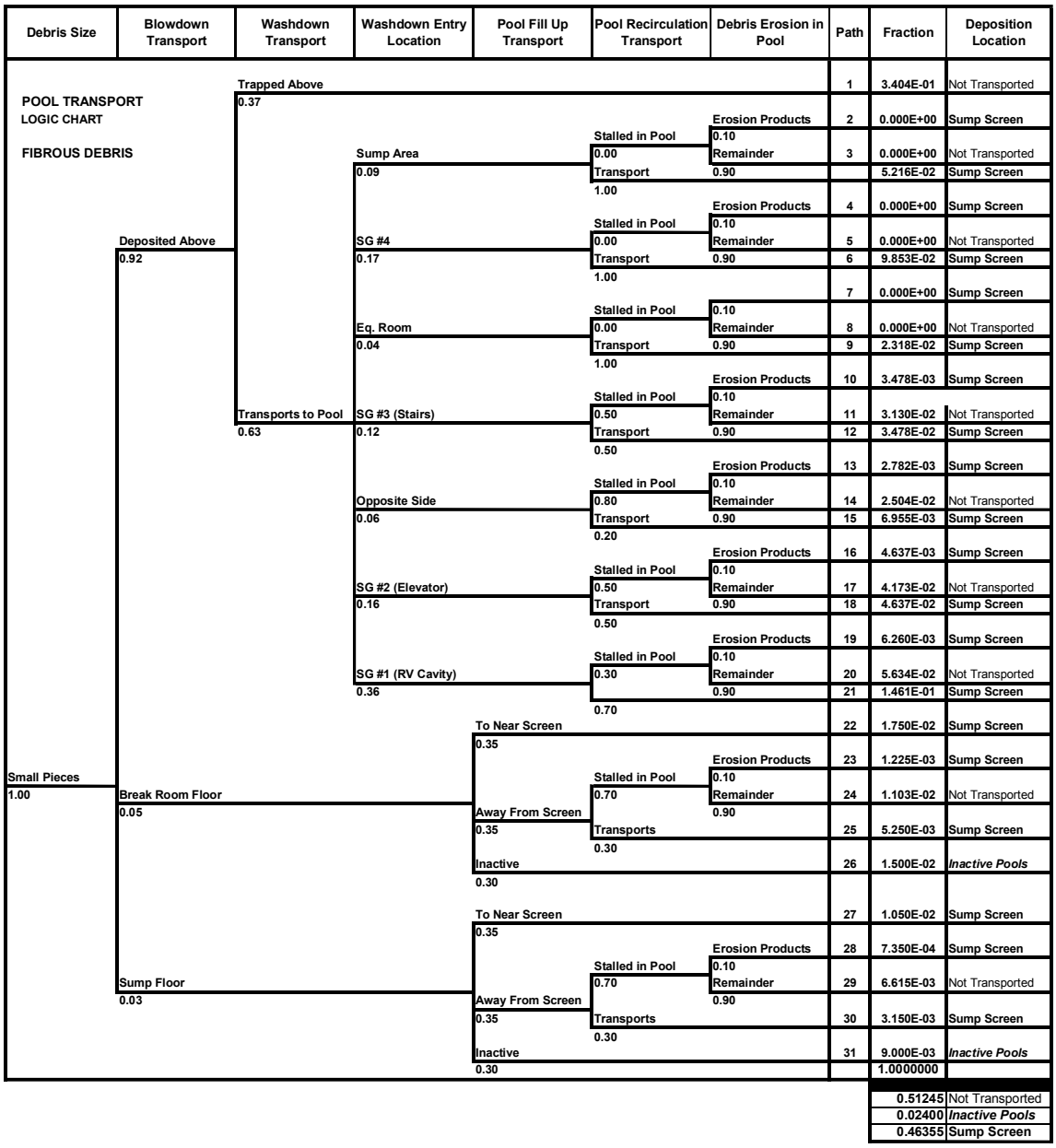

Figure III-50. Sump Pool Debris Transport Chart for Small-Piece Fibrous Debris

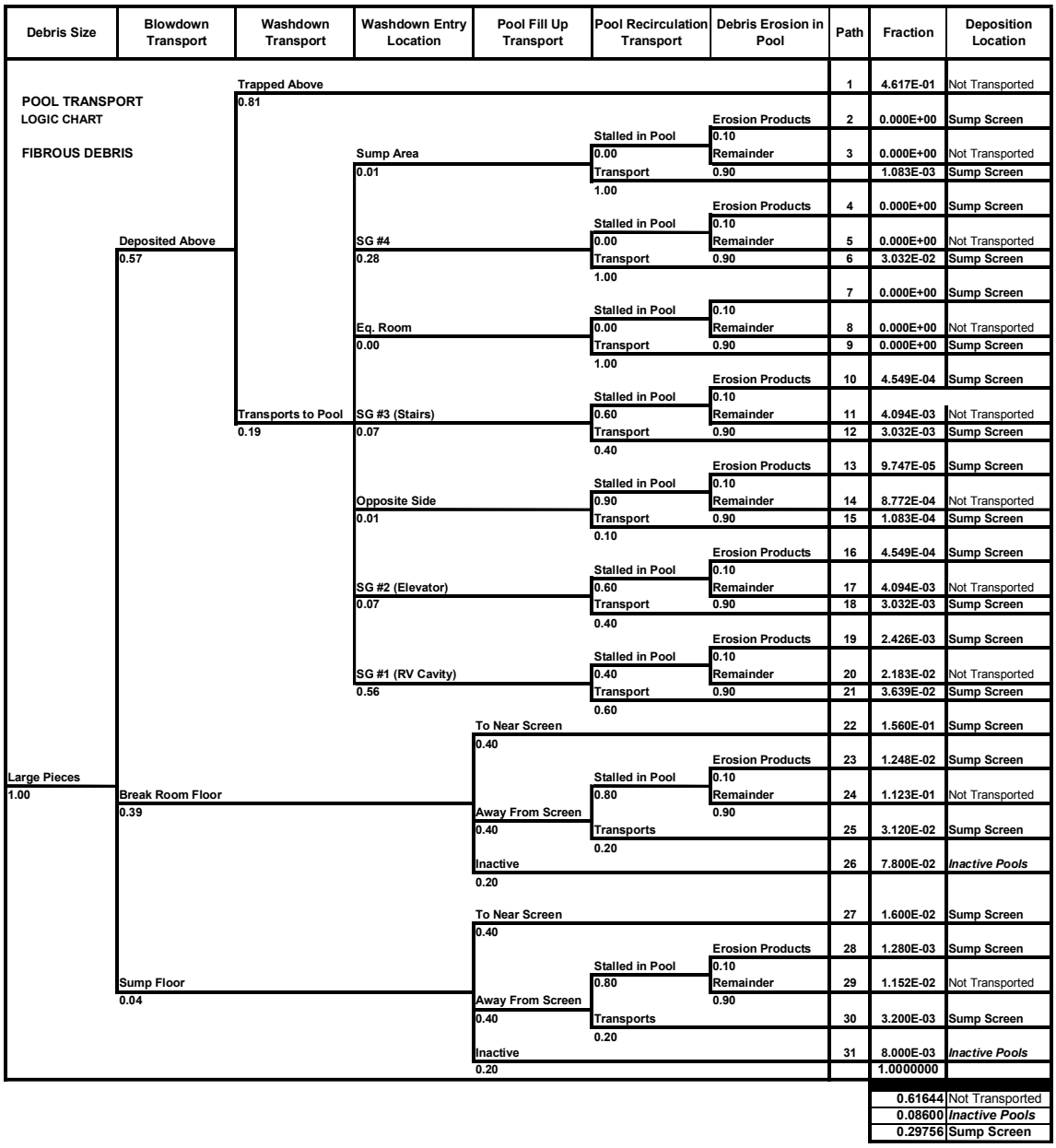

Figure III-51. Sump-Pool-Debris Transport Chart for Large-Piece Fibrous Debris

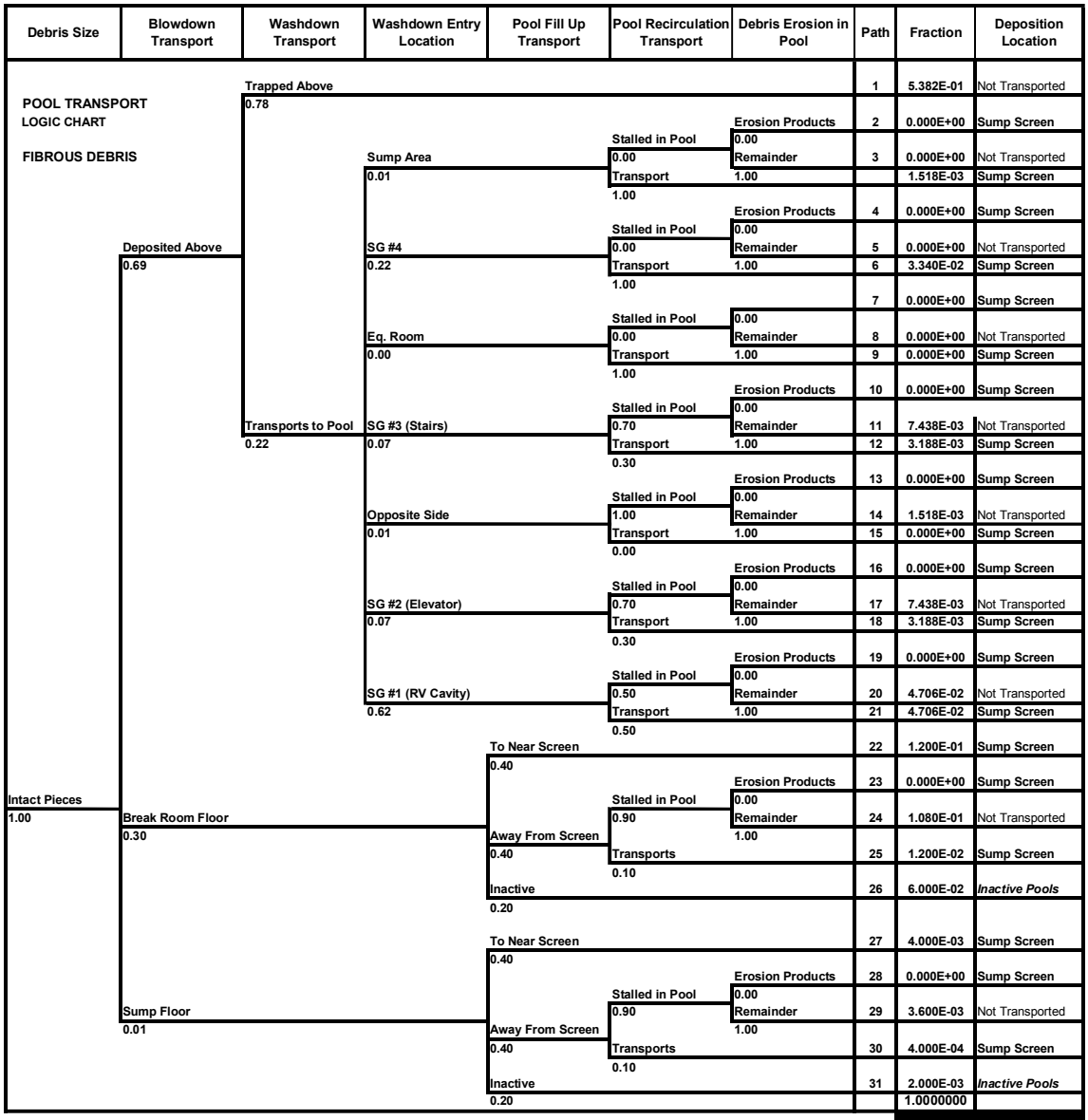

Figure III-52. Sump-Pool-Debris Transport Chart for Intact-Piece Fibrous Debris

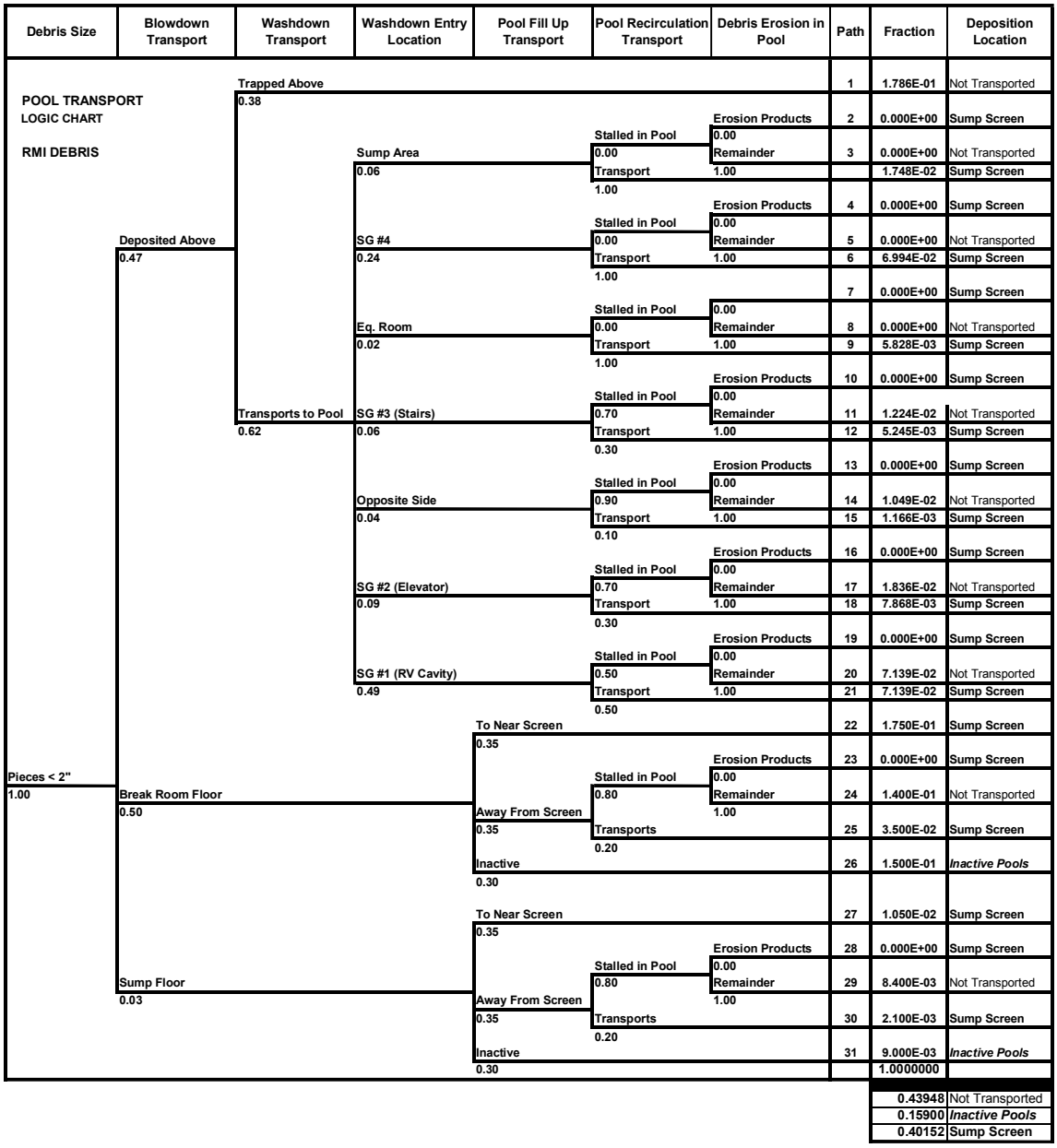

Figure III-53. Sump-Pool-Debris Transport Chart for <2-in. RMI Debris

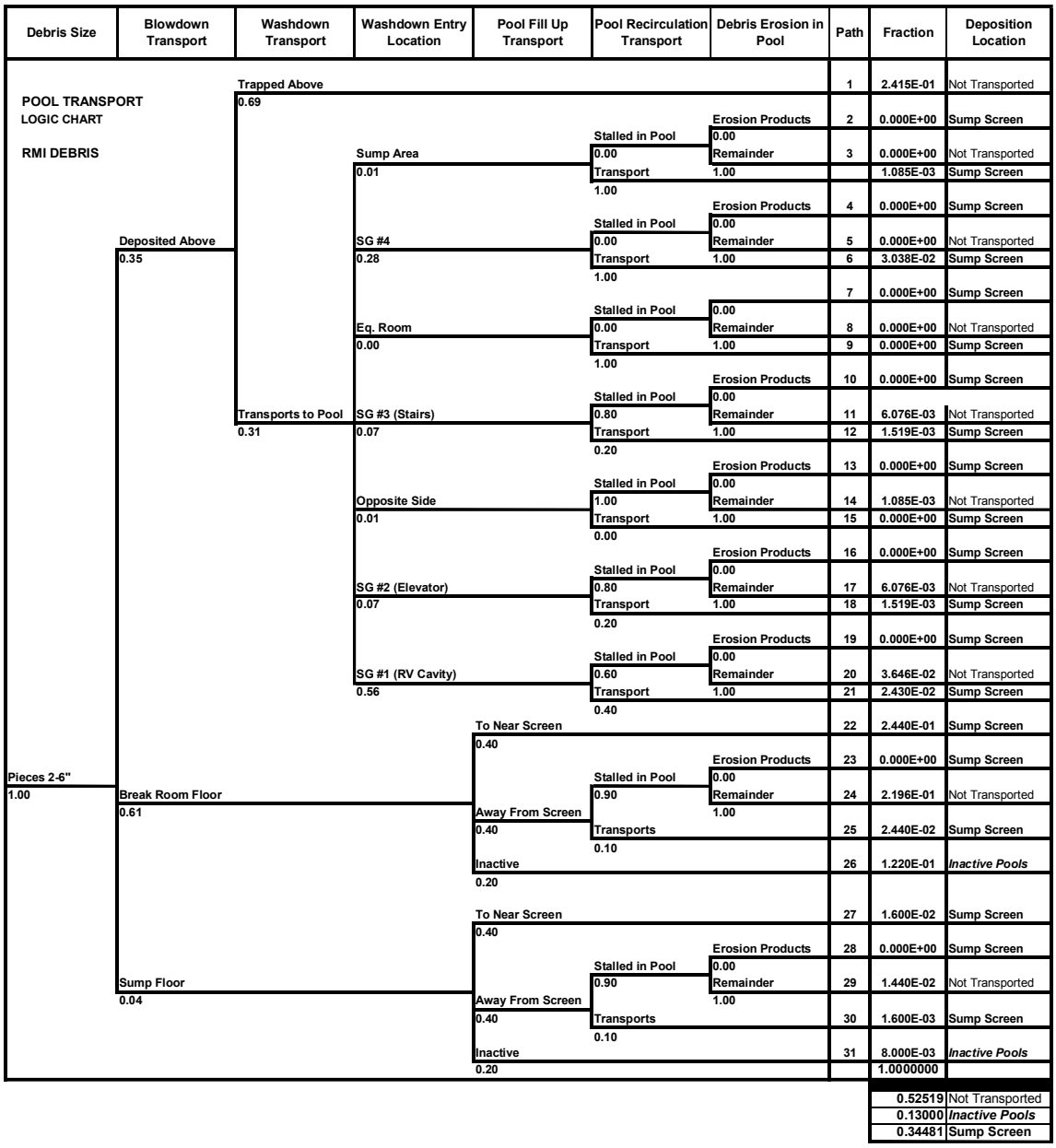

Figure III-54. Sump-Pool-Debris Transport Chart for 2- to 6-in. RMI Debris

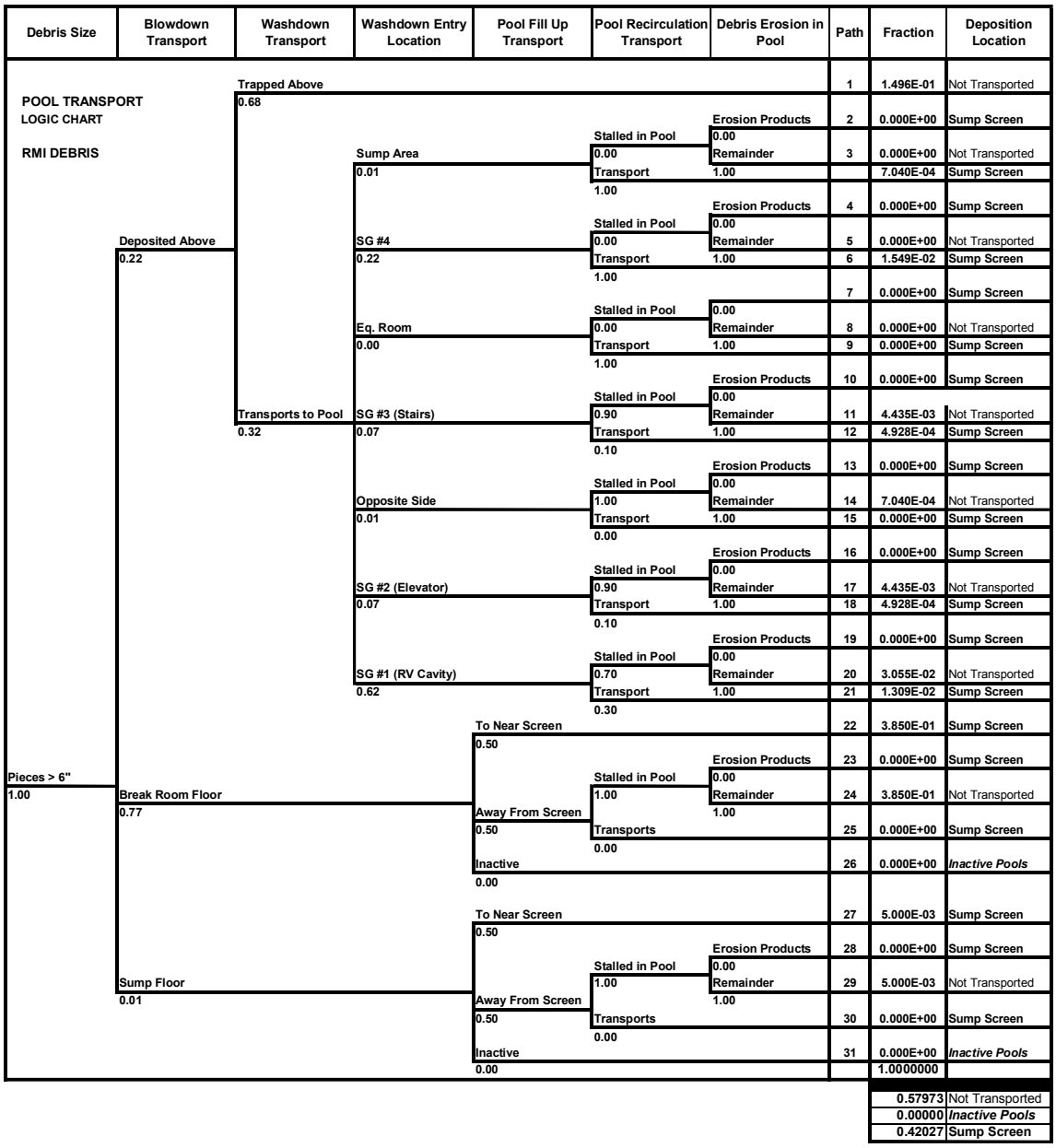

Figure III-55. Sump-Pool-Debris Transport Chart for >6-in. RMI Debris

Table III-9 shows the quantified results by debris category and insulation type, and Table III-10 shows the same results combined for each insulation type. The analysis indicates that about 52 percent of the fibrous and about 42 percent of the RMI debris would accumulate on the recirculation screens for a large LOCA in SG1. The sump pool transport fractions for the small- and large-piece debris are quite high, 97 and 96 percent, respectively. The high fraction for debris eroded contributed substantially to these numbers. However, to put this assumption into perspective, if only 10 percent had been assumed for the erosion, the pool transport fractions would still be 73 and 66 percent, respectively.

The large (greater than 6 in.) debris dominated the RMI debris transport fractions since 98.4 percent of the RMI was predicted to be in this category. This category includes quite large pieces including intact or nearly intact cassettes, which would require a faster flow to move the debris than the 0.28 ft/s used in the CFD analyses.

Table III-9. Quantified Category-Specific Sump-Pool-Debris Transport Results

Debris Category	Category-Specific Debris Transport Fractions				
	Size Distribution	Entering Pool	Into Inactive Pools	Sump Pool Transport	Overall Transport
Fibrous Debris					
Fines	0.133	0.90	0.032	1	0.90
Small Pieces	0.397	0.64	0.024	0.97	0.62
Large Pieces	0.235	0.45	0.086	0.96	0.44
Intact Pieces	0.235	0.40	0.062	0.56	0.23
RMI Debris					
<2 in.	0.011	0.66	0.15	0.61	0.40
2 to 6 in.	0.005	0.63	0.13	0.55	0.35
>6 in.	0.984	0.85	0	0.49	0.42

Table III-10. Quantified Insulation-Specific Sump-Pool-Debris Transport Results

Debris Category	Insulation-Specific Debris Transport Fractions			
	Entering Pool	Into Inactive Pools	Sump Pool Transport	Overall Transport
Fibrous	0.57	0.05	0.88	0.52
RMI	0.85	0.0024	0.50	0.42

The fractions of the sump pool floor where the floor-level flow velocity was slower than the threshold velocities for debris (0.12 and 0.28 ft/s for fibrous and RMI debris, respectively) were calculated from the CFD results presented in Section III.2. The floor fractions corresponding to a large break in SG1 (lower-right quadrant in the CFD results) are 0.41 and 0.22 for fibrous and RMI debris, respectively. Figure III-56 compares these floor area fractions with the sump pool transport fractions by insulation type and size categories. In this scenario, if the debris was uniformly introduced into the pool across the pool cross-sectional area and erosion was not significant, then the area fractions might be a reasonable indicator of the pool debris transport fractions. However, as shown, the area fractions are a poor indicator of debris transport when the debris is introduced into the pool in a more realistic and nonuniform manner and erosion is substantial. A uniform area fraction model can easily underpredict the pool debris transport by a factor of 2 or more.

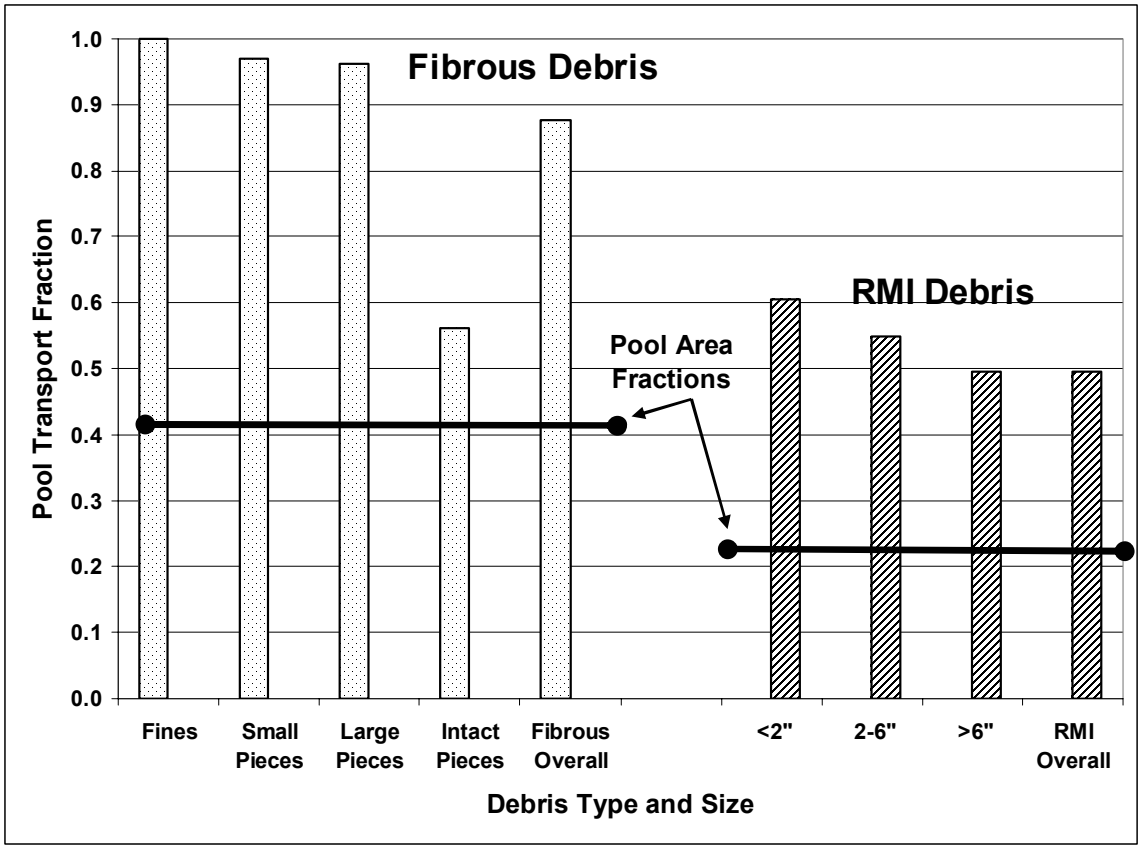

Figure III-56. Comparison of Sump Pool Transport Fraction with Velocity Area Fractions

The transport of debris from its generation in the zone of influence (ZOI) throughout the containment during the reactor coolant system (RCS) depressurization phase, then the washdown transport by the containment sprays, and then its transport through the sump pool to the recirculation sump screens is a rather intractable problem. A logic chart method was used to decompose the overall transport problem into many smaller problems that were subsequently either evaluated by analysis or simply conservatively judged. As such, the results of the volunteer analyses contain many sources of uncertainties; however, these uncertain results are plausible and offer insight into many aspects of debris transport that should be useful to subsequent evaluations. These sources of uncertainty regarding sump pool transport include (1) the timing and locations where debris enters the pool, (2) concerns regarding the effects of local pool turbulence that can move debris even when the bulk flow does not, (3) lack of data regarding erosion rates for debris that can decompose within the pool (e.g., fibrous debris), (4) the simplification of the analysis, and (5) the limited scenario space that can be realistically evaluated.

The debris transport results in this section pertain to a large LOCA in SG1. The same LOCA in another compartment could easily result in different transport results, which could be higher or lower than the scenario evaluated here. In addition, the transport of debris through the sump pool was evaluated here using simplified nodalization, as

discussed above. A more detailed evaluation would likely refine these transport results significantly; however, this analysis has demonstrated the transport methodology.

III.4 Conclusions and Recommendations

Section III.2 outlined a method for performing reactor containment pool flow dynamic analysis. A commercial CFD code was used to perform the simulations and assess the flow properties relevant to debris transport. The simulations obtained flow area fractions in excess of transport threshold velocities of debris. Transient containment pool fillup simulations were performed that could potentially be used to design debris diversion systems to sequester debris into zones that do not participate in the flow when sump pumps are engaged.

Recommendations for future simulations include performing grid-mesh convergence studies, further analysis of debris degradation mechanisms, and flow diversion. The grid-mesh convergence studies are required to have a defensible CFD analysis. Additional constraints on the grid mesh, not used or presented in this document, should include clustering grid points near the mass flow injection locations (break and splash locations) and development of a proper boundary layer grid near the no-slip walls, particularly on the containment floor. With additional grid points near the floor, a near-wall velocity profile will be established. The grid refinement study should thoroughly investigate this near-wall velocity gradient and drag forces which could have an impact on debris transport. The debris degradation mechanisms should also be further studied. This document shows examples of degradation, but no attempt to quantify the dynamics has been made at this time.

The transport of debris from its generation in the ZOI throughout the containment during the RCS depressurization phase, then the washdown transport by the containment sprays, and then its transport through the sump pool to the recirculation sump screens is a rather intractable problem. A logic chart method was used to separate the overall transport problem into many smaller problems that were subsequently either evaluated by analysis or by engineering judgment. As such, the results of the volunteer analyses contain many sources of uncertainty; however, these uncertain results are plausible and offer insight into the many aspects of debris transport that should be useful to subsequent evaluations. These sources of uncertainty regarding sump pool transport include (1) the timing and locations where debris enters the pool, (2) concerns regarding the effects of local pool turbulence that can move debris even when the bulk flow does not, (3) lack of data regarding erosion rates for debris that can decompose within the pool (e.g., fibrous debris), (4) the simplification of the analysis, and (5) the limited scenario space that can be realistically evaluated.

The debris transport results in this appendix pertain to one LOCA scenario (a large LOCA in SG1). The same LOCA in another compartment could easily result in different transport results that could be higher or lower than the scenario evaluated here. In addition, the transport of debris through the sump pool was evaluated here using simplified nodalization, as discussed above. A more detailed evaluation would likely refine these transport results significantly; however, the transport methodology has been demonstrated.

III.5 III.5 References

(NUREG/CR-6772, 2001) Rao, D. V., B. C. Letellier, A. K. Maji, and B. Marshall, "GSI-191: Separate-Effects Characterization of Debris Transport in Water," NUREG/CR-6772, LA-UR-01-6882, 2001.

(NUREG/CR-6773, 2002) Rao, D. V., et al., "GSI-191: Integrated Debris-Transport Tests in Water Using Simulated Containment Floor Geometries," NUREG/CR-6773, LA-UR-02-6786, December 2002.